Molecular and cell biology analysis of Rgnef, Trim71 and Gli2 in regulation of the Shh signalling pathway

Kayvan Hakim-Rad

Royal Holloway University of London

A thesis presented for the degree of PhD

October 2014

Declaration of Authorship

I Kayvan Hakim-Rad hereby declare that this thesis and the work presented in it is entirely my own. Where I have consulted the work of others, this is always clearly stated.

Signed: _____

Date: _____

Acknowledgement

I would like to express my sincere gratitude to my supervisor Jenny Murdoch for her solid support, for her guidance and reassurance.

I would like to thank my second supervisor Chris Wilkinson for his advice and support. I wish to thank all the academic staff in biological sciences for their support and use of their laboratories and research equipment. I am particularly grateful to Chris Rider, Philip Chen, Pavlos Alifragis and Laurence Bindschedler for their regular help and advice.

I would like to thank all the research technicians for their help and instruction. I am particularly grateful for the assistance given by Chris Gerrish, for taking time from his own busy schedule to introduce me to mass spectrometry and support me on my steep learning curve. Thanks also to Safina Khan for her help, training and kind support.

My gratitude goes to Baolin Wang, Gregory Wulczyn, Dominic Norris and Wouter Moolenaar for sharing cell lines, reagents and protocols.

I would also like to thank the following companies for their assistance. Thanks to Chris Hingley and Alison Davis from Primer Design Ltd for including me their student sponsorship scheme. I am very grateful to Julia Smith for her continued help and for inviting me to Bruker for training. Also thank you to the BBSRC and The Royal Society for funding this research.

Thanks to my lab partners Paul de Saram and Anila Iqbal for all their help and support. Thanks for making me laugh a lot and keeping me sane these past few months.

I wish to thank my family and friends for their solid support and understanding. I finally want to thank my wife Sharon who believed in me, always supported me and joined me in making all the sacrifices. To her I dedicate this thesis.

Abstract

The Sonic hedgehog signalling pathway is of key importance during embryonic development as well as adult disease. While much is known regarding the main intracellular signalling components involved, precise details of the regulation of the pathway remain undiscovered. In this thesis, I aim to further our understanding of the regulation of the Shh signalling pathway by investigating aspects of the molecular mechanism.

We have previously shown that Tulp3 acts as a negative regulator of the Shh pathway. More recently, we have found that Tulp3 interacts with Rgnef and Trim71. In this thesis, I test the hypothesis that Rgnef and Trim71 act as regulators of the Shh pathway. My investigations centre on assessing pathway activity in relation to changes in *Rgnef* and *Trim71* expression, using a cell biology assay. I show that reducing Rgnef expression leads to a reduction in Shh pathway activity, while increasing Rgnef expression stimulates pathway activity. I show also that increasing Rgnef expression significantly reduces the proportion of cells with a primary cilium, an organelle fundamental to Shh signalling. Within the embryo, I show that *Rgnef* is expressed in the developing neural tube. Shh pathway suppression was also induced by *Trim71* siRNA, but through validation tests I show this to be a false positive result and investigate the possible causes.

In addition, I have used mass spectrometry to identify putative novel sites of Gli2 post translational modification. Gli2 is one of three transcription factors conserved in vertebrate Shh signalling, and which are the ultimate target effectors of pathway activity. Gli2 is predominantly involved in pathway activation however precise regulation of Gli2 activity remains poorly understood. By using mass spectrometry, I aimed to reveal novel sites of protein modification that would help to understand the role of Gli2. Two potential novel sites of Gli2 phosphorylation have been discovered.

Table of Contents

Table of figures

Index of tables

Abbreviations

Ab	Antibody
ANP	Anterior neuropore
AP	Anterioposterior
BMP	Bone morphogenic proteins
BSA	Bovine serum albumin
C1	Closure 1
C2	Closure 2
C3	Closure 3
cAMP	Cyclic AMP
Ci	Cubitus interruptus
CID	Collision-induced dissociation
CK1	Casein kinase 1
coIP	Coimmunoprecipitation
Cos2	Costal2
Dhh	Desert hedgehog
DIG	Digoxygenin
DLHP	Dorsolateral hinge points
DMEM	Dulbeccos's Modified Eagle's Medium
DMSO	Dimethyl sulfoxide
DTT	Dithiothreitol
DV	Dorsoventral
E	Embryonic day
ENU	N-ethyl N-nitrosourea
ETD	Electron transfer dissociation
FAK	Focal adhesion kinase
Fam193a	Family with sequence similarity 193, member A
FAS	Fatty Acid Synthase
FGF	fibroblast growth factor
Fu	Fused
GAP	GTPase activating protein
GEF	Guanine nucleotide exchange factor
GDP	Guanosine diphosphate
Gli	Glioma associated oncogene
GPCR	G-protein coupled receptor
GSK3b	Glycogen synthase kinase3b
GTP	Guanosine triphosphate
HEK293T	Human embryonic kidney 293 cells, large T antigen
Hh	Hedgehog
hhkr	hitchhiker
HNP	hindbrain neuropore
HRP	Horse radish peroxidase
IFT	Intraflagellar transport

IHC	Immunohistochemistry
Ihh	Indian hedgehog
IMCD3	Inner medullary collecting ducts
IP	Immunoprecipitation
kDa	Kilodaltons
Ktn1	Kinectin 1
LB	Luria Bertani
MALDI-TOF	Matrix-assisted Laser Desorption/Ionization - Time Of Flight
MHP	Median hinge point
M-MLV	Moloney Murine Leukemia Virus
MRC	Medical research council
MS	Mass spectrometer
NT	Neural tube
NTD	Neural tube defect
Nup155	Nucleoporin 155
PBS	Phosphate buffered saline
PCP	Planar cell polarity
PCR	Polymerase chain reaction
PFA	Paraformaldehyde
PH	Pleckstrin homology
PKA	Protein kinase A
PNP	Posterior neuropore
polyA	Polyadenylation
Ptch1	Patched1
PTM	Post translation modifications
PVDF	Polyvinylidene fluoride
RA	Retinoic acid
Rgnef	Rho-guanine nucleotide exchange factor
RT	Room temperature
Shh	Sonic hedgehog
Smo	Smoothened
Sufu	Suppressor of Fused
TE	Tris-EDTA
TNF	Tumour necrosis factor
Trim71	Tripartite motif protein 71 (abnormal cell lineage 41)
Tulp	Tubby-like proteins
Tulp3	Tubby like protein 3
WB	Western blotting

Chapter 1: Introduction

1-01 Neural tube defects

In the UK birth defects account for over 12,000 live births per year with nervous system disorders amongst the most common (EUROCAT, prevelance data tables 2008-2012 (2014)). Neural tube defects (NTD) are one of the most prevalent forms of developmental embryo abnormality second only to congenital heart defects (Detrait et al., 2005). The main forms are anencephaly, which results in fetal and infant mortality and spina bifida, where almost all individuals affected have lower body paralysis and significant physical disability (Oakley, 1998, Detrait et al., 2005). Almost half a century has passed since links were first made regarding low folic acid and NTDs through clinical observations that lead to preliminary epidemiological research (Hibbard et al., 1965, Leck, 1974). The first definitive case for identifying folic acid deficiency as a factor for the prevalence of NTD came from the Medical Research Council (MRC) Vitamin Study (MRC, 1991). The main finding from this and subsequent intervention studies was to show that periconceptual use of folic acid supplements can lower the risk of NTD by 40% to 80% (Eichholzer et al., 2006). Since 1992 the consensus among national and worldwide health organisations was to promote awareness and recommend folic acid supplementation for women (Eichholzer et al., 2006). In 1998 the World Health Organisation reported that approximately 400,000 infants were born worldwide with NTD, mostly in China, Mexico and Central America (Oakley, 1998). In the same year mandatory folic acid fortification of bread and flour was introduced in the USA, a measure soon adopted in South America, Canada, Australia and other countries, although not with Europe (Eichholzer et al., 2006). Decreases in prevalence of NTD did occur, although progress was slow and results were not as high as predicted from the MRC vitamin study (Eichholzer et al., 2006). Despite such progress NTD still persists, even when the difficulty in implementing public health preventative measures are taken into account (Oakley, 2009, Copp et al., 2013). What has therefore become clear is that forms of NTD are folic acid resistant, a condition that has since been well established in mouse models of the disorder (Copp et al., 2003b).

The study of developing mouse embryos has proven to be an effective experimental method when identifying genes involved in neural tube development. Investigating the abnormal development of NTD mouse models provides a basis for comparison that can identify genes involved and investigate their relationship to environmental factors

(Copp et al., 2003b, Detrait et al., 2005). How genetic inheritance determines NTD is best summarised as genetic or multi-genetic susceptibilities to the extent and timing of environmental factors (Detrait et al., 2005). Identifying such genes in mutant mouse models enables a basis to test for environmental factor susceptibilities. For example, in folic acid resistant NTD mouse mutant *Grhl3*, a lack of inositol was identified as a potential contributing factor to prevalence of NTD (Greene and Copp, 1997). A factor that is currently being investigated in the UK by randomised clinical trial (Copp et al., 2013).

Observing the morphological changes after gene disruption by N-ethyl-N-nitrosourea (ENU) has become an extensively practiced form of forward mutagenesis screening (Cordes, 2005). Alkylating agent ENU is a highly potent mutagen that acts by transferring an ethyl group to nucleotides. ENU is toxic but correctly administered can produce low numbers of random mutations. Any observed defective phenotypes, including NTD, can then be sourced back to the dysfunction of specific genes (Cordes, 2005). Gene defects discovered in this way cannot be assumed to simply occur in human populations as inherited traits but provide a basis for human population screens of the same disorders (Detrait et al., 2005, Boyles et al., 2005). Such studies have identified risk factors based on genes of the folic acid metabolic pathway and to some extent on Wnt and Hedgehog signalling (Boyles et al., 2005). For example, elevated homocysteine observed in mothers of children with NTD metabolism could relate to three genes within the folic acid pathway; *cystathion-β-synthase* (CBS), *methionine synthase* (MS) and *5,10 –methylenetetrahydrofolate reductase*(MTHFR) (Boyles et al., 2005, van der Put et al., 1995). These genes may therefore, individually or collectively, infer a susceptibility to environmental factors that contribute to NTD.

In order to eradicate NTD, the challenge for the research community is to provide a complete model of gene involvement in neural tube development. Hence, a model to help collectively identify the genes involved as risk factors in human populations.

1-02 Morphological aspects of mammalian neurulation

Neurulation is the process of neural tube formation from a plane of columnar epithelial tissue in the dorsal region of developing embryos called the neural plate. There are two quite separate mechanisms of neurulation, primary and secondary.

Primary neurulation is responsible for the large majority of neural tube formation using a mechanism that folds the neural plate into a tube. Secondary neurulation only occurs at the very caudal end of the embryo using a mechanism that involves internally hollowing out a lumen to form a tube.

Primary neurulation starts with the formation of the neural folds. The edges of the neural plate elevate on either side of the dorsal midline (Figure 1-01 A-B). The neural folds converge and fuse along the midline to form the neural tube. The adjacent ectoderm joins to cover the neural tube by forming a layer of surface ectoderm (Figure 1-01 C). The precise morphology of the bending neural folds varies along the anterior-posterior axis of the embryo (Figure 1-01 D). Along most of the axis, a median hinge point (MHP) forms at the mid-line of the neural plate, and bending at this hinge point creates the emergence of the neural folds. In the upper spine, the MHP is the only bending region of the neural plate. At mid- and lower-spine levels, each neural fold forms a further bend called the dorsal lateral hinge point (DLHP) which helps to turn the neural fold ends towards each other for eventual fusion. At low spinal levels, DLHPs form in the absence of an MHP. These three forms of neural tube closure are referred to as the three modes of spinal closure (Shum and Copp, 1996).

Neural tube closure does not occur uniformly along the entire embryo but instead initiates at specific points where it then continues concurrently until completion (Figure 1-01 E). In mice neural tube closure is initiated at three points along the neural plate; closure 1 is at the base of the hindbrain and closes in both directions towards future brain and spinal regions. Bidirectional closure is also initiated at closure 2 at around the forebrain/midbrain boundary, although there is variation in precise position of closure 2, between different mouse strains (Copp et al., 2003b). Closure 3 occurs at the rostral end of the forebrain from where it can only proceed caudally. Closure between these points gives temporarily open regions of neural tube, between them; these are referred to as the neuropores. In the mouse brain, there are clear anterior and hindbrain neuropores. Final closure of the neural tube is seen in the posterior region, with closure of the posterior neuropore. In humans, it appears that there are only two sites of initiation of closure. It seems that the position of closure 2 is so far anterior that it becomes indistinguishable from closure 3. In mouse embryos,

neurulation takes place over 2 days of development, from embryonic day (E) 8.5 to E10.5. The initiation of neural tube closure 1 occurs at around the 5-6 somite stage, with closure 2 and 3 occurring at about the 12-somite stages. Completion of cranial closure, with closure of the anterior and hindbrain neuropores, is seen by about the 17-somite stage. Final completion of primary neurulation, with closure of the PNP, is observed usually by the 30-somite stage. Figure 1-01 is a summary of mammalian neurulation as outlined so far.

Formation of the lowest portion of the spinal cord does not require neural folding and is instead formed by a process of secondary neurulation. Here mesenchymal cells in the dorsal part of the tail bud around the posterior neuropore, condense into an epithelial rod that is effectively “hollowed out” to form a lumen continuous with the neural tube (Greene and Copp, 2009).

Prior to and during neurulation the neural epithelium simultaneously extends and this is due in part to growth of the caudal region and cell elongation. However most of the required lengthening and narrowing is achieved by coordinated intercalation of cells that move laterally towards the midline in a process, referred to as convergent extension (Keller, 2002). Furthermore, without convergent extension bilateral neural folds do not form sufficiently close enough to fuse (Copp et al., 2003a).

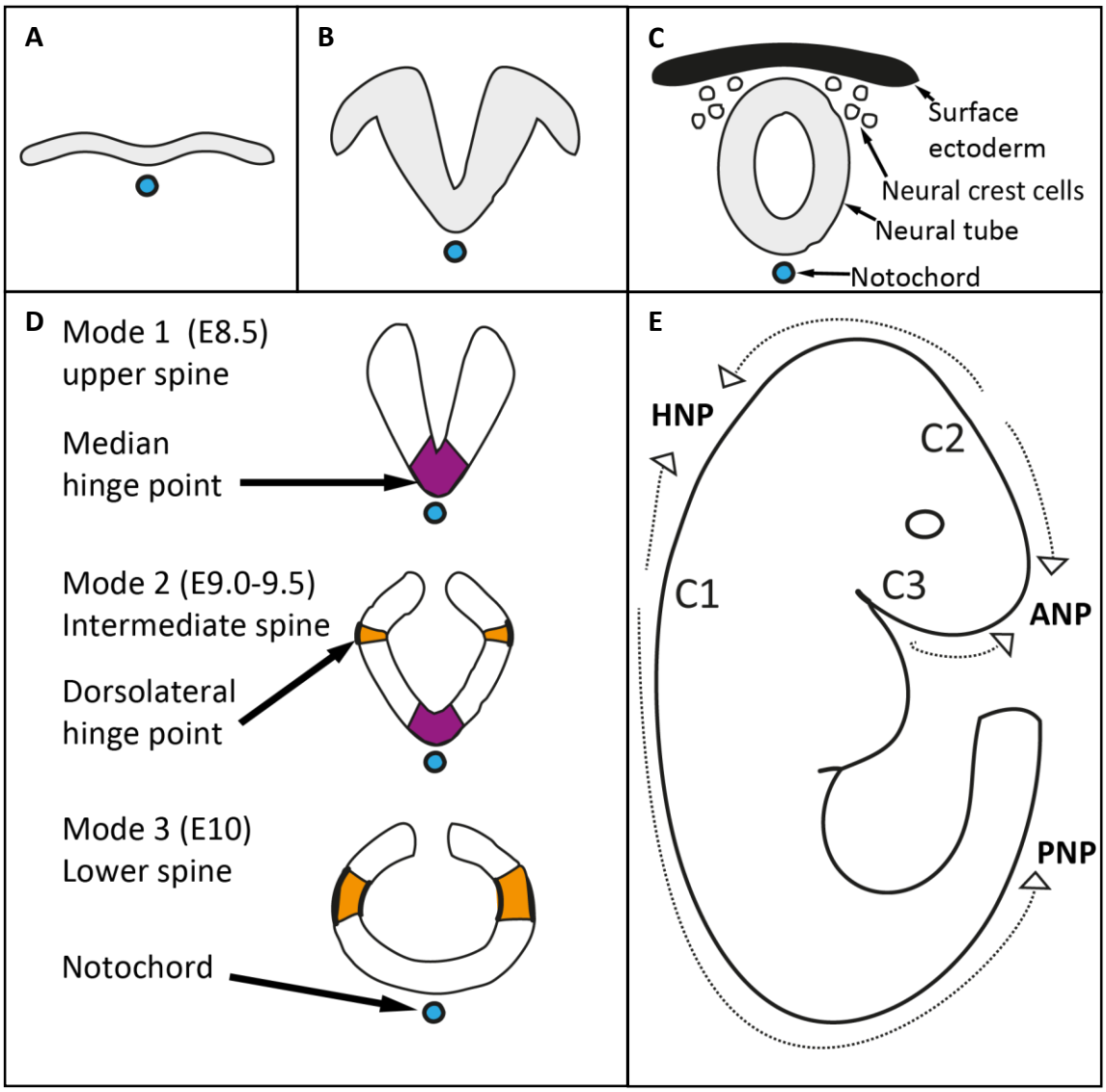
A
B
C
Surface ectoderm
Neural crest cells
Neural tube
Notochord
D
Mode 1 (E8.5)
upper spine
Median
hinge point
Mode 2 (E9.0-9.5)
Intermediate spine
Dorsolateral
hinge point
Mode 3 (E10)
Lower spine
Notochord
E
HNP
C2
C1
C3
ANP
PNP

Figure 1-01 Mammalian neurulation

(A-C) A summary of induction, bending and fusion required for NT closure. (A) The neural plate, a flat sheet of epithelial cells overlying the notochord (blue), an organising centre of the embryo. (B) Signalling from the notochord induces bending in the midline, elevating the neural folds and bringing them into proximity. (C) The neural folds fuse in the dorsal midline closing the tube and the adjacent ectoderm joins to cover the NT by forming a layer of surface ectoderm. The neural crest cells also migrate away from the site of closure. (D) Three modes of spinal closure along the rostrocaudal axis. Mode one in the upper spine, medial hinge point (MHP, purple) is the only bending region of the neural plate. Strong Shh signalling from the notochord induces the MHP while repressing formation of the dorsolateral hinge points (DLHP). Mode two closure occurs more caudally, where decreased Shh signalling from the notochord releases repression of DLHP formation (orange) but maintains the MHP. In mode three closure the MHP is lost due to decreased Shh signalling, and the DLHPs are induced. (E) Closure initiates at specific points along the rostrocaudal axis of the embryo. At E8.5 in mouse closure 1 (C1) occurs bidirectionally at the base of the hindbrain. Closure 2 (C2) initiates at the midbrain/hindbrain boundary and also progresses bidirectionally. Closure 3 (C3) starts at the rostral-most extent of the NT where fusion can only proceed caudally. The open NT between C3 and C2 is the anterior neuropore (ANP), between C2 and C1 is the hindbrain neuropore (HNP) and caudal to C2 is the posterior neuropore (PNP). Adapted from Copp et al (2003).

1-2-01 Molecular regulation of neurulation

Highly regulated molecular processes are involved in the complex morphological tissue remodelling required to shape and bend the neural plate for neural tube formation and closure. (Colas and Schoenwolf, 2001). Detailing the function of the many genes involved in this highly complex spatiotemporal regulation is required to clinically address the causes of neural tube defects. Central to the process is formation of the hinge points, required at variable modes along the nueroaxis to assist neural tube closure. The process is initiated by forming the MHP. The MHP is induced by signals from the underlying notochord as midline bending is absent as a result of suppressed notochordal development (Smith and Schoenwolf, 1989, Davidson et al., 1999, Ybot-Gonzalez et al., 2002). Whereas complete removal of the surface ectoderm prevents formation of the DLHPs. (Jacobson and Moury, 1995, Moury and Schoenwolf, 1995, Ybot-Gonzalez et al., 2002). Removal of any remaining adjacent regions of the paraxial mesoderm has no effect on either MHP or DLHP formation (Ybot-Gonzalez et al., 2002). These findings help establish the ventral notochord and dorsal surface ectoderm as regions providing the framework of molecular signals for MHP and DLHP formation. The regulation of DLHP formation in particular depends on the relationship between antagonistic signals from both these poles. Although DLHP is induced by the surface ectoderm, the notochord release of Shh suppresses DLHP formation (Ybot-Gonzalez et al., 2002). Morphogen Shh is secreted from the notochord to form a diminishing ventral to dorsal concentration gradient along each emerging neural fold (Jessell, 2000). DLHP is therefore only permitted to occur at the threshold point along each neural fold that is far enough away from the notochord source of Shh inhibition (Ybot-Gonzalez et al., 2002). Bone morphogenic proteins (Bmp) represent a key group of developmental signals emanating from the surface ectoderm. Regulation of DLHP formation pivots upon a negative feedback loop formed by Bmp2 inducing the expression of its own antagonist, Noggin. The molecular mechanism establishing the three modes of neural tube closure involve a cascade of negative regulation that centres on the relationships between Shh, Bmp2 and Noggin. In mode1 neurulation DLHP's are not formed due to unimpeded negative regulation by Bmp2 resulting from suppression of its antagonist Noggin by high Shh expression (Ybot-Gonzalez et al., 2007). Yet at more caudal ends of neural tube formation, notochord Shh expression is

reduced releasing Noggin suppression on Bmp2, but in a concentration dependant manner from the ends of neural fold. An opposing concentration gradient of Bmp2 emanates from the surface ectoderm, continuing to suppress DLHP formation. The molecular mechanism that regulates DLHP formation is based on the threshold level of antagonist Noggin that is sufficient enough to neutralise Bmp2 suppression on DLHP formation (Ybot-Gonzalez et al., 2007).

At a molecular level convergent extension depends on the planar cell polarity pathway (PCP), first discovered by disruption of PCP pathway effector *dishevelled* in frog resulting in shortened embryos and neural folds that could not fuse due to a broad neural plate (Wallingford and Harland, 2001, Wallingford and Harland, 2002). In mice, findings were repeated as lack of convergent extension resulted in neural tube defects from a range of independent gene disruptions either part of or related to the PCP pathway (Greene and Copp, 2009). The genes, well reviewed by Greene and Copp et al (2009) were *vangl2*, *dishevelled*, *Celsr1*, *Scrb1*, *Ptk7* as well as combined knock out of *frizzled-3* and *frizzled-6*.

1-03 Dorsoventral patterning of the neural tube

In vertebrates, the cells of the central nervous system originate from the neural tube. Dorsoventral (DV) patterning is the process by which differentiating neuroblasts are anatomically segregated and organised along a dorsal ventral axis (Jessell, 2000). DV patterning depends on the timing and extent of external signals, a model that centres on four main signalling pathways; BMP, retinoic acid (RA), fibroblast growth factor (FGF) and Shh (Jessell, 2000, Wilson and Maden, 2005). The neural tube therefore becomes an environment of opposing morphogen concentration gradients, providing a range of developmental cues that induce all neural cell types (Wilson and Maden, 2005).

A broad level of spatiotemporal regulation involves directing progenitor cells to either proliferate or differentiate. FGF signalling cues emanate from the mesoderm to promote proliferation, predominantly a requirement of neuroepithelial cells in the immature NT (Bertrand et al., 2000, Diez del Corral et al., 2002, Diez del Corral et al., 2003). RA signalling from the paraxial mesoderm inhibits FGF signalling promoting

instead an environment for neuroepithelium differentiation (Diez del Corral et al., 2003, Novitch et al., 2003).

The advancement of differentiation cues that give rise to DV patterning depend on the antagonistic relationship of BMP and Shh signalling within the NT. Specialisation of the cells in the dorsal region of the NT result from the high exposure to BMPs produced by the roof plate and the surface ectoderm. Yet exposure to a gradient of Shh is specifically the determining factor for ventral neural tube patterning (Marti et al., 1995, Chiang et al., 1996, Ericson et al., 1996, Briscoe et al., 2000, Wijgerde et al., 2002). Shh expression originates first from the notochord and the high concentration and long exposure time experienced by cells in the most ventral region of the neural plate, adjacent to the notochord, induces these cells to become the floorplate (Placzek et al., 1990, Echelard et al., 1993, Roelink et al., 1995). The cells of the floorplate then themselves start to express Shh. The Shh gene exhibits a highly localised region of expression, limited only to cells of the notochord and floorplate. The key molecular basis of ventral patterning is that the Shh protein diffuses dorsally, creating a ventral-to-dorsal gradient of Shh protein, within the neural tube; cells at different positions within the neural tube are then exposed to different concentrations of Shh protein and also receive Shh for differing lengths of time. Evidence in support of the model for NT DV patterning came first from experimental studies with neural plate explants, cultured for differing lengths of time and at different concentrations of Shh (Yamada et al., 1993, Marti et al., 1995, Roelink et al., 1995, Ericson et al., 1997, Briscoe et al., 2000). Those exposed to the highest concentration of the Shh signal, for the longest time, are induced to form the most ventral type of neuronal subtype, the V3 ventral neurons. Adjacent to these, cells receive a slightly lower and shorter exposure to Shh, and are induced to form motor neurons. At progressively more dorsal positions, the gradually decreasing Shh exposure induces the precursors to form the other ventral neuronal subtypes, the V2, V1 and V0 ventral interneurons. Striking evidence for the central role of Shh comes from the observation that ventral neural cell types are lost when Shh signal is omitted (Chiang et al., 1996). The relation between Shh gradient, transcription factor expression and the neuronal subtypes formed is summarised in figure 1-02 (Jessell, 2000).

In each neuronal precursor, Shh pathway transduction acts to regulate the balance of Gli protein transcription factors in activator and repressor form to reflect the graduated Shh signal. In response, the extent of Shh pathway activation determines the fate of cells by relative activation of specific progenitor proteins (Briscoe and Ericson, 2001, Guillemot, 2007). These are called the class II transcription factors, and include NK2 homeobox 2 (Nkx2.2), oligodendrocyte transcription factor 2 (Olig2), and others. Another set of transcription factors are repressed at high levels of Shh signalling, with differing thresholds of responsiveness. These Class I transcription factors include Pax6, Pax7 and Irx3. The Class II and Class I transcription factors then act to co-repress, in particular pairs of factors. For instance, Nkx2.2 and Pax6 co-repress, while Olig2 and Irx3 co-repress. The co-repression results in a clearly defined boundary of gene expression, between each pair of transcription factors. The position of the boundary differs between different pairs. The result is that at different positions along the dorso-ventral axis, the cells express different combinations of Class I and Class II transcription factors. The specific combination of transcription factors then determines the neuronal subtype that is induced at each position along the DV axis. For instance, V3 interneurons differentiate from neuronal precursors expressing Nkx2.2 and Nkx6.1, in a narrow band of cells adjacent to the floorplate.

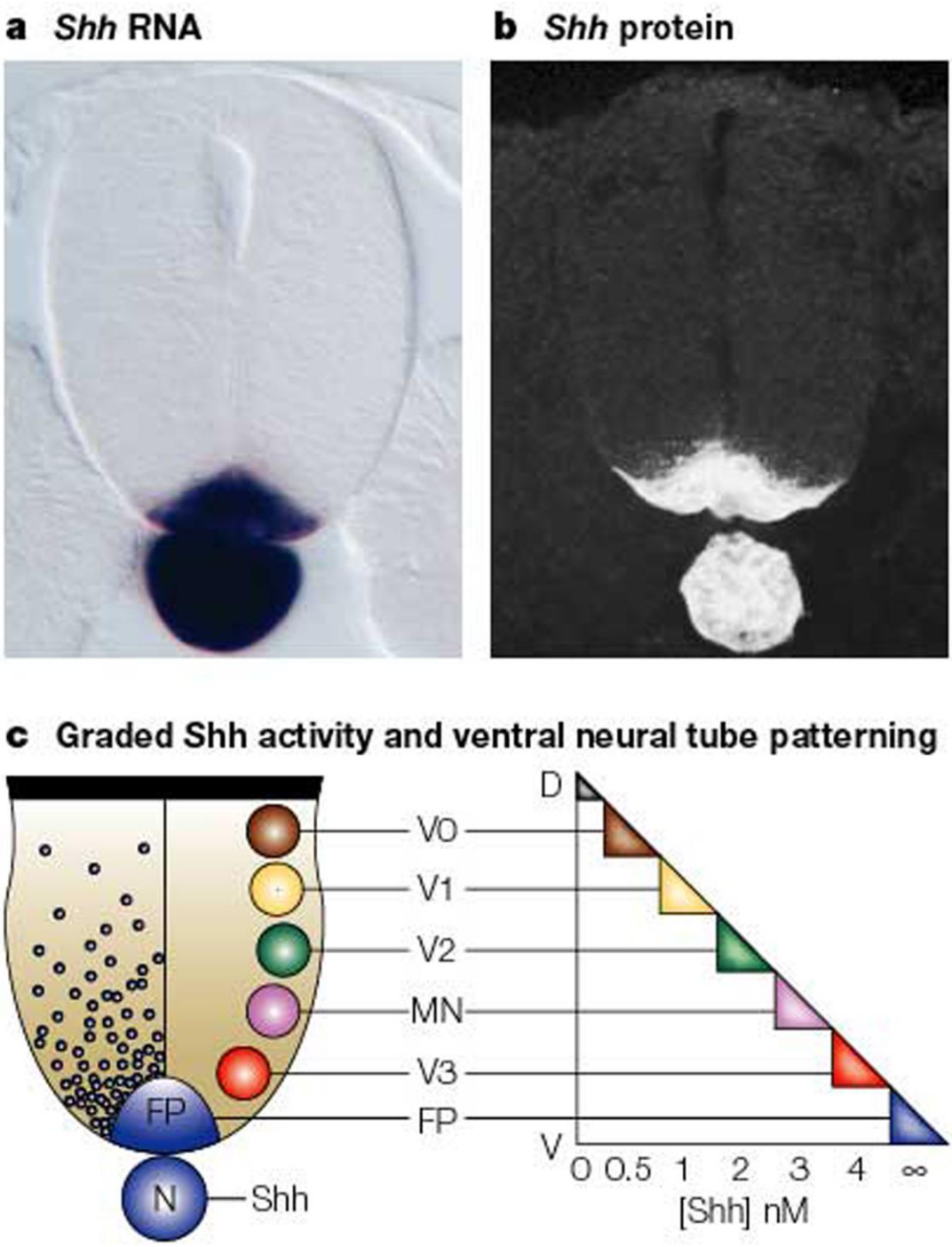

Taken from (Jessell, 2000)

Figure 1-02 Shh expression by notochord and floor plate controls ventral pattern

Cross-section through stage-18 chick spinal cord showing the expression in the notochord (N) and floor plate (FP) of (A) *Shh* RNA and (B) Shh protein. (C) Diagram of the neural tube showing the effect of high ventral to low dorsal Shh concentration gradient (blue dots) on the specification of ventral neuronal fates. Five classes of neurons are generated in response to graded Shh signalling; four different classes of ventral interneurons V0–V3, Motor neurons MN and floor plate FP. To the right is shown the profile of neuronal generation in intermediate neural plate explants grown in different concentrations of the recombinant amino-terminal fragment of Shh, termed Shh-N. The more dorsal the position of neuronal subtype generation *in vivo*, the lower the concentration of Shh required to induce the same neuronal subpopulation *in vitro*.

Taken from (Jessell, 2000)

1-04 The Shh Signalling pathway

The Shh pathway has been primarily identified for its crucial role in early development. Abnormal pathway signalling has been attributed to a wide range of birth defects, including holoprosencephaly, spina bifida, polydactyly, craniofacial and skeletal malformations (McMahon et al., 2003). Correct regulation of pathway activity is important across the entire life of an organism, noted by the oncogenic effects of increased pathway activity in adults (Pasca di Magliano and Hebrok, 2003).

1-4-01 In *Drosophila*

Essentially, the components of the Hedgehog (Hh) signalling pathway are well conserved across invertebrates and vertebrates (Huangfu and Anderson, 2006). Pathway effectors were first discovered through observing abnormal larva segmental development after gene disruption in *Drosophila*. It led to the early identification of morphogen hedgehog (Hh) and Patched (Ptc), discovered later to be the membrane receptor for Hh (Nusslein-Volhard and Wieschaus, 1980, Ingham et al., 1991). Hh effectors further identified downstream of Ptc were Smoothened (Smo), Fused (Fu), suppressor of Fused (Su(fu)), Costal2 (Cos2) and Cupitus Interuptus (Ci) (Nusslein-Volhard and Wieschaus, 1980, Preat, 1992, Forbes et al., 1993, Motzny and Holmgren, 1995, Alcedo et al., 1996, van den Heuvel and Ingham, 1996).

Ci is the single culminating transcription factor for the invertebrate Hh pathway and is bi-functionally responsible for either target gene activation or suppression (Methot and Basler, 1999). During pathway inactivity, when the Hh ligand is absent, Ci remains in the cytoplasm bound to Cos2 and Fu (Robbins et al., 1997). Formation of this complex initiates phosphorylation of Ci by protein kinase A (PKA), glycogen synthase kinase 3 (GSK3) and casein kinase 1 (CK1) (Chen et al., 1998, Chen et al., 1999, Price and Kalderon, 1999, Jia et al., 2002, Price and Kalderon, 2002, Jia et al., 2005). This sequential phosphorylation triggers targeting for proteolytic cleavage (Price and Kalderon, 1999, Jia et al., 2002, Price and Kalderon, 2002, Zhang et al., 2005). Ci is processed to a 75 kDa repressor form (Ci^R) and translocates to the nucleus for pathway suppression by inhibitive target gene promoter binding; Ci^R acts as a transcriptional repressor (Aza-Blanc et al., 1997, Jiang and Struhl, 1998). During pathway activation, Hh binds to membrane receptor Ptc releasing inhibition on transmembrane receptor

Smo (Hooper and Scott, 1989, Marigo et al., 1996, Stone et al., 1996, Alcedo et al., 1996, van den Heuvel and Ingham, 1996). Smo interacts with Cos2 to inhibit its association with Ci and this arrests processing of Ci to Ci^R. Full length Ci can now function as a transcriptional activator by translocation to the nucleus for target gene activation (Methot and Basler, 1999).

1-4-02 In mammals

Many elements of the Hh pathway first elucidated in *Drosophila* are essentially the same as the mammalian Shh signalling cascade. A key difference is that certain proteins in the invertebrate pathway are represented by a family of proteins in vertebrates. This includes vertebrate homologues of the Hh ligand, represented by a functionally divergent family of ligands, including Sonic hedgehog (Shh). Other members of the family in mammals are Desert hedgehog (Dhh) specialised for a role in male gonad development and Indian hedgehog (Ihh) for skeletal development (Bitgood et al., 1996, St-Jacques et al., 1999). Shh is the ligand that functionally relates to embryonic development, neural tube pattern formation and inducing proliferation in numerous tissues including the central nervous system (McMahon et al., 2003).

The homologue to Ci in mammals has also diverged to a family of proteins, named Glioma-associated oncogene homologs 1 to 3 (Gli1, Gli2 and Gli3) (Matise and Joyner, 1999, Sasaki et al., 1999). Although each Gli protein is specialised, they are functionally coordinated to a point that can be summarised in two states; Gli activator and Gli suppressor proteins, akin to the bi-functional activation states of Ci in *Drosophila* (Huangfu and Anderson, 2006). Simplistically, it is fair to functionally assign Gli3 as repressor and Gli2 as activator although full length Gli3 can act a weak activator and Gli2 also has as a weak repressor form (Bai et al., 2004, Pan et al., 2006). The conversion of full length 190 kDa Gli3 to repressor form involves proteolytic cleavage to form an 83 kDa Gli3 repressor that can directly block transcription promoter sites (Huangfu and Anderson, 2005). As mentioned, full length 185 kDa Gli2 is subject to the same processing mechanism to produce 78 kDa Gli2 but in comparison to Gli3, proteolysis is 6 times less efficient (Pan et al., 2006). Gli1 is a potent activator that only exists as a full length protein. However Gli1 activation is a product of Shh pathway

activation as *Gli1* is a Gli2 target gene and as such is not involved in onset of pathway activation (Bai et al., 2004).

As with Ci repressor processing in *Drosophila*, both Gli2 and Gli3 homologues are found to be subject to same sequential phosphorylation of PKA, GSK and CK1 (Wang et al., 2000, Pan et al., 2006, Pan et al., 2009). A significant difference however is that the vertebrate pathway requires the cellular mechanisms of primary cilium signalling, an organelle absent from invertebrate cells (Oh and Katsanis, 2012, Pal and Mukhopadhyay, 2014). Instead, ciliary regulation of Gli2 and Gli3 during pathway inactivation involves Shh membrane receptor Patched1 (Ptch1) localisation to the primary cilia and in conjunction with β-arrestin, prevents membrane receptor Smoothened (Smo) from entering the cilium (Rohatgi et al., 2007, Kovacs et al., 2008). As Shh binds and internalises Ptch1, it releases its inhibition allowing Smo translocation to the primary cilium (Rohatgi et al., 2007, Kovacs et al., 2008, Rohatgi et al., 2009). Accumulation of Smo on the ciliary membrane arrests Gli3 processing to repressor form as the pathway mechanism changes towards promoting Gli activator proteins, a process that is less well understood (Haycraft et al., 2005, Tran et al., 2008). Recent discovery of negative regulator Gpr161 has helped further understand the mechanism of ciliary cAMP activation of PKA phosphorylation and its pivotal role in regulating Gli repressor processing (Mukhopadhyay et al., 2013). During pathway activation, the reduction of cAMP levels in the primary cilia resulting from loss of Gpr161 is proposed to reduce PKA activity required to process Gli repression (Mukhopadhyay et al., 2013). Reduction of Gli3 repressor removes target gene inhibition of Gli2 increasing the incidence of successful Gli2 translocation to the nucleus for target gene activation.

Suppressor of Fused (Sufu) is a key regulator of Gli transcription factor activation states. During pathway inactivation Sufu can bind and sequester all Gli proteins in the cytoplasm, including Gli1, restricting Gli translocation to the nucleus (Ding et al., 1999, Dunaeva et al., 2003, Jia et al., 2009). Sufu-Gli complexes also promote active repression by recruiting GSK3β to help promote proteolytic cleavage of full length Gli3 to $Gli3^{R}$ (Kise et al., 2009). Dissociation of Sufu-Gli complexes during pathway activation requires primary cilia for Smo-mediated inactivation of Sufu (Corbit et al.,

2005, Huangfu and Anderson, 2005). The mechanism involves reduced primary cilia induction of PKA activity that in turn reduces stability of Sufu-Gli binding complexes (Humke et al., 2010, Tukachinsky et al., 2010, Chen et al., 2011a).

Also evident but less understood is the molecular mechanism of positive regulation in Shh signalling pathway. Serine/threoine kinase phosphorylation by Unc-51-like kinase 3 (ULK3) as is reported to increase nuclear localisation of Gli1 and Gli2, resulting in pathway activation (Maloverjan et al., 2010b). ULK3 is also regulated by Sufu in a Sufu-Ulk3 complex that blocks it from phosphorylating Gli2 for pathway activation (Maloverjan et al., 2010a).

Increasingly, certain mechanisms involved in the formation or function of primary cilia are also identified as Shh pathway effectors and regulators (Oh and Katsanis, 2012). Hence the focus of the next section has taken a ciliary centric view of the structure and function of primary cilia in the context of cell signalling. In particular, the requirement for bidirectional protein transportation to and from the primary cilia has identified intraflagellar transport (IFT) proteins as a class of pathway effectors in Shh pathway signalling. Main pathway related effectors can be divided into two functional groups; the IFT complex B proteins IFT57, IFT172, IFT88, IFT52 and the kinesin, Kif7, are involved in anterograde transport towards the ciliary tip and the IFT complex A proteins Dync2h1 (a dynein), IFT122 and Thm1 enable retrograde transport of proteins back to the ciliary pore (Huangfu et al., 2003, Haycraft et al., 2005, Huangfu and Anderson, 2005, Liu et al., 2005, Cortellino et al., 2009, Tran et al., 2008, Cheung et al., 2009, Liem et al., 2009, Qin et al., 2011, Mukhopadhyay et al., 2010). Interestingly, the discovery that Kif7 is the mammalian homologue of Cos2 suggests that these effectors are still integrated within the conserved elements of the pathway and not necessarily an appendage to it (Cheung et al., 2009, Liem et al., 2009).

In summary of the vertebrate Shh signalling pathway as detailed here, figure 1-03 illustrates the complex interactions of key pathway effectors before and after pathway activation.

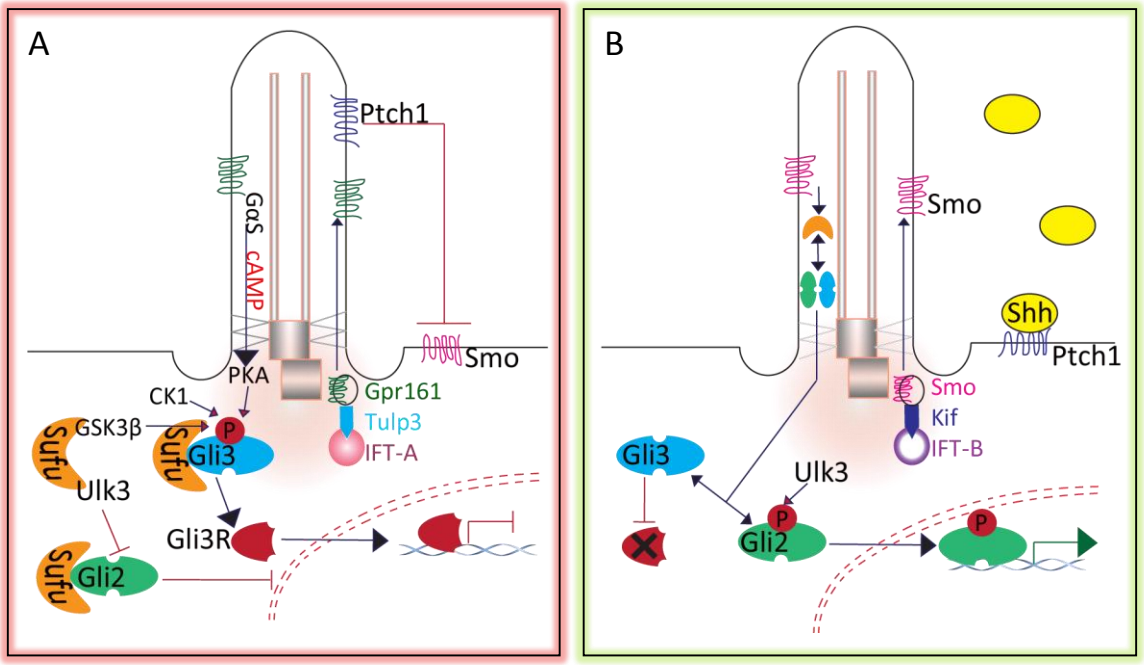

Figure 1-03 Sonic hedgehog signalling

(A-B) A simplified representation of the Shh signalling pathway. (A) In the absence of Shh ligand Ptch1 inhibits Smo, preventing its ciliary accumulation. Sufu binds and sequesters Gli2 preventing translocation to the nucleus. Sufu also binds positive regulator Ulk3 to prevent Gli2 phosphorylation. Gpr161 is transported to the cilium in complex with Tulp3 and IFTA proteins. Cilium levels of cAMP are increased by Gs alpha protein coupled receptor activation of the cAMP-dependant pathway. PKA phosphorylates Gli3 which primes Gli3 for further phosphorylation by CK1 as well as from GSK3β recruited from Sufu. Gli3 is then targeted for proteolytic cleavage to the repressor form which translocates to the nucleus to repress gene expression.

(B) In the presence of Shh, Pthc1 inhibition of Smo is relieved. Smo is internalised and translocated to the cilium in a Kif dependent manner. Gli2 and Gli3 localise to the cilium and dissociate from Sufu and Gli3 processing to Gli3 repressor is arrested. Instead suppression of Gli2 is relieved and activation is enhanced by Ulk3 phosphorylation. Gli2 processing to Gli activator induces expression of target genes.

1-05 Primary cilium

Primary cilia are microtubule-based sensory organelles that project singly from the cell surface of most vertebrate cells. All cilia originate from a modified form of the centriole, called the basal body, that is a barrel-shaped structure composed of nine triplet microtubule blades (Ringo, 1967). The centriole becomes the basal body when a complex structure of proteins form around the mother centriole as it migrates and integrates itself into the cell cortex (Marshall, 2008). Their inner barrel arrangement of nine microtubule doublets provides a structural template for tubulin polymerisation (Marshall, 2008). During early formation, a primary cilia vesicle attaches to projections on mother centriole and expands as tubulin polymerisation projects within forming a microtubule "shaft" (Molla-Herman et al., 2010). The surrounding "sheath" formed by the vesicle is the precursor to the ciliary membrane as it fuses with the plasma membrane prior to extracellular projection (Molla-Herman et al., 2010).

A feature of primary cilia is that they do not have a central microtubule doublet, a structure referred to as 9 + 0 cilia (Satir and Christensen, 2007). The 9 + 2 structure, in connection with axonemal dyneins, evolved as a functional requirement for motile cilia (Satir and Christensen, 2007). Figure 1-04 A and B provide a schematic cross sectional comparison of 9 + 2 motile cilia and 9 + 0 primary cilia. The role of microtubules in primary cilia is to provide structural support and tracks for intraflagellar transport (IFT) enabling bidirectional transport of large protein complexes (IFT particles) along outer doublets of the central microtubule structure (Rosenbaum and Witman, 2002). IFT-B complex cargo transport to the ciliary tip, referred to as anterograde transport, is achieved by kinesin-2 motor proteins whereas retrograde IFT-A complex cargo transport away from the ciliary tip requires cytoplasmic dynein 2 proteins (Kozminski et al., 1993, Kozminski et al., 1995, Pazour et al., 1999, Porter et al., 1999). The transport process also requires carriage of the dynein or kinesin motor proteins when inactive (figure 1-04 C).

Primary cilia are compartmentalised organelles that strictly regulate their environment and protein composition (Garcia-Gonzalo and Reiter, 2012). Devoid of ribosomes, Cilia depend on the cell body for synthesis and delivery of all proteins (Johnson and Rosenbaum, 1992). Proteins destined for the primary cilia arrive in golgi derived

vesicles that fuse with membrane at the base of the cilium to exocytose proteins into the transition zone. The transition zone is a diffusion barrier made up of tightly associated proteins and an opening at the base called the ciliary pore (Pazour and Bloodgood, 2008, Garcia-Gonzalo and Reiter, 2012). Entry to the cilium is therefore regulated within the transition zone and its ciliary pore complex of proteins. Unless actively transported, the ciliary pore restricts access, comparable to the nuclear pore where proteins larger than 30 kD are reported to be restricted access (Cook et al., 2007, Garcia-Gonzalo and Reiter, 2012). The influence of the transition zone extends across to the contiguous cell membrane where it can also regulate membrane proteins able to transverse across to the ciliary membrane. Hence passage of ciliary proteins across the transition zone depends on their specific association of with the IFT machinery (Qin et al., 2004). Only protein complexes containing specific ciliary protein motifs can continue through to the ciliary compartment via anterograde transport (Pazour and Bloodgood, 2008, Garcia-Gonzalo and Reiter, 2012). Retrograde transport back from the ciliary tip involves remodelling IFT protein complex and activating cytoplasmic dynein 2 proteins (Qin et al., 2004). IFT is a central process during ciliogenesis as it delivers axonomal precursors for assembly (Pedersen and Rosenbaum, 2008). It is a mechanism that continues even after cilia are formed to maintain constant turnover of the axoneme at the ciliary tip (Pedersen and Rosenbaum, 2008).

Evidence of protein trafficking for purposes other than axoneme formation is rapidly accumulating, particularly in relation to cell signalling (Pazour and Bloodgood, 2008, Oh and Katsanis, 2012). Regulating the interchange of select proteins within the cilia is key to understanding the mechanism of primary cilia signalling (Garcia-Gonzalo and Reiter, 2012). This is exemplified in the previous section by the regulated passage of receptors Ptch1, Smo and Gpr161 in Shh signal transduction (section 1-04).

The mature axoneme is a complex of many distinct tubulin isoforms, rather than a homogenous polymerisation of soluble tubulin (Redeker et al., 2005). Interestingly, most of the post translational modifications (PTM) seen in tubulin are not found in organisms that lack cilia and therefore thought to be cilia specific (Alfa and Hyams, 1991, Janke et al., 2005). The abundant arrays of highly conserved PTMs are broadly

categorised as acetylation (addition of an acetyl group), detyronisation (removal of C-terminal tyrosine to expose a glutamate), glutamylation and glycation (covalent bonding to a sugar molecule) (Westermann and Weber, 2003, Verhey and Gaertig, 2007, Marshall, 2008, Gaertig and Wloga, 2008, Wloga and Gaertig, 2010). Although the functions of tubulin PTMs are mostly related to structure and assembly, α-tubulin acetylation has been shown to directly regulate the transport of kinesin-1 cargo (Reed et al., 2006, Dompierre et al., 2007). Hence axoneme PTMs can regulate ciliary transport, a feature that may be integral to the mechanism of signal transduction and regulation.

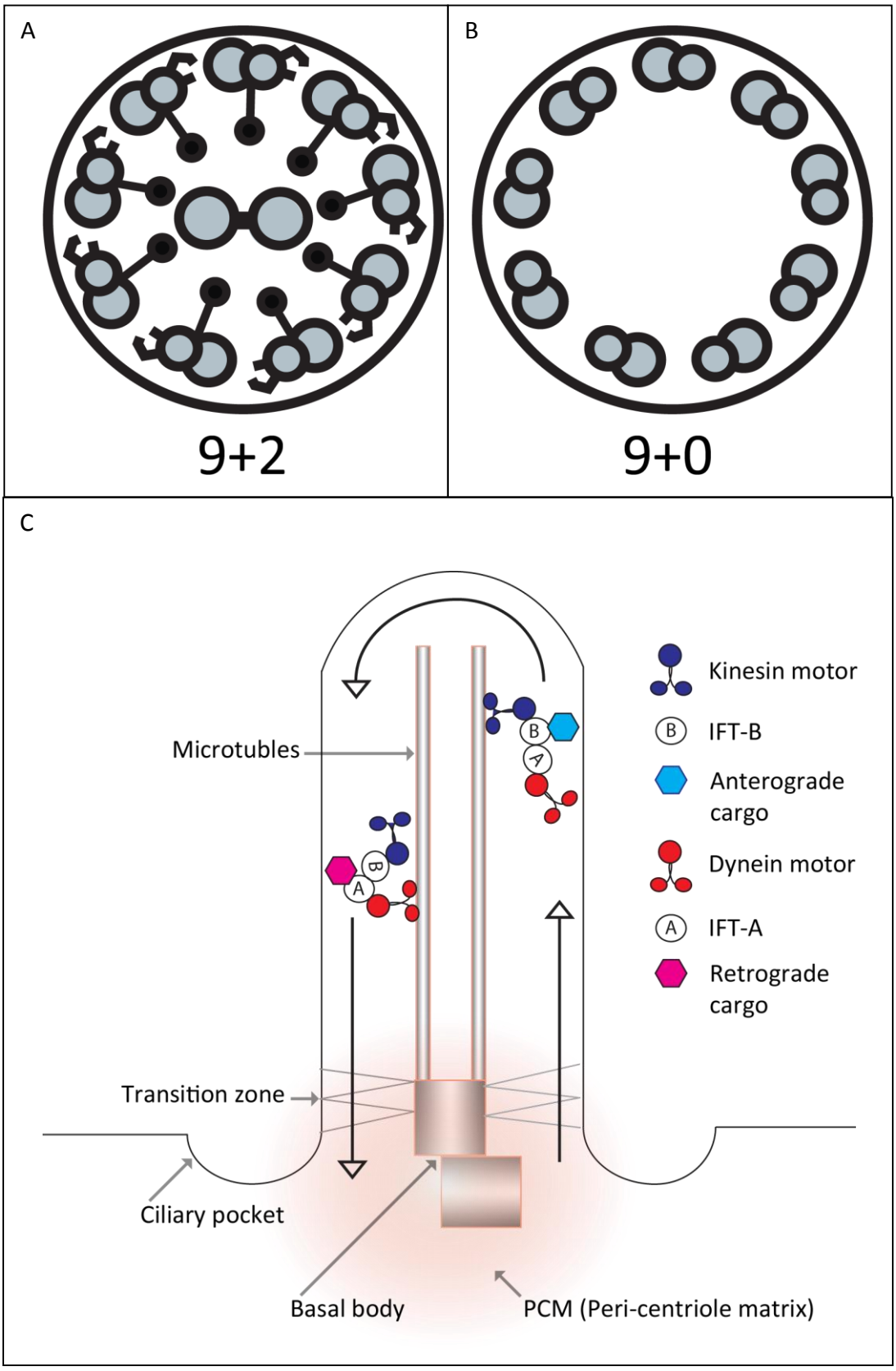
A
9+2
B
9+0
C
Microtubles
Transition zone
Ciliary pocket
Basal body
PCM (Peri-centriole matrix)
Kinesin motor
IFT-B
Anterograde cargo
Dynein motor
IFT-A
Retrograde cargo

Figure 1-04 Cilia structure and intraflagellar transport

(A and B) Cross section diagrams of the forms of cilia in vertebrate cells. (A) The motile cilium is formed of nine outer microtubule doublets arranged around a central pair in a 9+2 configuration. Dynein arms project from the microtubules, and radial spokes extend towards the central pair to facilitate motion. (B) Primary cilia have a 9+0 configuration, with similar arrangement of the outer microtubule doublets but loss of the central pair. (C) Movement along the cilium is achieved by Intraflagellar transport (IFT). Anterograde transport of cargo is mediated by kinesin complexes linked to IFT-B complex particles. Retrograde transport is mediated by dynein motors and the IFT-A complex proteins binding to the cargo. Components of the IFT machinery and IFT cargo accumulate near the basal body in preparation for loading but are prevented from diffusing into the cilium by the transition zone diffusion barrier at the base of the cilium.

1-5-01 Primary cilia in Shh signalling

The increased focus on primary cilia in the last 12 years is largely due to the identification of disorders resulting from dysfunctional cilia, termed ciliopathies (Goetz and Anderson, 2010). Primary cilia are now established in connection with a range of signal transduction pathways including canonical and non-canonical Wnt, fibroblast growth factor (FGF) and platelet-derived growth factor (PDGF) pathways (Gorbatyuk et al., 2007, Gerdes et al., 2009, Berbari et al., 2009, Oh and Katsanis, 2012). New pathways are expected to yet be identified given the increasing emphasis on primary cilia research in recent years (Oh and Katsanis, 2012). The organelle is therefore becoming understood to be a signalling nexus for enabling pathway to pathway interconnections or crosstalk and regulation. (Oh and Katsanis, 2012).

The Shh signal pathway was first to be identified in connection with primary cilia. Loss of cilia was observed along with NT closure and patterning defects in mutants for genes *polaris* and *wim* (the homologues of *Chlamydomonas* IFT88, IFT172) as well as kinesin transport protein *kif3a* (Huangfu et al., 2003). Hence loss of cilia, due to disruption of the IFT machinery, resulted in phenotypes consistent with lack of Shh pathway activation. Reduced Shh pathway activity was identified in the NT by absence of Shh-dependant ventral cell types, as compared with Shh mutants and with Gli2 and Gli3 double mutants, in particular (Huangfu et al., 2003). Disruption of cilia or IFT machinery also resulted in reduced Shh pathway activation in mutants for *Dync2h1*, *IFT52*, *IFT57*, *Ofd1* and *Ftm/Rgrip1* (May et al., 2005, Liu et al., 2005, Houde et al., 2006, Ferrante et al., 2006). Important also were examples of cilia disruption causing pathway activation as seen in *Arl13b* and *Thm1* mutants (Caspary et al., 2007, Tran et al., 2008). Together the evidence recognizes primary cilia regulation of Shh signal pathway as involved with both suppression and activation, ultimately based on its influence on the nuclear ratio of Gli transcription suppressor versus activator.

1-06 Tulp3 - negative regulator of the Shh signalling pathway

ENU mutagenesis derived "*hitchhiker*" is a mouse mutant with neural tube defects, as identified in our laboratory by observing embryonic phenotypes of anencephaly and spina bifida (Patterson et al., 2009). Where closure had occurred, histological sections revealed abnormal morphology of the neural tube, with expansion of the lumen

(Patterson et al., 2009). Abnormalities not related to the neural tube include preaxial polydactyly and forked rib formation (Patterson et al., 2009). Immuno-detection of cell differentiation markers Foxa2, Nkx2.2, Nkx6.1 and Oligo2 were revealed to have expanded dorsally from their normal domain of expression in the neural tube (Patterson et al., 2009). This revealed a disruption of dorso-ventral patterning in the spinal cord, with an expansion of the ventral marker domains, indicating ventralization of the neural tube.

The gene disruption responsible for the *hitchhiker* mutant was identified as a single point mutation in *Tubby-like-protein 3 (Tulp3)*, the result of T→A transversion at the splice acceptor site of intron 3 causing skipping of exon 2 (Patterson et al., 2009). This single base change results in deletion of 52 bp of the coding sequence, which leads to a frameshift and premature truncation of the protein. Almost complete absence of the Tulp3 protein was confirmed by Western blotting. Nevertheless, it seems that this altered splice site can function as an acceptor site with low efficiency. The Western blot analysis revealed some expression of the Tulp3 protein, at around 4% of the wild-type expression level (Patterson et al., 2009).

Previously identified Tulp3 mouse mutant *Tulp3^{tm1Jng}* generates a truncated form of Tulp3 that lacks the C-terminal Tubby domain. Homozygous *Tulp3^{tm1Jng}* mutant mice have similar phenotype to *hitchhiker* and exhibit exencephaly and spina bifida, with abnormalities in neural tube development apparent from E9.5 (Ikeda et al., 2001). The phenotype of the *Tulp3^{tm1Jng}* is a little more severe than *hitchhiker*, consistent with the complete absence of Tulp3 protein function in the knockout, but retention of a small amount of protein expression in *hitchhiker* (Patterson et al., 2009). Intercrosses between *Tulp3* knockout mice and *hitchhiker* mice produce embryos with the same phenotypes of exencephaly and spina bifida, consist with these mutations being allelic (Patterson et al., 2009).

The multiple phenotypes observed in mice with *Tulp3* disruption, including preaxial polydactyly, expansion of ventral markers and neural tube defects, were consistent with defects found in mice with *Rab23, FKBP8* or *Tectonic* disruption (Eggenschwiler et al., 2001, Bulgakov et al., 2004, Reiter and Skarnes, 2006). Hence, in comparison to these initial seminal studies, *Tulp3* was identified as amongst the group of negative

regulators in Shh pathway signalling (Cameron et al., 2009, Norman et al., 2009, Patterson et al., 2009).

Further epistasis was used to establish and place *Tulp3* within the Shh signalling pathway. Starting with Shh, compared to *hhkr*$^{-/-}$ mutants some distinct phenotypes of *Shh*^{tm1Amc} mutants are that they are reduced in size, exhibit cyclopia, holoprosencephaly and an expansion of dorsal markers in the NT (Chiang et al., 1996). Doubly homozygous *Shh*^{tm1Amc} */hhkr*$^{-/-}$ mutant embryos exhibit phenotypes that more resemble that of the *hhkr* and as such provide evidence that Shh is dependent on downstream effector Tulp3 (Patterson et al., 2009). Similarly, *hhkr*$^{-/-}$ phenotypes were expressed in doubly homozygous mutants *hhkr*$^{-/-}$ */smo smo*^{tm1Amc} mutants as opposed to the distinct *Smo*^{tm1Amc} mouse genotypes, including cyclopia and holoprosencephaly (Zhang et al., 2001, Patterson et al., 2009). Similar comparisons with *Tulp3*^{tm1jng} mutants again placed Shh and Smo upstream of Tulp3 (Norman et al., 2009). In addition IFT transport protein Kif3a and transcription factor Gli2 were identified as downstream of Tulp3 by demonstrating Gli2^{tm1Alj}*/Tulp3*^{tm1jng} and *Kif3a*^{tm1Gsn}*/ Tulp3*^{tm1jng} double mutants had phenotypes resembling single mutants of Gli2^{tm1Alj} and *Kif3a*^{tm1Gsn} respectively (Mo et al., 1997, Marszalek et al., 1999, Norman et al., 2009).

1-07 Interacting protein partners of Tulp3

In vertebrates, the tubby family of proteins comprises of 5 members; the founding TUB protein and 4 tubby-like proteins 1-4 (TULP 1-4) (Mukhopadhyay and Jackson, 2011). All share a signature carboxy-terminal tubby domain predicted to membrane interact with phosphatidylinositol 4,5-biphospahte (PIP_2) (Santagata et al., 2001, Boggon et al., 1999). The wide diversity of these proteins is mostly characterised by features in their amino-termini (Mukhopadhyay and Jackson, 2011).

In order to understand the role of proteins, it is useful to identify interacting protein partners. At the time of beginning the work for this thesis, no Tulp3 protein partners had been identified. More recently, Tulp3 interacting protein partners have been identified by another group. This was specifically a conserved helical domain in the amino-terminal of TULP3 that interacts with the core IFT-A proteins IFT122, IFT140 and WDR19 forming a TULP3/IFT-A complex (Mukhopadhyay et al., 2010). Formation of the TULP3/IFT-A enables ciliary localisation of a specific subset of G-coupled receptor

(GPCR) proteins and is a role independent to canonical IFT-A retrograde primary cilia protein transportation (Mukhopadhyay et al., 2010, Qin et al., 2011). More recently, G-coupled receptor Gpr161 was identified as a negative regulator of the Shh signal pathway through TULP3/IFTA mediated localisation to the primary cilia (Mukhopadhyay et al., 2013). Therefore Tulp3 mediates ciliary dependant regulation of the Shh signalling pathway IFT-A transport proteins.

In order to identify potential binding partners, before the IFT-A interactions were known, previous study in our laboratory was undertaken using a yeast-2-hybrid approach. The yeast 2-hybrid screens were performed by a company, Hybrigenics. The screens involved using full length Tulp3 as a bait protein to screen a library generated from an E10.5/12.5 mouse brain cDNA library. The procedure was outsourced to Hybrigenics, as they are specialists in protein interaction studies. Upon receiving our full length Tulp3 cDNA clone, Hybrigenics sub cloned the cDNA to create two N-terminal tagged Tulp3 bait proteins. One bait protein contained the Gal4 transcription factor DNA binding domain, while the second bait protein was tagged with the LexA DNA binding domain The two bait proteins were then screened for potential interacting proteins from a cDNA library generated from E10.5 and E12.5 embryonic mouse brain. These library clones were tagged with the corresponding activation domain of either Gal4 or LexA, converting them to prey protein clones. The protein to protein interaction of Tulp3 “bait” with binding partner “prey” would pair the Gal4 or LexA DNA binding and activation domains together, creating a functional transcriptional activator that would then permit colony survival.

All constructs were co-transfected into yeast cells, resulting in identification of 49 clones, sequenced to identify 16 proteins that potentially interact with Tulp3. After eliminating three common false positives, 11 sequenced proteins remained and of these only 5 produced 2 or more colonies from the screen. These were “Family with sequence similarity 193 member A” (Fam193a), Tripartite motif protein 71 (Trim71), Nucleoporin 155 (Nup155) Cyclin B1 (Ccnb1) and Rho-guanine nucleotide exchange factor (Rgnef). In particular, Trim71, Nup155 and Fam193a were identified from both the screens, indicating that the interaction is tag-independent. In our laboratories, further supportive evidence for Trim71 and Rgnef interaction with Tulp3 was obtained

from reciprocal co-immunoprecipitation experiments using tagged constructs in HEK293T cells (Anju Paudyal, Vikki Patterson, unpublished data).

It is notable that no IFT-A complex proteins were identified in this screen, which is perhaps surprising, given the recently published data from Mukhopadhyay et al. However, the IFTA interactions were found to occur with the N-terminal region of Tulp3. The bait proteins were created so that the tag was fused at the N-terminal end of Tulp3, in order to optimise the chance of obtaining proteins that interact with the conserved Tubby domain. The orientation of the tagged construct would likely make the N-terminal less accessible to interacting proteins. Indeed, proteins that interacted with the N-terminal region might then have prevented the DNA binding domain from binding to DNA, thus preventing positive identification in this assay. This may explain the reason for not detecting IFT complex proteins in the yeast 2-hybrid screen. Moreover, proteins can often function in multi-protein complexes. Thus, publication of the Tulp3-IFT-A interaction does not render our results meaningless but, rather, adds a greater importance to investigating their relevance. The aim is to therefore try and identify the function of Trim71 and Rgnef binding partners in relation to Shh signalling pathway and in conjunction with negative regulator Tulp3.

1-7-01 Potential Tulp3 binding partner, Rgnef

Previously named p190RhoGEF, Rgnef is a 190 kDa guanine nucleotide exchange factor (GEF) protein, containing PH –DH domains for membrane localisation (Gebbink et al., 1997). In their capacity to activate GTPases, the GEF proteins act as switches or activators in signal transduction by metabolising the energy transference of GDP to GTP (Machesky and Hall, 1996). Rgnef binds the depleted GDP bound form of RhoA to then facilitate its transfer to an activated GTP form (van Horck et al., 2001). Another key feature of Rgnef is that it can bind Focal Adhesion Kinase (FAK) , one of the integrin dependent factors involved in the maturation process of extracellular matrix (ECM) adhesion sites (Zhai et al., 2003). Focal adhesions (FA) comprise of a large complex of proteins that can provide mechanical anchorage to the ECM as well as a nexus for adhesion-mediated signalling (Zamir and Geiger, 2001). Cell motility requires FA structures to be dynamically regulated to the point that either under- or over-formation of these sites can restrict cell motility (Arthur and Burridge, 2001, Tomar et

al., 2009, Miller et al., 2012, Miller et al., 2013). Rgnef is responsible for providing a layer of FA regulation in its capacity to bind FAK and activate RhoA whilst holding the FAK complex in proximity of the cell membrane by its DH-PH domain attachment (Miller et al., 2013).

Interestingly, Rgnef has been shown to also bind scaffolding protein JIP-1, to then promote JNK activation (Meyer et al., 1999).It is a role completely unrelated to its capacity as GEF protein and provides an example of the functional diversity of Rgnef in connection with other binding partners for involvement in another signal transduction mechanism.

Another quite diverse role to consider is that Rgnef is involved in regulating light neurofilament neural expression by its ability to destabilise light neurofilament mRNA transcripts (Canete-Soler et al., 2001). Neurofilaments comprise of ordered bundles of three different types of filaments, each categorised by their molecular weight, hence light (NFL), medium (NFM) and heavy (NFH) (Yuan et al., 2012). Abundant in neural cell axons, they form an intricate network of fibres that are essential for radial growth during development and future maintenance of axon calibre (Zhu et al., 1997, Elder et al., 1998, Yum et al., 2009). Current focus on neurofilament modulation is mainly driven by the observed cellular phenotype of abundant unregulated neurofilaments in a range of neurological diseases. In In mice and other model organisms, NF knockout studies has largely shown normal development and a lack of any overt developmental phenotypes (Yuan et al., 2012). This Rgnef function is at least another example of its functional diversity. Although worth bearing in mind is that microtubule axoneme structure and function in neural cells is a potential model for understanding primary cilia. Like the axon, the primary cilium is compartmentalised and comprises of a central microtubule element. Protein regulation in the axon is also highly regulated either by selective protein targeting and removal of selective retention and exclusion (Garcia-Gonzalo and Reiter, 2012). By comparison, it offers further insight to Rgnef function and raises the question of whether Rgnef has a role in primary cilia.

In relation to Shh signalling pathway, RhoA has been shown to trigger Smo-induced Gαi-coupled protein receptor signalling cascade (Kasai et al., 2004). Coupled with the evidence in our laboratory of Tulp3 interaction provides the first links to Shh effectors.

Furthermore in our laboratory, preliminary expression studies in mutant mice embryos have also implicated Rgnef, in that *Shh* mutants lack Rgnef expression and yet in *Ptch* mutants Rgnef expression was found to be increased. The aim of finding further connection is now also coupled with identifying the possible role of Rgnef in Shh signal transduction.

In Rgnef knockout mice, numbers of Rgnef $^{-/-}$ mice born were lower and smaller in size compared to Rgnef$^{+/-}$ (Miller et al., 2012). At Embryonic stage E13.5 development was reported to be normal and neural tube closure defects were not observed. Embryos earlier than E13.5 were not examined in this study or the reason for the lower number of mice born. The evidence is therefore against the involvement of Rgnef in NT closure, although embryonic development defects may have been overlooked particularly in relation to DV patterning.

1-7-02 Potential Tulp3 binding partner, Tripartite motif protein 71

Tripartite motif 71 (Trim71), also known as mlin41, is the mouse homologue of lin-41, first discovered in *Caenorhabditis elegans*. The loss of Lin-41 in *C.elegans* results in premature cell cycle exit and differentiation resulting in adult phenotypes during larval stages of development. *Lin-41* is a heterochronic gene that is regulated by *Let-7*, a 21 nucleotide sequence of miRNA that destabilises Lin41 by binding to sites along the 3' UTR of the *Lin-41* transcript (Reinhart et al., 2000, Slack et al., 2000, Vella et al., 2004). The Let-7 miRNA pathway regulation of *Lin-41* is a mechanism found conserved in more complex organisms such as zebra fish, chicken, mouse and human and although precise function is unknown, it is reasonably hypothesised to regulate cell proliferation or differentiation timing cues (Pasquinelli et al., 2000, Kloosterman et al., 2004, Lancman et al., 2005, Schulman et al., 2005, Kanamoto et al., 2006). Preliminary evidence of a Shh signalling pathway connection was identified by inducing c*Lin-41* (Trim71 chick homologue) with Shh-coated bead implant in chick embryo and an observed inverse relationship with Gli3 expression during chick limb development (Lancman et al., 2005). In mice, Trim71 mutants exhibit exencephaly, an anterior neural tube closure defect although the precise mechanism is not known (Maller Schulman et al., 2008). *Trim71* is of particular interest, as it is a heterochronic gene and temporal regulation is a relatively undefined mechanism in NT closure and patterning.

The Trim71 protein is characterised as an E3 ubiquitin ligase as part a large TRIM/RBCC domain family, identified by its tripartite motif, a RING type zinc finger domain consisting of two B Box zinc fingers and coiled-coil domain (Slack et al., 2000, Meroni and Diez-Roux, 2005). Trim71 negatively regulates miRNA processing protein Argonaute 2 (Ago2) *in vitro*, by ubiquitination of Ago2, targeting for proteosome mediated degradation (Rybak et al., 2009). Ago2 is the only Argonaute protein (Ago1-4) required for embryonic development as discovered by NTD in Ago2-deficient mice, particularly in the cranial region, as observed in Trim71-deficient mice (Liu et al., 2004, Maller Schulman et al., 2008). However the protein interaction between Trim71 and Ago2 is disputed, particularly as neural progenitor cells from wild-type mice had similar Ago2 levels and ubiquitylation patterns *in vivo* (Chen et al., 2012). Trim71 is alternatively proposed to maintain proliferation of neural progenitor cells as a temporal regulator of the FGF pathway (Chen et al., 2012). The reasons why these studies differ is unclear and may simply reflect the inherent aberration of Lin41 overexpression in different cell lines (Ecsedi and Grosshans, 2013). Nevertheless, despite questions regarding the mechanism, evidence for the involvement of Trim71 in neural tube development is accumulating. Particularly in our laboratory, Trim71 was identified as a Tulp3-interacting protein and Tulp3 is negative regulator of the Shh Signal pathway.

1-08 Project summary

In this thesis I test the hypothesis that Rgnef and Trim71 act as regulators of the Shh signalling pathway. The hypothesis is based on their interaction with Tulp3, identified by previous studies in our laboratory using yeast-2-hybrid screen and CO-IP investigation. Tulp3 is an established negative regulator of Shh signalling pathway involved in a mechanism that involves primary cilia, an organelle fundamental to Shh signalling. My investigations centre on using Shh Light-II cell based assay to monitor states of Shh pathway activation in relation to changes in Rgnef and Trim71 expression. Using siRNA, I show *in vitro* that reducing Rgnef expression significantly reduces the extent of induced Shh pathway activation. To investigate the contrasting effect of increasing Rgnef expression, I use an established HA tagged Rgnef expression construct (pcDNA3-HA-p190RhoGEF) as well as sub-clone a mammalian expression vector pCAGGS Rgnef, for untagged expression. Increasing Rgnef expression is then

shown to stimulate pathway activity, hence opposite to the effect induced previously by siRNA *Rgnef* suppression. Investigation as to the possible causes of Rgnef regulation of Shh signal transduction was taken at a cellular level by investigating the effects on the primary cilia organelle. Through fluorescent immunocytochemistry, I demonstrate that increasing Rgnef expression significantly reduces the proportion of cells with a primary cilium. At an organismal level I also show that within the mouse embryo *Rgnef* is expressed in ventral floorplate of the developing neural tube.

Shh pathway suppression was also induced by Trim71 siRNA, but through validation tests I discover Trim71 is not expressed in the NIH 3T3 cell line, used to construct the Shh-LIGHT2 cell based assay. In discovering my results to be a false positive, I endeavour to investigate possible causes and identify the result to be from a single siRNA amongst the total mix used for the experiments.

My thesis also investigates established effectors of Shh signalling pathway by focusing on the vertebrate pathway transcription factor Gli2, by using mass spectrometry to identify putative novel sites of Gli2 post translational modification. Gli2 is one of three transcription factors conserved in vertebrate Shh signalling and is predominantly involved in pathway activation. By using mass spectrometry, I aimed to reveal sites of protein modification that would help to understand the role of Gli2. The challenge was to devise methods to adequately identify Gli2 by SDS PAGE electrophoresis and best practice techniques to ensure adequate protein extraction and preparation for MS. I also compared the use of two Mass spectrometers, The MALDI-ToF and AmaZon ETD ion Trap mass spectrometer. Using the Amazon ETD I was able to sequence specific regions of Gli2 protein. I was also able to identify established sites of Gli2 phosphorylation as well as discover potentially novel sites.

In summary my thesis aims are broadly to help build towards a more comprehensive model of the Shh signalling pathway. I aimed to further confirm and investigate potential new effectors of the Shh signalling Pathway, Rgnef and Trim71 and to further understand one its key effectors, Gli2. The model of Shh signal transduction and its relationship with the primary cilia organelle has also been a key focus.

Chapter 2: Materials and Methods

2-01 Mouse Embryo protocols

2-1-01 Riboprobe synthesis

The Rgnf expression plasmid, pBS Rgnef, was linearised (37°C, 2 hr) with XbaI restriction enzyme and appropriate buffer (Fermentas fast digest). Sample digests were then analysed using gel electrophoresis to check for digest completion. Linearised DNA plasmids were precipitated (0.15 M sodium acetate, 66% ethanol, -20°C, 1 hr), centrifuged (13,000rpm, 4°C, 10 min) and washed with 70% ethanol. Resulting pellets were then air dried and re-suspended in RNase-free water.

Dioxigenein-labelled (DIG-labelled) riboprobe was synthesised by incorporating digoxygenin-labelled dUTP during targeted transcription from the linearised plasmid (37°C, 2 hr). Each 20 µl reaction mix consisted of 1 x transcription buffer (Roche), 1 x digoxygenin labelling mix (Roche), 1 µg linearised plasmid, 20 units of RNase inhibitor (Invitrogen) and 10 units of T3 RNA polymerase (Roche). Transcription efficiency was tested by analysing a 1 µl aliquot on a 1% agarose electrophoresis gel. Successful DIG-labelled riboprobe transcription would reveal an RNA band to be approximately 10 times as intense as the plasmid band. The probe was then precipitated using 100 µl TE, 10 µl 4M LiCl and 300 µl ethanol and incubated at -20°C for 2 hr. Finally probe was pelleted (13000 x g, 20 min at 4°C), then washed with 70% ethanol to remove salt and immediately re-suspended in RNase-free TE buffer. The dioxigenein-labelled riboprobe (DIG-labelled) could then be identified using anti-digoxygenin antibody conjugated to alkaline phosphatase. Visualisation requires incubation with substrates nitro-blue tetrazolium chloride (NBT) and 5-bromo-4-chloro-3'-indolyphosphate phosphotoluidine (BCIP).

2-1-02 Wholemount *in situ* hybridisation

Wild type E10.5 mouse embryos were obtained from previously processed stock, stored in 70% ethanol at RT. Embryos were fixed overnight with 4% paraformaldehyde in PBS. Following day, embryos were dehydrated through a methanol series and then rehydrated to PBT (0.1% Tween-20 in PBS) and then bleached (6% H_2O_2 in PBT, 1 hr). After short treatment with proteinase K (10 µg ml^{-1}, 10 min, RT) followed by glycine (2 mg ml^{-1}), embryos were washed and refixed for 20 min (0.2% glutaraldehyde in 4% PFA/PBS). Once washed embryos were incubated (4 hr, 70°C) in prehybridisation

solution (50% formamide, 4x saline sodium citrate buffer (SSC; 0.6 M sodium chloride (NaCl), 0.06 M sodium citrate in ddH_2O, pH4.5), 50 µg ml^{-1} yeast tRNA, 1% SDS, 50 µg ml^{-1} heparin) before adding 0.1 µg ml^{-1} digoxygenin-labelled riboprobe in prehybridisation solution for overnight incubation (70°C).

Following day, embryos were washed twice (70°C, 30 min) in solution 1 (50% formamide, 5x SSC (pH4.5), 1% SDS) and twice (70°C, 30 min) in solution 2 (50% formamide, 2x SSC (pH 4.5), 1% SDS). Prior to blocking, embryos were washed in Tris buffered saline with Tween 20 (TBST: 0.14 M NaCl, 3 mM potassium chloride, 25 mM Tris-HCl (pH7.5), 1% Tween-20, 0.05% Levamisole) and then blocked by incubation in 10% sheep serum/TBST (4 hr, RT).

Anti-digoxygenin alkaline phosphatase antibody (anti-DIG-AP (Roche) 1:500) was incubated (4°C, 4 hr) in pre-absorbing solution (embryo powder, 1% sheep serum in TBST) before centrifugation (3000 rpm, 10 min). Supernatant was made up to volume with 1% sheep serum/TBST and applied to embryos (4°C, overnight).

Embryos were washed with 6-8 changes of TBST (over 24 hr), equilibrated in NTMT (0.1M NaCl, 0.1M Tris-HCl (pH9.5), 0.05M magnesium chloride, 0.1% Tween-20, 0.05% Levamisole) incubated with nitro-blue tetrazolium chloride (NBT) and 5-bromo-4-chloro-3'-indolyphosphate phosphotoluidine (BCIP) salt (20 µl ml^{-1} TBST) and washed in PBT.

Photographs were taken using a Leica MZ16 microscope, and then embryos were embedded for Vibratome sectioning.

2-1-03 Vibratome sectioning

Embryos were fixed (20 min, 4% PFA/PBS) then washed in PBS. Embryos were coated in vibratome embedding mixture (0.56% gelatine 300 bloom, 22.5% sucrose, 33.75% albumin/ PBS). Glutaraldehyde (10 µl of 25% stock/100 µl) was added to embedding mixture in a mould, mixed quickly and embryos were immediately positioned in the desired orientation. Blocks were allowed to set (30 min, RT) then removed from the mould and stored in PBS (4°C).

Embryos were sectioned using a Vibratome^{tm} series 1000 sectioning system. Blocks were trimmed into a trapezoidal shape and glued to the mounting plate, which was secured to the vibratome. Sections of 30 µm were collected on slides. Sections were mounted (50% glycerol/PBS), and photographed with a Zeiss AxioPhot 2 microscope.

2-02 Cell culture

2-2-01 Cell lines

The mouse fibroblast (Shh-LIGHT2) cell line was provided by James Briscoe MRC, London (Taipale et al., 2000). The Human Embryonic Kidney (HEK293T) and NIH 3T3 cell lines were provided by George Dickson RHUL, London. Inner Medullary Collecting Duct cell line (IMCD3) was provided by D. Norris, MRC Harwell.

Sterile plastic ware and media were used, and equipment was washed (70% ethanol) and solutions warmed (37°C) prior to use. Shh-LIGHT2, NIH 3T3 and HEK293T Cells were grown in Dulbeccos's Modified Eagle's Medium (Sigma D6546) with 2 mM L-Glutamine (Sigma G7513) added, 10% Foetal Bovine Serum (Gibco 10500-064) and 1% Antibiotic-Antimycotic (Gibco 15140-122). Selective antibiotics for Shh Light cells were added to a concentration of 0.4 mg ml^{-1} for Geneticin (Gibco 10131-019) and 0.15 mg ml^{-1} for Zeocin (Invitrogen 46-0509). IMCD3 cells were grown in DMEM: Nutrient mixture F-12 plus GlutaMAX™ (Gibco 31331-028), 10% Foetal Bovine Serum (Gibco 10500-064) and 1% Penicillin-Streptomycin (Gibco 15140-122).

2-2-02 Waking, plating and growth culture

Frozen cell aliquots (1 ml) were rapid-thawed (37°C, gentle shaking) and gradually over 2 min 5 ml culture media was added. To remove trypsin, Cell suspension was centrifuged (1000 g 10 min) and supernatant removed. Cell pellet was then re-suspended in 10 ml culture media, transferred to T75 cell culture flasks and placed in an incubator (37°C, 5% CO_2). At between 85-95% cell confluence a portion of cells were sub cultured to new flasks to continue cell line growth.

2-2-03 Subculturing

Culture media was aspirated and cells washed twice with PBS (without calcium or magnesium (Gibco)). Trypsin (TryPLE™ Select Gibco 12563-029) was added (1 ml for 75 cm^2 flask and 0.5 ml for 25 cm^2 flask) and flask incubated (2-3 min, 37°C) enabling cell

detachment. Once cells were detached, 5 ml medium was added to inhibit trypsin and entire cell suspension was then transferred to a 15 ml falcon tube. To remove trypsin the cell suspension was centrifuged (1000 g, 10 min) so that the supernatant could be separated from the resulting cell pellet. The pellet was suspended in culture medium (10 ml) and apportioned to new culture flasks depending on requirement and incubated (37°C, 5% CO_2). At 85-95% confluence cells were again sub cultured.

2-2-04 Counting cells

Spent media was aspirated; cells were washed twice, and trypsinised and pellets collected as described (section 2-2-03). 16 µl of cell suspension was applied to a haemocytometer and cells were counted in 3 individual 10^{-4}ml sections. An average was taken of the three counts and multiplied by $x10^4$ to give an estimation of cells/ml.

2-2-05 Freezing cells

To store, cells were trypsinised as described (section 2-2-03), centrifuged (1000 g, 10 min) pellets were resuspended in Recovery™ cell culture freezing medium (Gibco 12648-010) at 1 ml/million cells concentration. One ml cell suspensions were aliquoted into 1.5 ml cryotubes (Nunc) and stored at -70°C overnight in a CoolCell® (BioCision) to ensure a controlled -1°C per minute temperature drop before long term storage in a liquid nitrogen dewer.

2-03 Mammalian cell transfection

2-3-01 siRNA reverse transfecting cells with Dharmafect

Assay samples were prepared in sterile 96 well plates (corning). All siRNA and transfection reagent Dharmafect was supplied by Dharmacon (Thermo Fisher Scientific). In each well was added 18 µl Optimem serum-free, antibiotic-free medium (Gibco), 2 µl Dharmafect and 100 nM siRNA (Table 2-01 for siRNA smartpools). The siRNA and Dharmafect were then incubated for 20 min, to optimise transfection complex formation. A $2x10^5$ cells ml^{-1} suspension of Shh-LIGHT2 cells were prepared and 80 µl was added to each well containing pre-prepared 20 µl transfection complex. The total 100 µl Optimem preparation therefore consisted of $1.6x10^4$ cells/well and complexed 20 nM siRNA concentration. Shh-LIGHT2 cells were incubated overnight (37°C, 5% CO_2) to produce adherent transfected cells at 80-95% confluence.

Table 2-01 - siRNA sequences*

ON-TARGETplus SMARTpool - Mouse Rgnef (L-040493-01-0005)		
Name	**Catalogue reference**	**sequence**
Rgnef siRNA(1)	J-040493-09	GUGAUGAAGUCUACGCUAA
Rgnef siRNA(2)	J-040493-10	CAUCAAACUCUUCCGGAAA
Rgnef siRNA(3)	J-040493-11	ACAUUGACCCUGACCGUUA
Rgnef siRNA(4)	J-040493-12	GCGAAUACGAGAAGAACCA
ON-TARGETplus SMARTpool - Mouse LOC636931 (L-161015-00-0005)		
Name	**Catalogue reference**	**sequence**
Trim71 siRNA(1)	J-161015-01	GAUCAUAGUGGCCGACAAA
Trim71 siRNA(2)	J-161015-02	CAUCAUAGUGGCUGACCGA
Trim71 siRNA(3)	J-161015-03	CAAGAAGAUGACCGCCAUUA
Trim71 siRNA(4)	J-161015-04	GGGCAAGAUCCUCGUUUCA
ON-TARGETplus Non-targeting pool		
Name	**Catalogue reference**	**sequence**
Non-Targeting pool	D-001810-10-05	Unknown

*All siRNA was supplied by Dharmacon (Thermo Fisher Scientific)

2-3-02 Lipofectamine 2000 DNA transfection

Cells were grown to 80-95% confluence and transfected with Lipofectamine 2000 (Invitrogen) according to optimised manufacturer's instructions. Lipofectamine (6 µl/µg DNA) was diluted in required amount of Optimem serum-free, antibiotic-free medium, incubated (5 min, RT), added to the DNA (0.2-0.4 µg μl^{-1}) in serum-free, antibiotic-free medium) and incubated (30 min, RT). Cell medium was replaced and DNA/Lipofectamine mix was introduced. Cells were incubated (4 hr-overnight, 37°C, 5% CO_2), media was replaced with serum-positive, antibiotic-free medium and incubated (37°C, 5% CO_2, overnight).

2-04 Gene expression protocols

2-4-01 RNA extraction

Total RNA was extracted from whole 3T3 cell pellets with the GenElute™ Mammalian Total RNA Purification Kit (Sigma RTN70-1KT) according to the manufacturer's

instructions. Samples were lysed (with a series of needles) in lysis buffer (500 µl) containing guanidine thiocyanate (a protein denaturant which releases RNA) and 2-mercaptoethanol (which inactivates RNase). Lysate was then filtered through a column to remove cell debris and shear DNA. Ethanol was added to the filtrate before application to a high capacity silica column which binds total RNA. Contaminants were washed away and the RNA eluted in RNase-free water. Concentrations were determined using a NanoDrop ND-1000 spectrophotometer (Thermoscientific) to read absorbance at 260 nm.

2-4-02 cDNA Synthesis

A 14 µl genomic DNA elimination reaction was prepared for each sample on ice, adding 0.3 µg total RNA in 12 µl RNase-free water with 2 µl gDNA wipeout buffer. The reaction mix was incubated for 2 min (42°C) then immediately placed on ice. A 6 µl master mix was added to each reaction containing 4 µl Quantiscript RT buffer, 1 µl Quantiscript Reverse Transcriptase and 1 µl RT primer mix (a mix of random and oligo dT primers). The final 20 µl reverse transcriptase reaction was incubated for 15 min (42°C) followed by 3 min at 95°C to inactivate the reverse transcriptase. Preparations were used immediately or stored at -20°C for long term use.

2-4-03 Polymerase chain reaction

PCRs were performed as a 25 µl reaction consisting of 0.5 µM of each primer and 25 ng DNA or cDNA in 1x PCR Master Mix (BIOTAQ DNA polymerase, 1.5 mM $MgCl_2$, 200 µM of each dNTP, 1 x NH_4 buffer). Reactions were performed with a Chromo4 thermo cycler (MJResearch) and the appropriate primer combinations.

The program comprised initial denaturation (95˚C, 5 min) followed by up to 38 cycles of denaturation (95°C, 15 sec), annealing (60˚C, 30 sec) and extension (72˚C, 15 sec), followed by a final extension (72˚C, 5 min).

Table 2-02 Site directed primer sequences

PCR	Forward	Reverse
Rgnef	GCGCGCGCGATATCATGGAGTTG	GCGCGCGCGCTAGCTCAGAGGTAAAGAAT
Trim71	CAGCACCACGACGATGAG	GACTTGAGGGCGAGGTACAG

RT-qpcr	Forward	Reverse
Rgnef	CAGCCACAGACACTCACAAC	GCCACACAATCAGAGGTAAAGA
Trim71	CTTCTCCATTCTCTCGGTGTTC	CAGAGCAGGTGTCACAGTAGA

2-4-03 Real Time quantitative PCR

The thermal cycler used for RT qPCR was a Rotor-Gene 6000 (Qiagen). Each individual 20 µl sample was prepared by Qiagility, a robotic automated sample preparation system (Qiagen) pre-loaded with master mixes for SYBR green, Gene specific primer and cDNA preparations. Each 20 µl sample preparations consisted of 10 µl 2X SYBR green jumpstart Taq (Sigma, S4438), 5 µl gene specific primer mix (1 µM) and 5 µl of cDNA preparation (1:5 dilution from cDNA synthesis (section 2-5-02)). The cycling program comprised of initial denaturation (94˚C, 2 min) followed by 40 cycles of denaturation (95°C, 15 sec), annealing (60˚C, 60 sec) and extension (72˚C, 20 sec), during which a read was taken. The melt curve analysis program comprised of temperature ramping form 65 ˚C to 95 ˚C by 1 ˚C increments every 5 sec.

Expression changes were calculated using the $2^{-\Delta\Delta C}{}_{T}$ method, a method that depends on using the stable expression of selected reference genes for normalisation of initial template RNA variations (Livak and Schmittgen, 2001). In order to select sufficient controls, the effect of experimental conditions on the expression of 6 reference genes was assessed by RT-qPCR. The genes selected were *GAPDH*, *β2-Microglobulin*, *ribosomal protein L13a*, *ubiquitin C*, *ATP synthase subunit* and *β-Actin*. Reference gene primers were designed and purchased from Primer Design Ltd and were pre-validated to ensure they targeted their specific genes. Visual basic application GeNorm, incorporated in Biogazelle qbase+ software tool, was used to manage the large amount of data and recurring calculations required for assessment of the most stable reference gene in any specific experimental condition (Vandesompele et al., 2002). Assessment is based on the principle that expression between any two reference genes should be the same in all samples. Hence measurable differences between them indicate that one or both of these genes are not constitutively expressed (Vandesompele et al., 2002). By using 6 different control genes, all possible permutations of gene by gene stability ratios can be calculated to provide an overall value ratio M. Therefore M has an inverse relationship to stability; a lower value will

indicate the most stable gene expression. The worst-scoring reference gene (highest M value) was eliminated to then recalculate M values for all remaining genes and so on. By ranking the genes in this way, the optimal number of the most stable reference genes are identified also taking into account V; the inherent systematic variation from factors like machine, enzymatic and pipette variations.

2-4-04 Agarose gel electrophoresis

DNA was analysed by electrophoresis using agarose gels (1-2% agarose in 1 x TAE (Tris/Borate/EDTA: 89 mM Tris base, 89 mM Boric acid, 20 mM EDTA) containing 1x Sybrsafe (Invitrogen) in TBE buffer. Samples were prepared with loading buffer (25% glycerol in TAE with dye) and applied to the gel along with a DNA ladder Generuler 1kb plus DNA ladder (Promega) for bands of 0.5-12 kb or 1 kb plus DNA ladder (Invitrogen) for bands of 0.1-12 kb) to allow estimation of band size. A voltage of 90 V was applied across the gel for 30-45 min, and bands were visualized with a UV transilluminator.

2-4-05 Sequencing

PCR fragments and sequencing primers were sent by post to GATC for sequencing following the company guidelines for volume, concentration and labelling instructions. The results were sent via email and analysed by search and alignment tools Vector NTi (Invitrogen) and NCBI blast (http://blast.ncbi.nlm.nih.gov/Blast.cgi).

2-05 Cloning and Subcloning

2-5-01 Bacterial transformation

Prior to use, competent *Escherichia coli* (*E. coli*) cells (α-Select^{tm} competent cells silver efficiency, Bioline (Cat# Bio-85026)) were stored at -70°C. When required, each sample aliquot (25 µl) was thawed on ice and gently mixed with 50 ng of plasmid before 30 min incubated on ice. To facilitate plasmid transformation, cells were subjected to short heat-shock treatment (42°C, 45 sec) and cooled on ice. Cells were allowed to recover by adding 250 µl Luria Bertani (LB) broth (shaking, 37°C, 1 hr).

Depending on plasmid induced resistance, respective antibiotic was added (50 µg ml^{-1} ampicillin or 20 µg ml^{-1} kanamycin or 25 µg ml^{-1} zeocin (Invitrogen)) to melted Luria Bertani (LB) agar. The mixture was poured into sterile 90 mm plates. Once set, plates were warmed to 37°C and cells were streaked out. Plates were incubated overnight

(37°C). Individual colonies were picked and grown (37°C, 8 hr with shaking) in 3 ml LB broth (10% tryptone, 5% yeast extract, 10% NaCl, pH7.0), again with appropriate antibiotic (50 μg ml^{-1} ampicillin or 20 μg ml^{-1} kanamycin or 25 μg ml^{-1} zeocin).

2-5-02 Plasmid purification

LB broth with appropriate antibiotic (30 ml) was seeded with transformed bacterial culture (30 μl) and incubated (37°C, overnight with shaking). Plasmids were purified using Plasmid Purification Midi kit (Promega) according to manufacturer's instructions.

Cells were pelleted by centrifugation (5000 x g, 15 min) and subjected to a modified alkaline lysis procedure and RNase A. Lysed cells were cleared through a filter cartridge, and applied to an anion-exchange resin column under low-salt and pH conditions. Contaminants are washed away with medium-salt wash and plasmid is eluted in high-salt buffer. DNA is precipitated (0.7 volumes isopropanol), pelleted (15000 x g, 30 min, 4°C), washed (70% ethanol) and re-suspended in Tris-EDTA (TE) buffer (10 mM Tris, 1 mM EDTA).

Purification was quantified using a NanoDrop ND-1000 spectrophotometer (Thermoscientific) to read absorbance at 260 nm.

2-06 Protein extraction, quantification and analysis

2-6-01 Protein extraction

Cells were harvested in 300-1000 μl lysis buffer (50 mM HEPES (pH 7.5), 150 mM NaCl, 1 mM EDTA, 10% Glycerol, 1% Triton-X 100) containing 3-10 μl 100X HALT protease and phosphatase inhibitor (HALT #1861281 Thermo scientific) for 20 min at 4°C. Cell debris and nuclei were removed by centrifugation (10,000 x g, 10 min, 4°C) and supernatants stored at -20°C or used immediately.

2-6-02 Protein quantification

The DC Protein assay kit (Bio-Rad) was used to quantify protein. The protein reacts with copper, causing reduction of Folin reagent and development of the blue colour such that intensity reflects protein concentration. DC reagent A (an alkaline tartrate solution) was mixed with DC reagent S (50:1 ratio) and combined with sample or

protein standard (5 µl) in wells of a flat bottom 96 well plate. DC reagent B, Folin reagent (200 µl) was added and the mixture incubated (45 min, RT).

A series of BSA standards (0.25 mg ml^{-1}, 0.5 mg ml^{-1}, 0.75 mg ml^{-1}, 1.0 mg ml^{-1}, 1.25 mg ml^{-1} and 1.5 mg ml^{-1}) were prepared by diluting BSA stock (Sigma) in the buffer used to extract the protein. If sample protein concentrations were expected to be high, 1:10 dilutions were prepared to ensure measurements were taken within the assay's optimal range of between 0.2 and 1.5 mg/ml. The absorbance at 750 nm was measured with µ Quant (Bio-tek Instruments).

Quantification of each sample and standard was performed in duplicate, and absorbance values for the BSA standards were used to generate a standard curve to which sample absorbance values could be compared.

2-6-03 SDS-PAGE

Protein samples (1-16 µg) were added to SDS-PAGE buffer (1 x orange loading buffer (Licor) and, 1 x reducing agent (Invitrogen). Samples were then heated to denature proteins (70°C, 10 min) and chilled on ice until loaded. Pre-made NuPAGE 3-8% or 7% Tris Acetate gels (Life Tech EA03752) were used depending on molecular weight resolution requirements. Once removed from sealed packaging, gel preparation involved rinsing in water, removing comb and taking care to wash lanes with 1 x NuPAGE® Tris-Acetate SDS Running Buffer. Gels were secured in the XCell SureLock® Mini-Cell electrophoresis chamber (Life Tech), creating inner and outer chambers. Inner chamber was filled using 200 ml 1 x NuPAGE® Tris-Acetate SDS Running Buffer with 500 µl NuPAGE® antioxidant. Outer chamber was filed with 600 ml 1 x NuPAGE® Tris-Acetate SDS Running Buffer. Protein samples were loaded (1-16 µg) together with marker ladder, using either HiMark Prestained Protein Standard (Invitrogen) for 3-8% TA gels or Novex Sharp Pre-stained Standard (Invitrogen) for 7% TA gels. Gels were then electrophoresed for 70 min at 150 V.

2-6-04 Western blotting

Electrophoresed gels were removed from cassettes by carefully trimming edges. Prior to blotting, the electrophoresis gel, membranes, filter paper and sponges were soaked in transfer buffer (25 mM Tris base, 0.2 M glycine, 10% methanol/H_2O) for 10 min

before assembly of the blotting system. When using ECL detection nitrocellulose membranes were used (Hybond-ECL, GE Healthcare) and when using fluorescent antibody detection PVDF-FL membranes (Millipore) were substituted to reduce background signal. PVDF-FL membranes (Millipore) were first activated by soaking in methanol for 15 sec.

During blot assembly care was taken to ensure that the membrane was on the positively charged side of the tank relative to the gel. The tank was then filled with transfer buffer and transfer was performed at 100 V for 1 hr. An ice pack and magnetic stirrer were also included in the tank to prevent against over-heating and enable uniform heat distribution.

2-6-05 Immunodetection

After proteins of interest were transferred, the nitrocellulose membranes were blocked (1hr at RT with shaking) using 2% ECL Advance blocking reagent (GE Healthcare) in TBST (0.14 M NaCl, 20 mM Tris-HCl pH 7.6, 0.1% Tween 20). In the case of PVDF membranes, the blocking solution used was Odyssey blocking solution (Licor) to reduce background fluorescence. Blocking solution was then removed and replaced with primary antibody diluted in respective block for overnight incubation (4°C with gentle rocking). Following day, antibody solution was removed and membrane washed in TBST (2 rinses, 1x 15 min then 3 x 5 min at RT) to remove excess antibody. The appropriate HRP-conjugated or fluorescent secondary antibody was diluted in block and incubated with the nitrocellulose or PVDF membrane respectively (1 hr, RT with gentle rocking). The membrane was then washed with TBST (2 rinses, 1 x 15 min then 3 x 5 min at RT).

The Enhanced Chemiluminescence (ECL) Advance Western Blotting Detection Kit (GE Healthcare) was used for detection. Solution A (containing hydrogen peroxidase) and Solution B (containing luminol) were equilibrated to RT then mixed in a 1:1 ratio in a volume of TBST equal to the combined volume, then applied to the nitrocellulose and incubated in the dark (5 min, RT). The HRP-conjugated secondary antibody catalyses the oxidation of luminol, producing luminescence. Blots were drained and mounted between acetate sheets in a light-proof cassette. Blots were exposed to X-ray film (GE Healthcare) and developed (using an automated X-ray developer) in a darkroom.

The Odyssey fluorescent reader (Licor) was used for fluorescent secondary antibody detection. The damp membrane was loaded onto the glass plate and loaded into the Odyssey for two channel near-infrared fluorescence detection, at 800 nm and 700 nm.

Detailed below is a summary table of primary and secondary antibodies used for immunoblotting (IB), immunocytohistochemistry (IHC) and protein pulldowns. This includes working concentrations, species antibody was raised and source.

Table 2-03 Antibody

Primary Antibody	**IB**	**IHC**	**Species**	**Source**
Acetylated α-tubulin	-	1:100,000	mouse	Sigma
Fatty Acid Synthase	1:5000	-	mouse	Santa Cruz
Gli2	1:2000	-	rabbit	B Wang
Gli2 (AB26056)	1:1000	-	rabbit	Abcam
Gli2 (AB7195)	1:1000	-	rabbit	Abcam
HA (Clone 16B12)	1:1000	1:1000	rabbit	Sigma
Rho A B and C	1:2000	-	rabbit	Thermo Sci
β-tubulin	1:5000	-	rabbit	Santa Cruz
mLin41	1:1000		rabbit	G. Wulczyn
Secondary Antibody	**IB**	**IHC**	**Species**	**Source**
IRDye 680RD anti-mouse	1:15000	-	Goat	Li-Cor
IRDye 680RD anti-rabbit	1:15000	-	Goat	Li-Cor
IRDye 800CW anti-mouse	1:15000	-	Goat	Li-Cor
IRDye 800CW anti-rabbit	1:15000	-	Goat	Li-Cor
Anti-mouse Alexa Fluor 594		1:250		Invitrogen
Anti-mouse Alexa Fluor 488		1:250		Invitrogen
Anti-rabbit Alexa Fluor 488		1:250		Invitrogen
Anti-rabbit Alexa Fluor 594		1:250		Invitrogen
Anti-mouse HRP	1:1000			DAKO
Anti-rabbit HRP	1:1000			DAKO
Anti-qoat HRP	1:1000			DAKO

2-07 Shh-LIGHT2 cell based assay

Media is removed from 96-well plates containing cell sample preparations to be assayed and replaced with 100 µl serum free medium (Dulbeccos's Modified Eagle's Medium (Sigma; D6546) with 2 mM L-Glutamine added (Invitrogen), 1% Antibiotic-Antimycotic, 0.5% 1M HEPES buffer). Shh pathway stimulation was achieved by Smoothened-agonist purmorphamine. Cells were incubated for 24 hr and cells requiring pathway stimulation were given 25 µl of 25 µM Purmorphamine (Calbiochem, 540223) in 1.25% DMSO in serum free media, making a final concentration of 5 µM Purmorphamine, 0.25% DMSO in each well. Cells to remain unstimulated were given 25 µl of 1.25% DMSO in serum free media. After 24 hr the medium was removed and replaced with 70 µl DMEM as well as adding 70 µl DMEM to an additional column of wells. All wells were assayed using the Dual-Glo® luciferase assay system (Promega E2920) as per manufacturer's instructions. Plate readings were measured on the Glomax – 96 microplate luminometer (Promega). Initial readings were made by adding firefly luciferase substrate (beetle luciferin) to generate luminescence relative to Gli transcription activity. Initial luminescence is quashed by the second reagent and instead replaced by luminescence from renilla luciferase substrate (coelenterazine). The background luminescence was assessed from DMEM media only assay and subtracted from all readings. Calculation of a firefly luminescence/Renilla luminescence ratio provides a normalised Gli Response factor relative to cell number.

2-08 Immunocytohistochemistry

Microscope slide preparation was achieved by first seeding adherent cells on coverslips that were in turn inserted in 6 well plates. Cells were then left overnight to adhere and grow on coverslips in antibiotic free culture media (37°C, 5% CO_2). Cell transfection and control procedures were then carried out on the following day as described previously (section 2-03). Each sample transfection medium was then replaced with serum-free medium and cells incubated for 48 hr to promote ciliogenesis (37°C, 5% CO_2). After removing medium and rinsing once with PBS, cells were fixed using 4% formaldehyde, 2% Triton-X in PBS (10 min, RT). Non-specific binding was blocked (2% BSA in PBS, 1 hr, RT) followed by primary antibody in block incubated overnight (4°C). Cells were washed and secondary antibody was added

suspended in block for 1 hr incubation (gentle rocking, RT). After removing secondary antibody and washing cells three times with PBS, coverslips were mounted face down onto slides with Vectashield (Vector Laboratories) and fixed at edges with nail varnish.

2-09 Active Rho pull-down and detection

For each sample and control preparation, NIH 3T3 cells were cultured in T75 flasks and transfected according to requirement (Section 2-02; Section 2-03). Active Rho Pull-Down and Detection Kit (Thermo Scientific 16116) was used to identify Rho activity, as per manufacturer's instructions. After completion of sample transfection and control preparations, cells were cultured for 48 hours. Protein extraction was achieved by first removing all media from the flasks by aspiration and PBS wash. Then by adding 1 ml of Lysis buffer (25 mM Tris HCl, pH7.2, 150 mM NaCl, 5 mM $MgCl_2$, 1% NP-40 and 5% glycerol) containing 10 µl 100X HALT protease and phosphatase inhibitor (HALT #1861281 Thermo scientific) for lysate preparation (20 min at 4°C). Cell debris was pelleted (16,000 x *g* at 4°C for 15 min) and the supernatant was measured for total protein (section 2-6-02). Lysate required for each sample was then taken, ensuring there was 500 µg of total protein per preparation (recommended range between 500 – 1000 µg). Positive and negative controls were prepared by first adding 10 µl 0.5 M EDTA pH8 to 1 ml un-transfected lysate. The positive control was prepared by adding 5 µl 10 mM GTPγS to 500 µl lysate preparation and 5 µl 10 mM GDP to remaining 500 µl lysate for the negative control. These control samples were then agitated and incubated (30°C, 15 min) before stopping the reaction with 32 µl 1 M $MgCl_2$.

The Rho pull-down spin cups were prepared with 100 µl glutathione agarose (50% resin slurry), 400 µg of GST-Rhotekin-RDB. For each sample 700 µl (500 µg total protein) was added to a spin cup, as well as the for the 500 µl negative and 500 µl positive controls. Sample reaction mixture were incubated at 4°C for 1 hr with gentle rocking. The spin cup samples were then washed three times by centrifugation (6000 x *g*, 20 sec) with lysis buffer. Sample proteins were eluted with 50 µl SDS-PAGE loading buffer and prepared for SDS-PAGE and immunoblotting (section 2-6-03 to 2-6-05). The primary antibody used was rabbit anti-Rho (RhoA, RhoB and RhoC) at a concentration of 1:2000 (Table 2-03).

2-10 Mass Spectrometric protein preparation and analysis

2-11-01 Cell culture protein production

HEK293-T cells were grown in vented T75 cell culture flask (Corning) using DMEM supplemented with 10% fetal bovine serum and 1% Penicillin/Streptomycin. Cells were seeded, grown overnight and then transfected with a plasmid encoding the HA-tagged gene of interest using Lipofectamine 2000. After 48 hr, cells were harvested in lysis buffer (50mM HEPES (pH 7.5), 150 mM NaCl, 1 mM EDTA, 10% Glycerol, 1% Triton-X 100) containing 1 x HALT protease and phosphatase inhibitor cocktail (Thermo Scientific) for 20 min at 4°C. Cell debris and nuclei were removed by centrifugation at 10,000 x *g* (10 min, 4°C).

2-10-02 Enrichment of Gli proteins using a biotinylated DNA oligonucleotide

Both the Gli binding site sequence and the mutated binding site control sequence oligonucleotides (oligo) were resuspended in water to a final concentration 5 µg μl^{-1}. The sense sequence oligo, with biotin at the 5' end, was annealed to the reverse sequence oligo by incubating for 2 min at 90°C followed by 10 min at 65°C and 10 min at 37°C. The mix consisted of 5 µl sense oligo, 5 µl antisense oligo and 5 µl 10 x annealing buffer (100 mM Tris-HCl (pH 8.0), 10 mM EDTA, 500 mM NaCl). Final volume of 50 µl was prepared by adding 35 µl water.

The sequences used for Gli binding and mutated Gli binding site was as follows (Pan et al., 2006):

Gli binding sequence

```
GAC GCG TGG ACC ACC CAA GAC GAA ATT CAC A
CTG CGC ACC TGG TGG GTT CTG CTT TAA GTG T
```

Mutated sequence (changes underlined)

```
GAC GCG TGG ATT ACA TAA GAC GAA ATT CAC A
CTG CGC ACC TAA TGT ATT CTG CTT TAA GTG T
```

Streptavidin conjugated magnetic beads (New England BioLabs) were prepared by washing A 100 µl of beads 4 times with TNE buffer (10 mM Tris (pH8), 100mM NaCl, 1 mM EDTA). Beads were then resuspended in 200 µl TNE and equally divided for addition of the sample and control oligo preparations. Prepared double-stranded

oligos (2 ug) were added to 100 µl beads, then rotated 30 min at RT. Beads were then washed with TNE buffer and resuspended in 100 µl TNE buffer.

Confluent cells from T75 cell culture flask (corning) were lysed in 300 µl lysis buffer (50mM HEPES (pH 7.5), 150 mM NaCl, 1 mM EDTA, 10% Glycerol, 1% Triton-X 100) containing 1X HALT protease and phosphatase inhibitor cocktail (Thermo Scientific) for 10 min at RT, then incubated with 20 µl of earlier prepared beads whilst being rotated for 1-2 hr at 4°C. The magnetic beads were pulled down and washed with lysis buffer four times (using 500 µl or more for each wash). Proteins were then eluted with 20 µl Elution buffer (50mM HEPES (pH 7.5), 1M NaCl, 1 mM EDTA, 10% Glycerol, 1% Triton-X 100) at RT for 15 min.

2-10-03 In-gel trypsin digestion

Gels were loaded and electrophoresed as detailed previously (section 2-6-03). Electrophoresed gels were removed from the plastic cassettes and trimmed to remove the stacking gel and wells. Proteins were silver stained using Sigma ProteoSilver™ silver stain kit, as per manufacturer's instructions. Required protein regions or bands were excised from the gel with a sharp scalpel and fragmented to 15 mm^3 cubes, then destained in a 1:1 mixture of 30 mM $K_3Fe(CN)_6$ and 100 mM $Na_2S_2O_3$ until completely clear. Gel fragments were equilibrated in 50 mM ammonium bicarbonate before drying in acetonitrile in three 15 min washes. Once dry gradual (5 µl volume) additions of 12.5 ng μl^{-1} Trypsin (Promega Cat:V5111) in 50 mM ammonium bicarbonate buffer was made to allow absorption into the gel until the gel pieces were rehydrated to their original size. After 30 min on ice to allow the enzyme to saturate gel pieces, 25 µl 50 mM ammonium bicarbonate buffer was added and preparations were incubated for 36 hr at 37°C.

The supernatant from the in-gel digest was removed by pipette from the gel pieces into a 1.5 ml protein LoBind tube (Eppendorf 022431081). To the gel pieces was added 25 µl of 50% acetonitrile solution with 5% formic acid for 15 min sonification. The supernatant was removed and added to the previous supernatant collection and the procedure then repeated twice more. The peptides were concentrated down to 1-2 µl using a speed-vac then enriched and purified using a C_{18} Zip tips© (Merck Millipore). The Zip Tip C_{18} is a disposable pipette tip containing a 0.5 µl plug of C18 reverse phase

resin tips, used for concentrating and desalting procedures for peptides up to 40 kDa. Peptides were then eluted with 80% acetonitrile solution with 5% formic acid for MALDI-ToF mass spectrometry.

2-10-04 Anti-HA magnetic bead Immunoprecipitation

The method required magnetic beads covalently coupled to high-affinity mouse IgG1 monoclonal antibody (Pierce clone 2-2.2.14). For each sample preparation, 25 µl (0.25 µg) anti-HA magnetic beads (Pierce 88836) were mixed with 125 µl of 0.05% TBS-T in 1.5 ml protein LoBind tubes (Eppendorf 022431081). The supernatant was removed using a magnetic stand to hold the beads and the beads were washed twice more with 1 ml 0.05% TBS-T. Sample containing the HA-tagged protein was added to the pre-washed magnetic beads and incubated at room temperature with gentle rocking. Remaining lysate supernatant containing unbound protein was collected for analysis and beads were washed twice more with 0.05% TBS-T, followed with a final ultra-pure water wash. Protein elution was achieved by adding 100 µl 50mM NaOH to the beads at room temperature for 5 min with mixing. The eluent was magnetically separated from the beads and stored at -20°C if not used immediately.

2-10-05 In-solution trypsin digest

Protein was precipitated from the sample eluents by adding five volumes of ice cold acetone and incubating overnight at -20°C. To pellet precipitated proteins, samples were centrifuged (13,000 x *g* for 30 min at 4°C), then supernatant discarded and pellets allowed to partially dry for 10 min. Samples were then re-suspended for a 15 min incubation at 50°C in 20 µl of 45 mM dithiothreitol (DTT) in 50 mM ammonium bicarbonate buffer (ABC) in LC-MS Chromasolv water (Sigma 39253). Samples were then incubated for 15 min at room temperature in the dark after adding 20 µl of 100 mM solution of iodoacetamide (IAA) dissolved in 50 mM ABC in LC-MS Chromasolv water (Sigma 39253). To destroy any excess IAA a further 20 µl of 45 mM DTT in 50 mM ABC in water was added followed by 20 µl 12 ng μl^{-1} in 50 mM ABC water to make a final concentration of 3 ng μl^{-1} trypsin in 80 µl 50 mM ABC water. Samples were incubated overnight at 37°C where proteins were reduced to trypsin digested fragments. Sample peptide enrichment and purification was achieved by C18 column packed pipette tips Zip tips© (Merck Millipore) following manufacturer's instructions.

2-10-06 Mass spectrometric analysis – AmaZon ETD

LC-MS/MS analysis was performed on an Ultimate™ 3000 RSLCnano HPLC system (Thermo Scientific Dionex) coupled to an Amazon ion trap mass spectrometer (Bruker) by a nano spray ion source (Bruker). Tryptic peptide mixtures were automatically injected (3 µl) and loaded at a flow rate of 4 µl min^{-1} in loading solvent (2% acetonitrile and 0.1% formic acid in HPLC-grade water) onto a nano trap column (75 µm i.d. × 2 cm, packed with Acclaim PepMap100 C18, 3 µm, 100 Å; Dionex). Peptides were eluted and separated on the analytical column (75 µm i.d. × 25 cm, Acclaim PepMap RSLC C18, 2µm, 100 Å; Dionex) by a multi-step gradient. Starting conditions consisted of 96% solvent A (0.1% formic acid in HPLC grade water), 4% solvent B (0.1% formic acid in acetonitrile) at a flow rate of 250 nl min^{-1}. Peptides were eluted from the column by graduated introduction of solvent B to 25% at 70 min, the rate was increased up to 60% at 90 min and to 90% at 90.5 min. The column was washed with solvent B (90%) for 10 min before equilibration in the starting conditions for a further 20 min. The complete runtime was 120 min.

The eluted peptides were analyzed using an AmaZon ion trap ETD mass spectrometer. From the mass spectrometry (MS) survey scan with a mass range of 300–1,500, the 5 most intense multiply charged ions were selected for fragment analysis in the ion trap if they exceeded an intensity of at least 2500 counts. Every ion selected for fragmentation was excluded for 20 sec by dynamic exclusion. Fragmentation was actioned consecutively by both collision-induced dissociation (CID) and electron transfer dissociation (ETD). The normalised collision energy for CID was optimised automatically by Smartfrag (Bruker).

For qualitative results the raw data were analyzed using Mascot (Matrix Science; version 2.4.0). Tandem mass spectra were extracted, charge state deconvoluted and deisotoped by DataAnalysis (ESI Compass, version 4.0) and BioTools. All MS/MS spectra were searched against the SwissProt database using Mascot. The search was restricted to Mammalia (Mammals), 2014_01 to 03 database, assuming the digestion enzyme trypsin, a fragment ion mass tolerance of 0.5 Da and a parent ion tolerance of 0.5 Da. Carbamidomethyl of cysteine was specified as a fixed modification and oxidation of methionine as a variable modification. For identification of

phosphorylation events Serine, Threonine and Tyrosine was specified in Mascot as variable modifications. Protein identifications were only accepted if they contained at least 2 identified peptides and the ion score values (-10log(P)) above a 95.0% probability threshold value ($p<0.05$) that the observed match was not a random event.

2-10-07 Mass spectrometric analysis – MALDI ToF

All analyses were prepared on a MALDI-ToF instrument in positive reflectron mode (Bruker) and peptide mass fingerprints were searched using the MASCOT search engine (Perkins et al., 1999). Calibration was achieved using peptide calibration standard (Bruker 206195) in 0.1% formic acid water (CHROMASOLV, Sigma 39253). Peptide standards covered a mass range between 1000 Da – 3200 Da and were; angiotensin II, angiotensin I, Substance P, Bombesin, ACTH clip 1-17, ACTH clip 18 – 39 and Somatostatin 28. During analysis, calibration was conducted before first analysis and every hour thereafter. Samples were prepared by premixing 1:1 with a saturated solution of HCCA matrix. HCCA matrix was prepared by sonification of 3 mg α-cyano-4-hydroxycinnamic acid (HCCA, (Bruker 201344)) in 300 µl high grade acetone (CHROMASOLV® plus, Sigma 650501) before adding 600 µl molecular grade ethanol (Sigma E7023). A 0.5 µl of each sample was spotted to MTP AnchorChip 600/385 target plate (Bruker), mixed with 0.5 µl HCCA matrix suspension. Once all samples were prepared they were left to dry, forming crystallised complexes. Monoisotopic peptide masses in the mass range 800-3500 Da were collected and used in the database search. The search parameters allowed for an error of 0.5 Da, carbamidomethyl modification of cysteine residues, oxidation of methionine and assumed trypsin enzyme digestion. The search was restricted to Mammalia (Mammals), 2013_06 to 09 database.

Chapter 3: Investigation of the role of Rgnef in the Shh signalling pathway

Rgnef is a 190 kDa guanine nucleotide exchange factor (GEF) that binds and activates RhoA by facilitating energy transfer exchange of bound GDP to GTP. Rgnef has largely been associated with cytoskeleton remodelling, specifically in the regulation of a large complex of proteins called focal adhesions that provide mechanical anchorage to the ECM. Focal adhesions are also a hub for integrin and adhesion-mediated signalling. In this chapter I test the hypothesis that Rgnef acts as regulator of the Shh signalling pathway. The hypothesis is based on being identified as a Tulp3 binding partner by previous yeast-2-hybrid screen and CO-IP investigations in our laboratory. Tulp3 is an established negative regulator of Shh signalling pathway involved in a mechanism that involves primary cilia, an organelle fundamental to Shh signalling.

My investigations centre on using a Shh-LIGHT2 cell based assay to monitor states of Shh pathway activation in relation to changes in *Rgnef* expression. Using siRNA transgenic suppression, I show *in vitro* that reducing *Rgnef* expression significantly reduces the extent of induced Shh pathway activation. To investigate the contrasting effect of increasing *Rgnef* expression, I use an established HA tagged Rgnef expression construct (pcDNA3-HA-p190RhoGEF) and sub-clone a mammalian expression vector pCAGGS Rgnef, for untagged expression. Increasing *Rgnef* expression is then shown to stimulate pathway activity, consistent with the pathway suppression results induced by *Rgnef* suppression. Investigation as to the possible causes of Rgnef regulation of Shh signal transduction was taken at a cellular level by investigating the effects on the primary cilia organelle. Through fluorescent immunocytochemistry, I demonstrate that increasing *Rgnef* expression significantly reduces the proportion of cells with a primary cilium. At an organismal level I also show that within the mouse embryo *Rgnef* is expressed ventrally in the floorplate of the developing neural tube.

3-01 In developing embryos Rgnef is expressed in the neural tube.

The aim was to examine the expression of *Rgnef* in the developing mouse embryos. Whole mount *in situ* hybridisation (WMISH) can effectively provide snapshots of localised gene expression during different periods of embryonic development. This required the sub-cloning of *Rgnef* cDNA into a suitable plasmid vector to allow RNA probe synthesis. The full length *Rgnef* cDNA was obtained from Dr Moolenaar in plasmid construct pcDNA3-HA-p190RhoGEF (Gebbink et al., 1997). However the

information available on the multiple cloning site was found to be incomplete after preliminary restriction enzyme mapping. The aim was to therefore remove the whole *Rgnef* sequence from pcDNA3-HA-p190RhoGEF and insert it into pBluescript (KS). The vector pBluescript is a well-established high yield plasmid containing RNA polymerase promoter sites for probe synthesis.

3-1-01 pBS Rgnef: Subcloning Rgnef from pRgnefHA (pcDNA3) into pBluescript (KS)

The first step was to remove the *Rgnef* cDNA insert from pcDNA3-HA-p190RhoGEf; an Rgnef expression construct that adds a 5' HA tag epitope (Gebbink et al., 1997). A working schematic of pcDNA3-HA-p190RhoGEF was devised by a combination of published pcDNA3 sequence and *Rgnef* sequence MMU73195 (Figure 3-01 A). Multiple cloning site information was found to be incomplete after preliminary restriction enzyme mapping. *Rgnef* insertion site regions were sequenced to detail the multiple cloning sites flanking the inserted 6.2 kb *Rgnef* sequence. This was then used to accurately combine sequences for pcDNA3 and 6.2 kb *Rgnef* (MMU73195). This revealed that there were no restriction sites that could remove the 6.2 kb *Rgnef* coding sequence from the pcDNA3 vector in a single fragment.

It was however possible to remove *Rgnef* in two fragments using *Sac*II and *Eco*RI restriction enzymes (Figure 3-01 A). Restriction enzyme *Sac*II digest of pcDNA3-HA-p190RhoGEF produced a 3 kb product consisting approximately of the first half of the *Rgnef* sequence, named 5'-*Rgnef* fragment. This fragment contained an *Xba*I restriction site situated 12 bp upstream from the *Rgnef* sequence start codon. *XbaI* enzyme digest provided a 5' cleavage restriction site that is not repeated along *Rgnef's* entire sequence. The second half of *Rgnef* was removed by an *Eco*RI digest, producing a 2.4 kb product, referred to as the 3'-*Rgnef* fragment. The overlap of 113 bp with the *5'-Rgnef* fragment was removed with *Sac*II digest. An entire *Rgnef* sequence would require both fragments to be ligated.

The 2.4 kb *Sac*II-*Eco*RI 3'-*Rgnef* fragment was first ligated into pBluescript, prepared by double digest with *Sac*II and *Eco*RI. This plasmid was subsequently linearised with *Sac*II and the *Sac*II-*Sac*II 5'Rgnef fragment inserted, to complete the entire *Rgnef* sequence. As both ends of the 5' fragment have *Sac*II overhangs, this fragment can insert in either orientation. Clones were tested by *EcoR* I digest fragment analysis to reveal those with

the *Sac*II-*Sac*II insert cloned in the correct orientation. Correct orientation of the 5'-*Rgnef* fragment would be identified by the presence of 5.9 kb and 2.4 kb fragments following *Eco*RI digestion, as opposed to 5.2 kb and 3 kb fragments. Once identified, respective colonies were further cultured for high yield followed by maxi-prep plasmid purification of pBS Rgnef (figure 3-01 B). It was then possible to synthesise antisense RNA probes from the 3' end of the full length cDNA sequence of *Rgnef* (Figure 3-01 C).

3-1-02 Rgnef ventral neural tube expression in developing embryos

Whole mount *in situ* hybridisation (WMISH) on six E10.5 embryos using *Rgnef* antisense RNA probes revealed defined *Rgnef* expression all along the neural tube (Figure 3-02 B). WMISH on E10.5 embryos using *Shh* antisense RNA probes were also prepared and demonstrated a comparable, although more intense, expression pattern along the neural tube (Figure 3-02 A). Transverse sections of neural tube revealed *Rgnef* expression was localised to the ventral region of the neural tube, in the floor plate (Figure 3-02 D). This was similar to the floor plate expression domain observed for Shh although, unlike Shh, *Rgnef* was not expressed in the notochord (Figure 3-02 C and D). This expression pattern was not observed in *Rgnef* sense controls. The results are consistent with *Rgnef* expression potentially playing a role in neural tube development and Shh signalling.

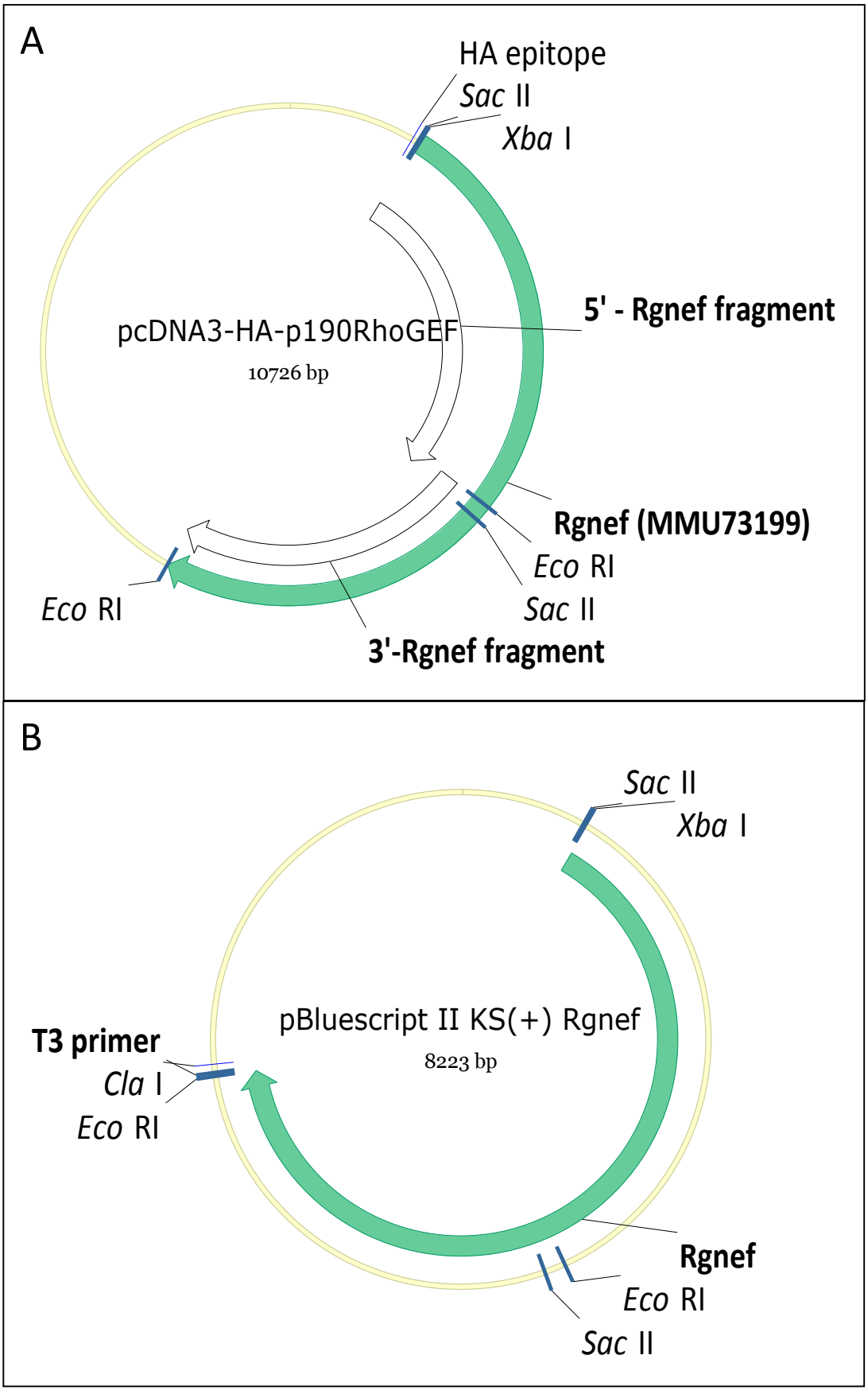
A
HA epitope
Sac II
Xba I
pcDNA3-HA-p190RhoGEF
10726 bp
5' - Rgnef fragment
Rgnef (MMU73199)
Eco RI
Sac II
Eco RI
3'-Rgnef fragment
B
Sac II
Xba I
pBluescript II KS(+) Rgnef
8223 bp
T3 primer
Cla I
Eco RI
Rgnef
Eco RI
Sac II

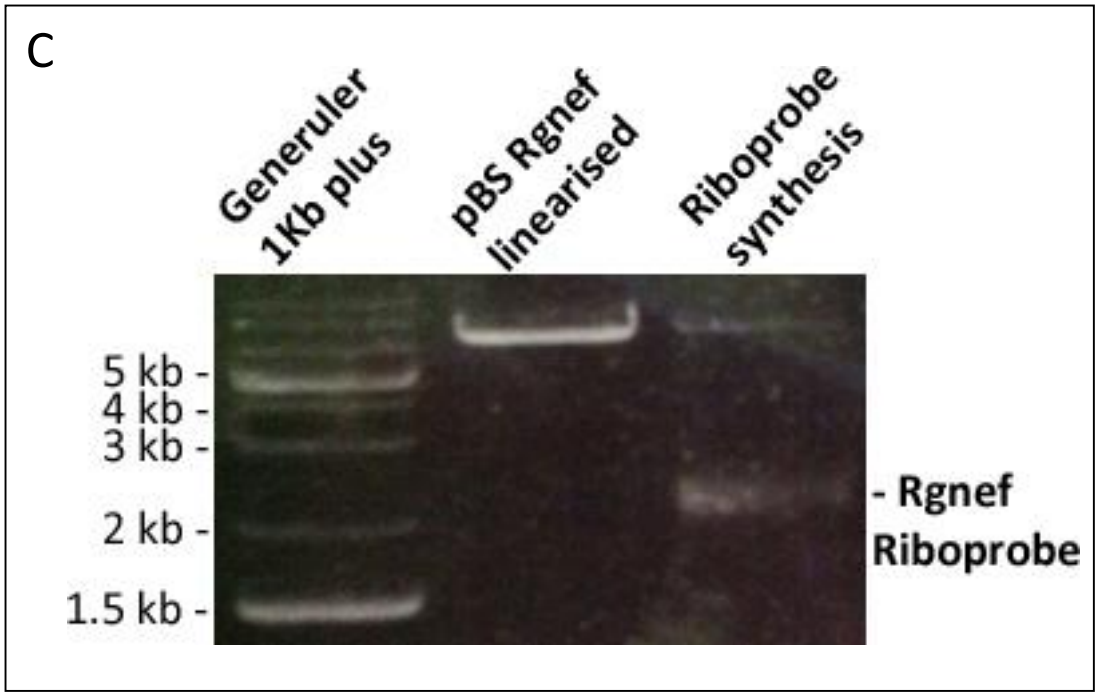

Figure 3-01 Working schematic of pcDNA3-HA-p190RhoGEF and Rgnef Riboprobe synthesis

(A) A working schematic of pcDNA3-HA-p190RhoGEf; an *Rgnef* expression construct that adds a 5' HA tag epitope (Gebbink et al., 1997). Multiple cloning site information was found to be incomplete after preliminary restriction enzyme mapping. *Rgnef* insertion site regions were sequenced to detail the multiple cloning sites flanking the inserted 6.2 Kb *Rgnef* sequence. This was then used to accurately combine sequences for pcDNA3 and 6.2 Kb *Rgnef* (MMU73195). It was then possible to discover a means of removing *Rgnef* in full by restriction digest removal of two fragments, 5'-Rgnef and 3'-Rgnef using SacII and EcoRI restriction enzymes. (B) A schematic of p blusescript II (K+) Rgnef (pBS Rgnef), the final plasmid construct that was used to synthesise Rgnef riboprobe used in this study. (C) Validation of riboprobe synthesis results by loading 5 µl sample of synthesised product onto 1% agarose gel. Results show a 2.2 Kb *Rgnef* riboprobe synthesised from pBS Rgnef. Antisense riboprobe is synthesised from the 3' end of *Rgnef* by T3 RNA polymerase.

A – Shh expression E10.5

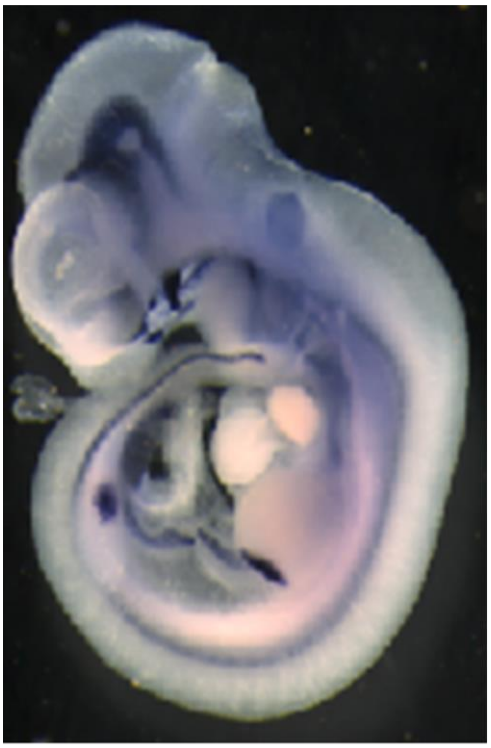

B – Rgnef expression E10.5

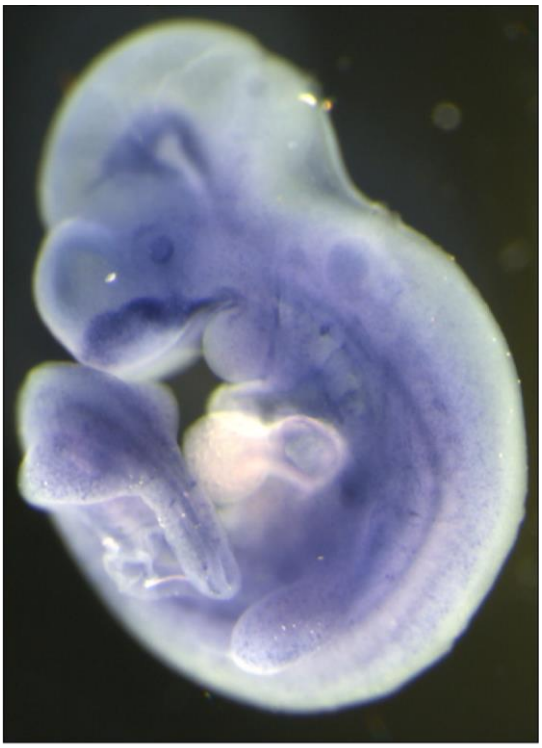

C – Shh expression E10.5

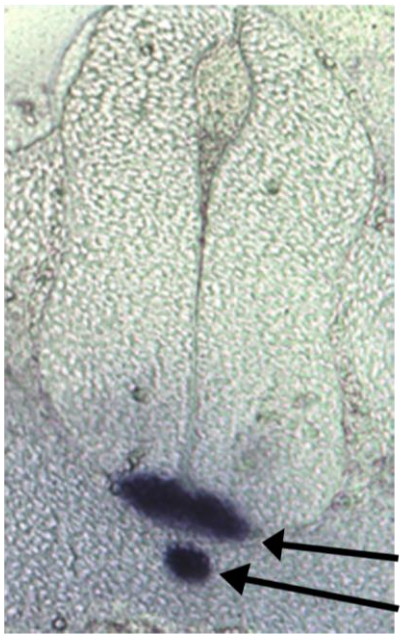

D – Rgnef expression E10.5

E – Rgnef sense control E10.5

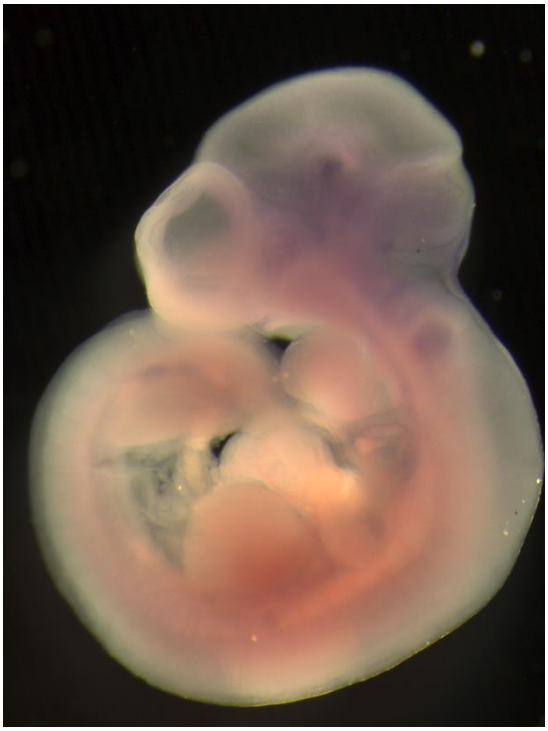

Figure 3-02 In developing embryos *Rgnef* is expressed in the neural tube

Representative example of wholemount *in situ* hybridisation on E10.5 wild-type embryos with antisense probe for (A) *Shh* and (B) *Rgnef* expression.(A-B) *Rgnef* antisense probe reveals expression all along the neural tube that is comparable to neural tube expression of Shh neural tube expression. (C) Mid region neural tube transverse sections reveals intense Shh expression in floorplate and notochord (D) *Rgnef* expression is also detected in the floorplate but not in the notochord. (E) Negative control preparation using Rgnef sense probe on E10.5 wild-type embryo reveals a distinct lack of neural tube expression demonstrated in (B) when using Rgnef antisense probe.

3-02 Efficacy of Shh-LIGHT2 cell assay in monitoring Shh pathway activation

The hypothesis that *Rgnef* is involved in regulating the activity of the Shh signalling pathway was tested functionally using the Shh-LIGHT2 cell assay. The aim was to test whether changes in pathway activation were detectable following forced changes in *Rgnef* expression level. Shh-LIGHT2 cells provide a cell based assay that can monitor states of Shh pathway activation. Initially a mouse fibroblast NIH 3T3 cell line, these cells were adapted by stably transfecting with two reporter constructs (Taipale et al., 2000). Quantitative assay of Gli activity is achieved using a firefly-luciferase reporter gene with 8 copies of the Gli-binding site promoter (Sasaki et al., 1997). Shh signalling pathway Gli activator transcription factors will attach to the Gli binding sites and drive firefly-luciferase expression to providing a detectable readout of activity in the presence of a luminescent substrate. The second reporter enables cell number normalisation between experimental replicates as it encodes a stable Renilla luciferase enzyme and different luminescent substrate (Taipale et al., 2000). Tests were carried out in order to ensure that in our hands, the Shh-LIGHT2 cells provided a viable test for Shh pathway activation. Shh pathway stimulation was achieved by Smoothened-agonist purmorphamine. Shh pathway stimulation was tested by purmorphamine in a dose response manner with readings taken at 0.05, 0.5, 5 and 50 µM purmorphamine concentrations (Figure 3-03 A). Readings conform to a dose response curve with maximum activation at 5 µM and 0.6 µM EC50. At the highest dose of purmorphamine, luciferase activation starts to drop. Cell toxicity is not observed as there are no changes in relative cell number indicated by the renilla reporter. The assay window is the measure of minimum and maximum levels, calculated here as the difference between unstimulated and purmorphamine-stimulated signalling states. The maximum level of activation was calculated as the normalised Gli luciferase response at 5 µM purmorphamine, ensuring luminescence reading from a blank (DMEM culture media) was subtracted. Taking the background level of response as the baseline, 5 µM purmorphamine activation led to an approximately 10-fold increase in response (Figure 3-03 B). The assay window was also tested across a range of cell confluence levels. The results show that above 50% cell confluence it is possible to clearly discern between cell activation states (Figure 3-03 C).

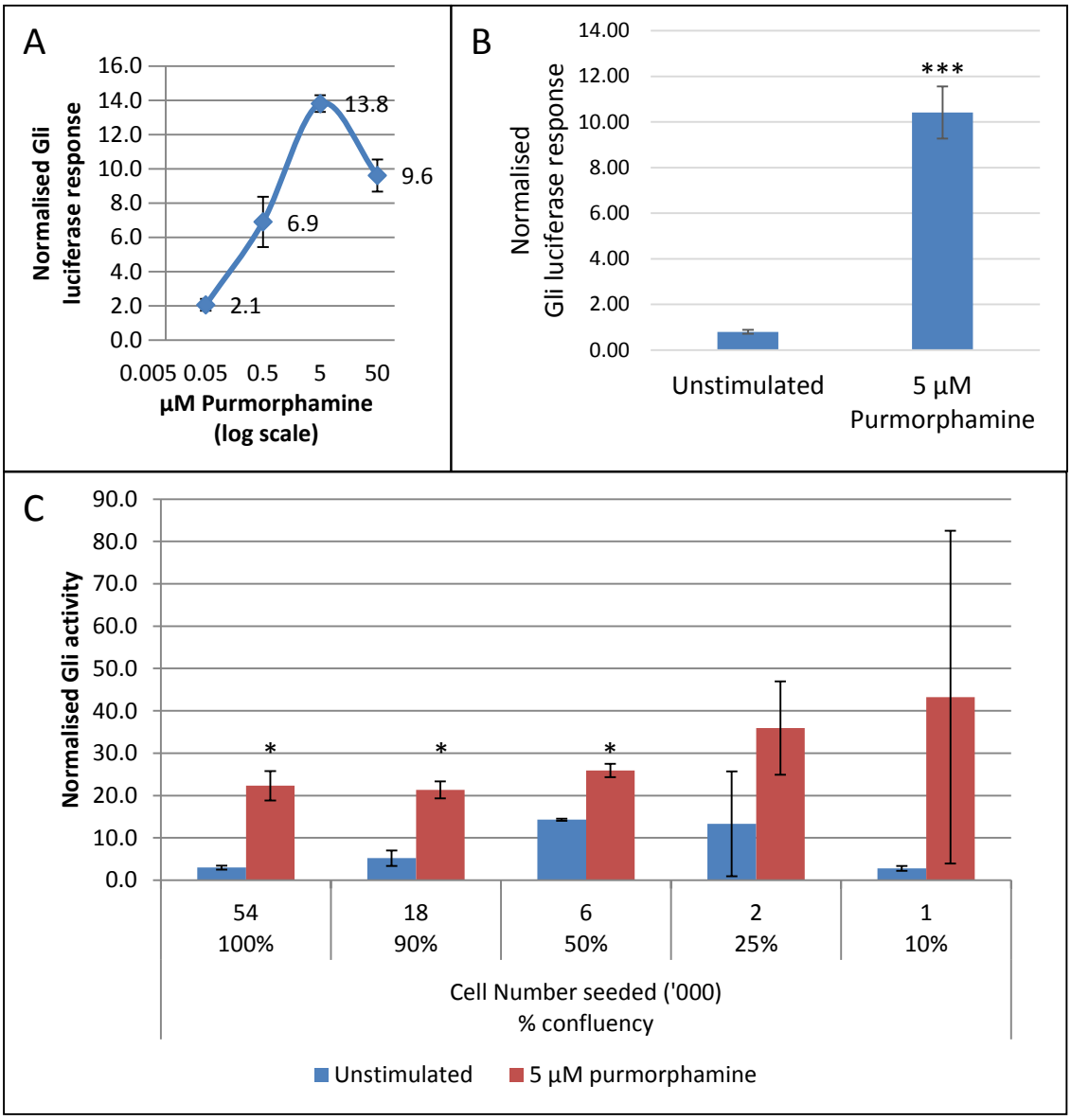
A
Normalised Gli luciferase response
16.0
14.0
12.0
10.0
8.0
6.0
4.0
2.0
0.0
13.8
9.6
6.9
2.1
0.005 0.05 0.5 5 50
µM Purmorphamine (log scale)
B
Normalised Gli luciferase response
14.00
12.00
10.00
8.00
6.00
4.00
2.00
0.00
***
Unstimulated
5 µM Purmorphamine
C
Normalised Gli activity
90.0
80.0
70.0
60.0
50.0
40.0
30.0
20.0
10.0
0.0
*
*
*
54 100%
18 90%
6 50%
2 25%
1 10%
Cell Number seeded ('000)
% confluency
Unstimulated
5 µM purmorphamine

Figure 3-03 Shh-LIGHT2 cell reporter assay detects Shh pathway activation

(A) Dose response Purmorphamine activation of Shh-LIGHT2 reporter assay. At 95% confluence, cells were serum starved for 24 hours before Shh pathway was stimulated at 0.05, 0.5, 5 and 50 µM purmorphamine concentrations (n=4). The resulting dose response curve shows maximum activation at 5 µM and the EC50 at 0.6 µM purmorphamine (B) The difference between purmorphamine stimulated and unstimulated cells. A concentration of 5 µM purmorphamine used to activate the cells led to an approximately 10 fold increase in luciferase activity and is a measure of the potential assay window ($p<0.001$, n=12). (C) The effects of reducing cell number on normalised Gli activity. Cells were seeded in 96-well plates using the range of initial cell numbers indicated. Following overnight incubation the percentage cell confluence was approximately determined before being left 24 hours in low serum conditions. Cells were incubated for a further 24 hours in the presence (red) or absence (blue) of 5 µM purmorphamine. The resulting combined Gli-luciferase normalised activation level is stable and comparable between experiments provided confluence is above 50% ($p<0.05$, n=2).

3-03 Rgnef siRNA transfection validation

Shh pathway activation in Shh-LIGHT2 cells can provide a means to monitor any changes in relation to variation in *Rgnef* expression. To achieve *Rgnef* gene suppression cells were transfected with a 20 nM pool of 4 *Rgnef* siRNA oligonucleotides. Once bound to their targets, creation of dsRNA evokes RNA-induced silencing complex (RISC) proteins that effectively remove them before they can direct protein synthesis (Filipowicz, 2005).

Identification of endogenous *Rgnef* expression in Shh-LIGHT2 cells was first achieved by standard PCR (Figure 3-04). Following on from this, the effect of targeted siRNA knockdown on *Rgnef* expression was monitored by quantitative RT-PCR (RT-qPCR), using SYBR green assays. Experiments compared cells transfected with *Rgnef*-targeted siRNA against cells transfected with non-target siRNA. Expression changes were calculated using the $2^{-\Delta\Delta C_T}$ method and accurate normalisation was achieved by using GeNorm to ensure stable reference genes were selected (section 2-4-03) (Livak and Schmittgen, 2001, Vandesompele et al., 2002). The overall results show the average of all geNorm values M was less than 0.2, an indication of very high reference target stability. Specifically, the optimal number of reference targets in this experimental situation is 2 (geNorm V <0.15). ATP synthase subunit and β-Actin were identified as the two most stable reference genes for optimal normalisation (Figure 3-05 A). When using ATP synthase subunit and β-Actin as calibrators, *Rgnef* siRNA transfection was found to reduce *Rgnef* gene expression by 50% (Figure 3-05 B).

In summary, Rgnef siRNA transfection has been shown to reduce endogenous *Rgnef* expression. Also highlighted is the importance of identifying stable reference genes particularly in relation to the sensitivity required when detecting a reduction in gene expression.

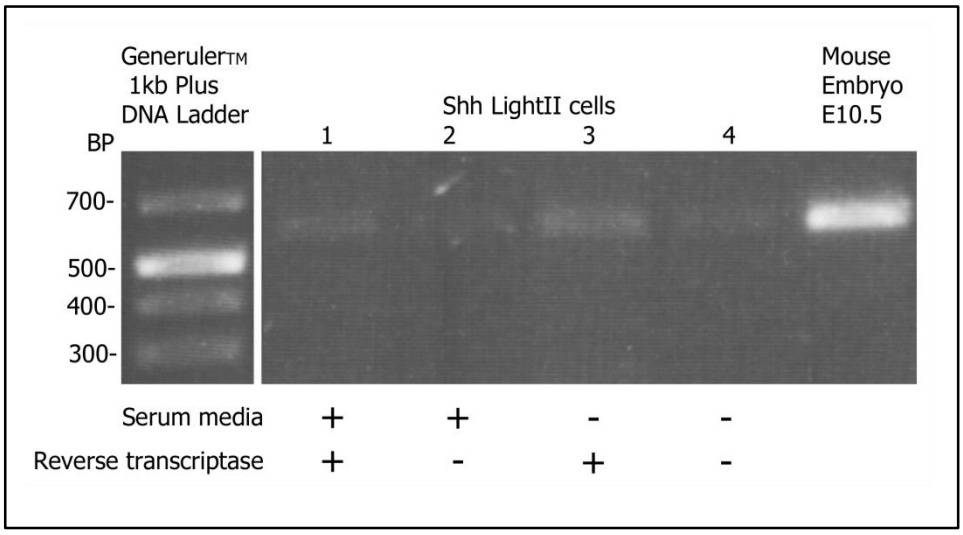

Figure 3-04 PCR detection of endogenous rgnef expression in Shh-LIGHT2 cells

(A) Primers designed from *Rgnef* sequence accession number NM_12026.2 are predicted to produce a PCR product of 585 bp. These primers successfully detected *Rgnef* from E10.5 mouse embryo cDNA. Detection of *Rgnef* in Shh-LIGHT2 cells is shown by bands in lane 2 and 4. The faintness of the bands suggests a low amount of template cDNA synthesis or initial RNA extraction. Lanes 1-2 and 3-4 differ by the presence or absence of serum in the culture media; lanes 3-4 are from cells cultured in serum free media whereas lane 1-2 are from cells cultured in standard 5% serum media. These two types of culture media are required during each Shh LII experimental assay. Lane 2 and 4 cDNA synthesis controls are RT reactions without the reverse transcriptase enzyme. The bands here are considerably fainter than *Rgnef* primer detection in lane 1 and 3. Genomic DNA is not detected as primers were designed to be intron spanning and RNA samples were treated with DNAse to remove any contaminating genomic DNA prior to cDNA synthesis. In conclusion, the contrast in intensity only provides preliminary evidence that endogenous *Rgnef* is detected in Shh Light cells.

A

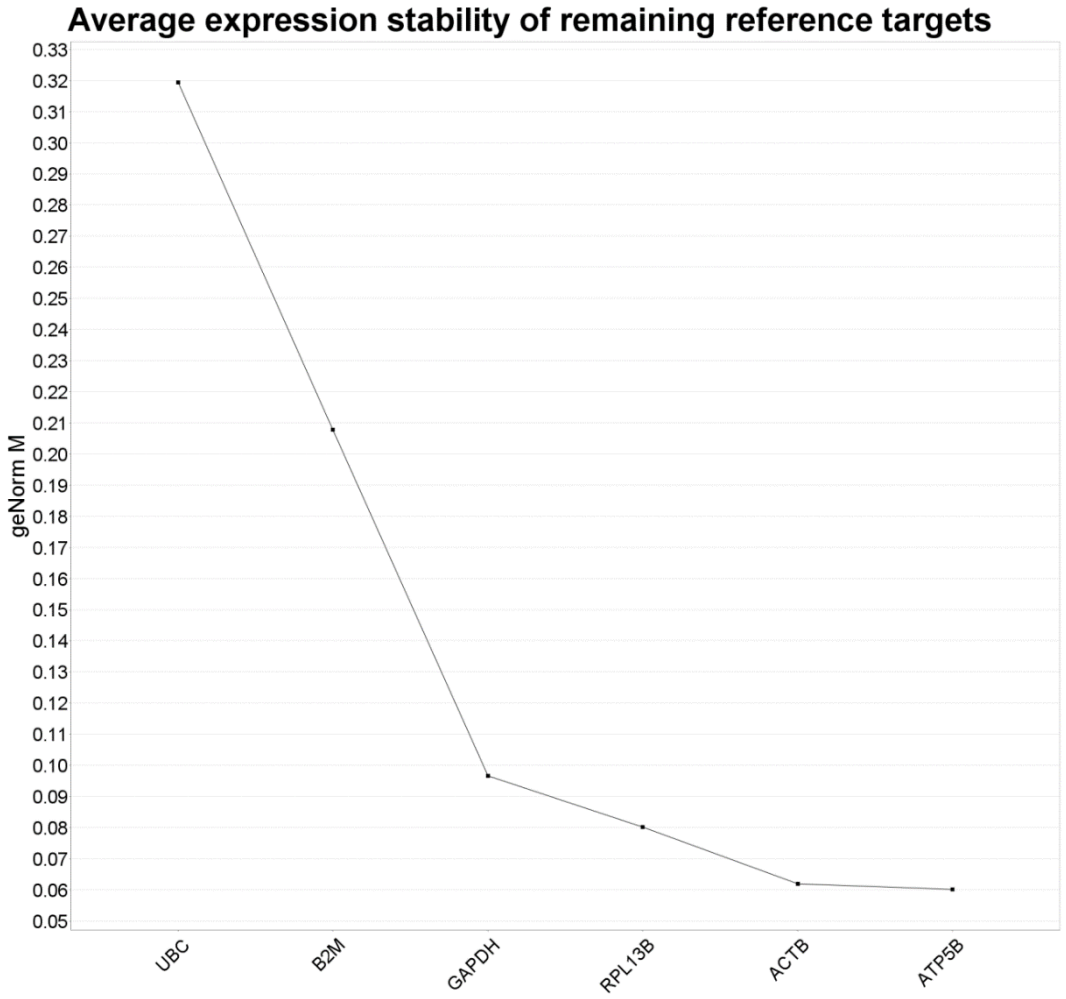
Average expression stability of remaining reference targets
geNorm M
0.33
0.32
0.31
0.30
0.29
0.28
0.27
0.26
0.25
0.24
0.23
0.22
0.21
0.20
0.19
0.18
0.17
0.16
0.15
0.14
0.13
0.12
0.11
0.10
0.09
0.08
0.07
0.06
0.05
UBC
B2M
GAPDH
RPL13B
ACTB
ATP5B

B

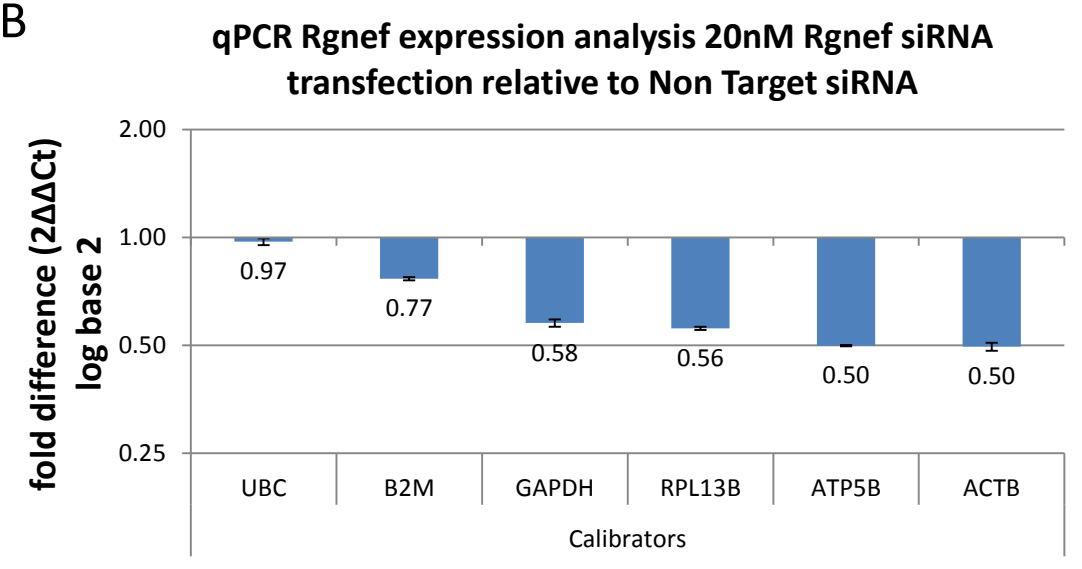
qPCR Rgnef expression analysis 20nM Rgnef siRNA transfection relative to Non Target siRNA
fold difference (2ΔΔCt) log base 2
2.00
1.00
0.50
0.25
0.97
0.77
0.58
0.56
0.50
0.50
UBC
B2M
GAPDH
RPL13B
ATP5B
ACTB
Calibrators

Figure 3-05 RT-qPCR validation of Rgnef siRNA knockdown in Shh-LIGHT2 cells

(A) RT-qPCR using 6 reference genes; GAPDH, β2-Microglobulin (B2M), ribosomal protein L13a (RPL13A) ubiquitin C (UBC), ATP synthase subunit (ATP5B) and β-Actin(ACTB). The stability of the reference genes could be assessed ,under these specific experimental conditions, based on relative expression with each other (Vandesompele et al., 2002). (B) The two most stable reference genes were ATP5B and ACTB and both equally concluded the highest level of suppression, a 50% reduction of *Rgnef* expression.

3-04 Lipid based transfection reagents reduce the Shh-LIGHT2 cell based assay window

Investigating loss of targeted gene function in the Shh-LIGHT2 cell based assay was achieved through transfection of siRNA oligonucleotides. To assist the passage across cell membranes siRNA is complexed with lipid-based transfection reagent Dharmafect® (Dharmacon Ltd). However tests revealed that Dharmafect® treated cells had suppressed activation when stimulated with 5 μM purmorphamine ($p<0.001$, $n=12$) (Figure 3-06 A). Furthermore the baseline level of activation detected in unstimulated cells was also reduced when cells were treated with Dharmafect ($p=0.013$, $n=12$), thus demonstrating an effect produced by Dharmafect alone and not in combination with stimulating agent purmorphamine (Figure 3-06 A). Although the assay window is reduced, Dharmafect treated cells are still able to show significant differences between activation states ($p=0.001$, $n=12$) (Figure 3-06 A).

Although the integrity of the assay window from Dharmafect treatment is still sufficient to measure changes in Shh pathway activation, this in itself cannot be taken to imply that the cell and molecular mechanisms of the Shh signalling pathway are now entirely representative of a normal state. One organelle in particular, the primary cilium, is hypothesised here to be particular susceptible to lipid-based transfection reagents. In allowing passage through cell membranes, lipid based transfection reagents are disruptive to cell membranes and the proteins they contain. Hence Dharmafect may directly disrupt the primary cilia or the process of ciliogenesis, putting into question the efficacy of these cells in representing the Shh pathway. The effect of Dharmafect on primary cilia was examined by immunocytochemistry comparison of Dharmafect treated and untreated NIH 3T3 cells. Cells were stained with mouse anti-acetylated tubulin primary antibody, as tubulin acetylation is a post translational modification found predominately in primary cilia and visualised in red with secondary antibody anti-mouse Alexa Fluor 594. Preparations were mounted with Vectashield™ mounting media (Vector Labs) plus nuclear stain DAPI and viewed with 60X oil immersion objective. Images taken at random clearly displayed contrasting nuclei in blue and and cilia in red (Figure 3-06 B). Comparisons of the proportion of cells exhibiting cilia were found to not be significantly different between treated and untreated cells (Figure 3-06 C). These results provide evidence that transfecting with

Dharmafect does not lower primary cilia numbers. Given the importance of primary cilia in Shh signal transduction, a lack of primary cilia in Shh-LIGHT2 cells would make this assay an obsolete reporter of Shh pathway activity. Hence the results provide a level of confidence for Dharmafect treated Shh-LIGHT2 cells as adequate reporters of pathway activity.

A

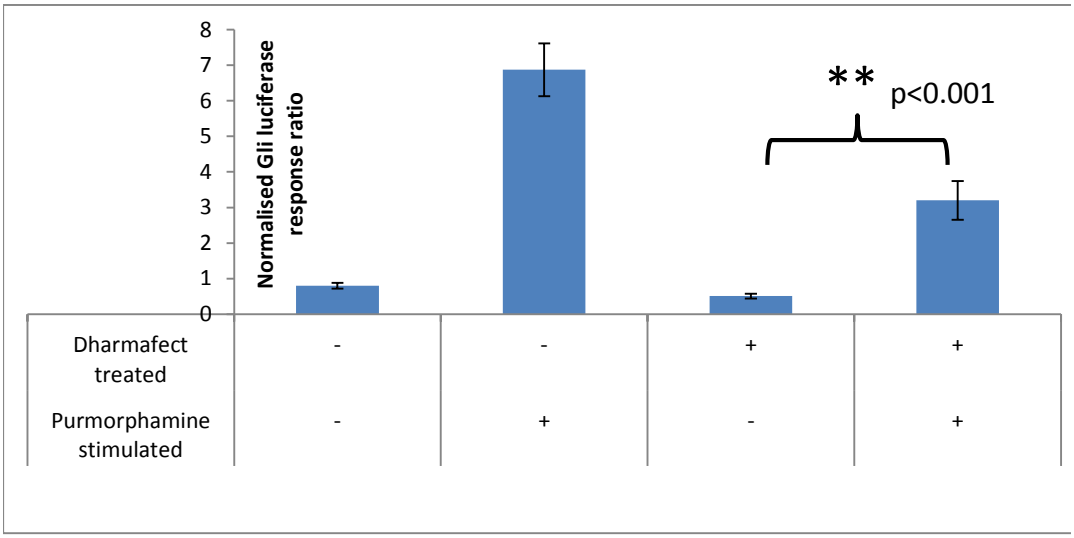

B

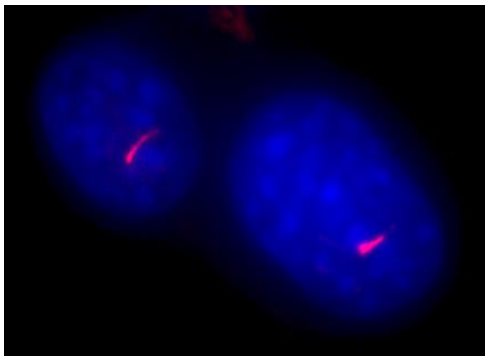

Blue = DAPI nuclear stain
Red = acetylated tubulin

C

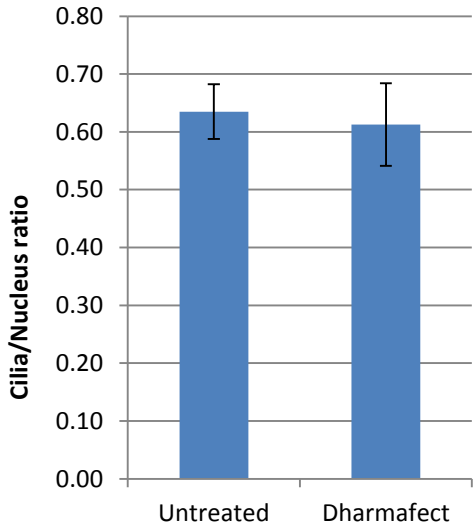

Figure 3-06 Dharmafect suppresses Shh pathway cell assay response without affecting number of cells expressing cilia.

(A) NIH 3T3 cells grown in 96 well plate wells were incubated in transfection reagent before 24 hour serum starvation. Transfection reagent Dharmafect suppresses both the background level of Gli reporter activation ($p<0.001$, $n=12$) and the level of 5 µm purmorphamine stimulated activation ($p=0.013$, $n=12$). Despite the effect of Dharmafect, the Shh-LIGHT2 assay window can still distinguish between activation states ($p=0.001$, $n=12$). (B) An example image of well contrasted cell nucleus in blue and primary cilia in red. Cells were probed with mouse anti-acetylated tubulin primary antibody and stained in red with Alexafluor anti-mouse 585 fluorescent secondary antibody. Preparations were mounted with Vectorshield plus DAPI (blue). (C) Results summarising image counts of cilia and nucleus in repeated images of stained cells. The ratio of cilia to nucleus in 190 Dharmafect treated cells is not significantly different when compared to ratio of cilia to nucleus in 163 untreated cells.

3-05 Investigating the role of Rgnef in Shh pathway regulation

The assay results of Shh-LIGHT2 cells transfected with 20 nM *Rgnef*-targetted siRNA were compared with Non-target siRNA transfected cells to ensure the changes were based only on the effect of specific *Rgnef* targeting sequences. Shh Pathway activation was induced by 5 µM purmorphamine and luminesce measured using the Promega dual-Glo Luciferase assay.

Results show a significant 22% suppression of normalised Gli-luciferase activity following *Rgnef* siRNA knockdown compared to non-target siRNA transfected cells ($p=0.01$, $n=52$) (Figure 3-07). A further increase of *Rgnef* siRNA concentration to 100 nM resulted in 43% suppression. As shown above (Section 3-03) the knockdown of *Rgnef* expression identified by RT-qPCR was 50%, so that at best not even a near complete knock down of expression and yet suppression of pathway activation was observed. The results therefore provide evidence for Rgnef requirement during Shh pathway activation.

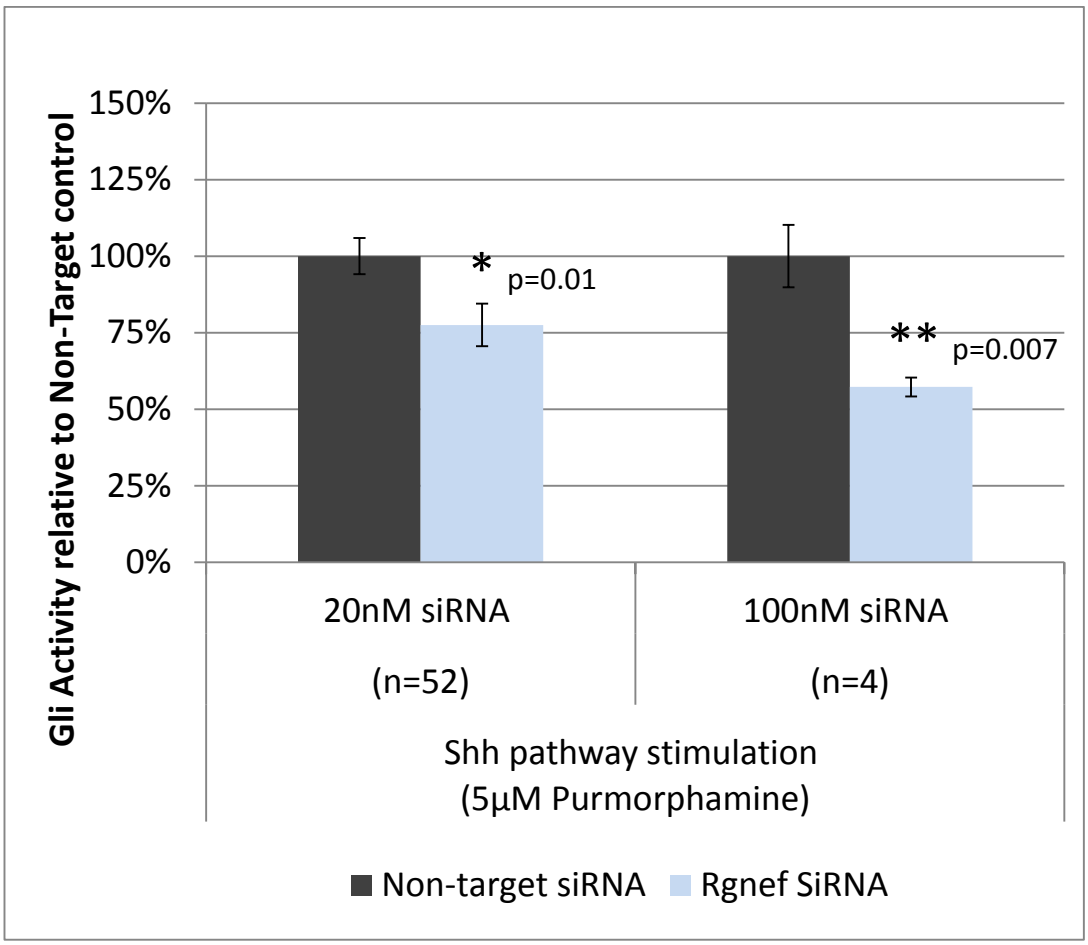

Figure 3-07 Investigating the role of Rgnef in Shh pathway regulation

Shh-LIGHT2 cells are serum starved to induce ciliogenesis prior to Shh pathway activation induced by 5µM purmorphamine. Shh-LIGHT2 cell assay results show that pathway stimulation is significantly suppressed in cells transfected with *Rgnef* siRNA compared to cells transfected with non-target siRNA under the same conditions. A five-fold increase of *Rgnef* siRNA treatment to 100 nM further suppresses activation. The results identify Rgnef as a Shh pathway activator.

3-06 Investigation of Rgnef over-expression on Shh signalling pathway

A further test for the involvement of Rgnef in regulating Shh signalling was achieved by observing the effect of Rgnef overexpression on the Shh signalling pathway. The overexpression of HA tagged Rgnef was possible by using plasmid construct pcDNA3-HA-p190RhoGEF (Gebbink et al., 1997). The expressed HA-taggedRgnef protein can assist in future protein purification or protein localisation studies. However, as the addition of an HA tag may impair normal protein function, a second sub-clone of Rgnef in pCAGGS-IRES-nls-GFP plasmid vector was also constructed. Expression vector pCAGGS-IRES-nls-GFP (pCAGGS) is a bicistronic mammalian expression vector consisting of a gene insertion site upstream of an internal ribosomal entry site (IRES) and nuclear localization sequence (nls) (Niwa et al., 1991). Therefore pCAGGS Rgnef can independently express untagged Rgnef protein and GFP protein , hence a means of validating plasmid transfection without adding (potentially) functionally interfering attachments to your protein of interest. Furthermore pCAGGS Rgnef is an ideal construct for *in ovo* electroporation of chick embryo, a powerful system to study *in vivo* effects of increasing *Rgnef* gene expression on dorsal ventral patterning (Voiculescu et al., 2008, Briscoe and Ericson, 2001).

3-6-01 pCAGGS Rgnef: Subcloning Rgnef from pBS Rgnef into pCAGGS

Full length Rgnef was extracted from pBS Rgnef (Section 3-01) through *Xba*I and *Cla*I double digest, then ligated into pCAGGS plasmid multiple cloning sites prepared by *Nhe*I and *Cla*I double digest. The overhanging DNA strand created by *Xba*I digest at the 5' end of Rgnef fragment complements the *Nhe*I overhang at the 3' end of pCAGGS. The *Cla I* site on pCAGGS was initially found to be blocked by *Dam* I methylation, which was overcome by preparing the plasmid in *Dam* I methylation mutated *E.coli* SCS110 Competent cells. These cells lack the ability to produce Dam1 methylation, so that the block on the *ClaI* restriction sites was removed.

The *Nhe*I and *Xba*I enzyme digests produce complementary DNA strand overhangs, but once ligated both the *Nhe*I and *Xba*I restriction enzyme sites are lost. After ligation, the construct was tested by *Eco*RV restriction enzyme digestion that produced the expected result for correct insertion; two fragments sized at 7kb and 4kb. Sequencing

of the entire Rgnef insert was also conducted, including both insertion sites to confirm that pCAGGS Rgnef was achieved without introducing any mutations.

Testing for GFP expression was also conducted by transfection into NIH 3T3 mouse fibroblast cells. Before Rgnef gene insertion, the vector pCAGGS produced detectable GFP expression. However, after Rgnef insertion the GFP expression was almost undetectable, sometimes just visible. Excision of the majority of the Rgnef insert, by *Eco*RV enzyme digestion and religation again enabled the expression of GFP. This verified that there was no mutation within the GFP expression part of the construct. Thus the presence of an Rgnef insert diminishes GFP expression from the bi-cistronic construct. As it is not possible to monitor pCAGGS Rgnef transfection, the construct cannot be used in chick electroporation studies. However pCAGGS Rgnef was still viable as an Rgnef expression construct to be used to assess overexpression in Shh-LIGHT2 assay experiments.

3-6-02 Rgnef over-expression stimulates the Shh signalling pathway

Quantitative validation of Rgnef expression increase induced by pCAGGS Rgnef and pcDNA3-HA-p190RhoGEF transfection was validated by quantitative RT-PCR using the $2^{-\Delta\Delta C_T}$ method. Under these experimental conditions, a geNorm stability analysis was conducted using 6 reference genes; GAPDH, β2-Microglobulin, ribosomal protein L13a, ubiquitin C, ATP synthase subunit and β-Actin. All primers were pre-validated to ensure they targeted their specific genes and ubiquitin C, ATP synthase subunit and β-Actin were designed to be intron-spanning. The expression changes could now be assessed by identifying the most stable reference gene under these specific experimental conditions (Claes et al., 2002). Overall the results show very high reference target stability (geNorm < 0.2) and amongst them GAPDH was found to be the single most stable gene under these experimental conditions (Figure 3-08 A). Using GAPDH for reference gene calibration, an increase in Rgnef expression of 356 fold was detected in cells transfected with pCAGGS Rgnef and 86 fold with regards to pcDNA3-HA-p190RhoGEF (Figure 3-08 B).

Significant Shh pathway activation was detected by the Shh-LIGHT2 cell assay when transfected either with pCAGGS Rgnef ($p=0.013$, $n=12$) or pcDNA3-HA-p190RhoGEF ($p=0.041$, $n=12$) without inducing any prior activation (Figure 3-09 A and B). In order to

also account for the possibility of pathway suppression, transfected cells were monitored after pathway activation induced by 5 µM purmorphamine. Surprisingly, significant pathway activation was also detected in relation to pCAGGS Rgnef transfection ($p=0.035$, $n=12$) in addition to the stimulation induced by potent smoothened agonist purmorphamine (Figure 3-09 A). Possible conclusions are that pCAGGS Rgnef is counteracting the assay window reduction caused by the transfection reagent. Also increased Rgnef in the cells may be affecting pathway suppressors and as such increasing the extent of pathway stimulation.

This increase in pathway activation was not observed in cells transfected with pcDNA3-HA-p190RhoGEF (Figure 3-09 B). Three possibilities may account for the difference between the results for the two Rgnef expression constructs after activation. First the increased gene expression detected by RT-qPCR was 86 fold for pcDNA3-HA-p190RhoGEF, approximately a quarter of the increase induced by pCAGGS Rgnef. Secondly, during pcDNA3-HA-p190RhoGEF transfection experiments, the assay window was reduced by 30% due to a higher baseline level of activation. An increase in the number of experimental samples may therefore provide a statistically significant increase in activation, particularly as an increased trend was observed (Figure 3-09 B). Finally, although pathway activation was induced under unstimulated assay conditions, the addition of an HA tag may have specifically restricted Rgnef's ability to extend pathway activation even after pathway stimulation.

Although the unexpected increase in activation in cells already stimulated should not detract from the main findings of these experiments; Shh pathway activation due to Rgnef over-expression, identifies Rgnef as a Shh pathway activator (Figure 3-09 A and B).

A

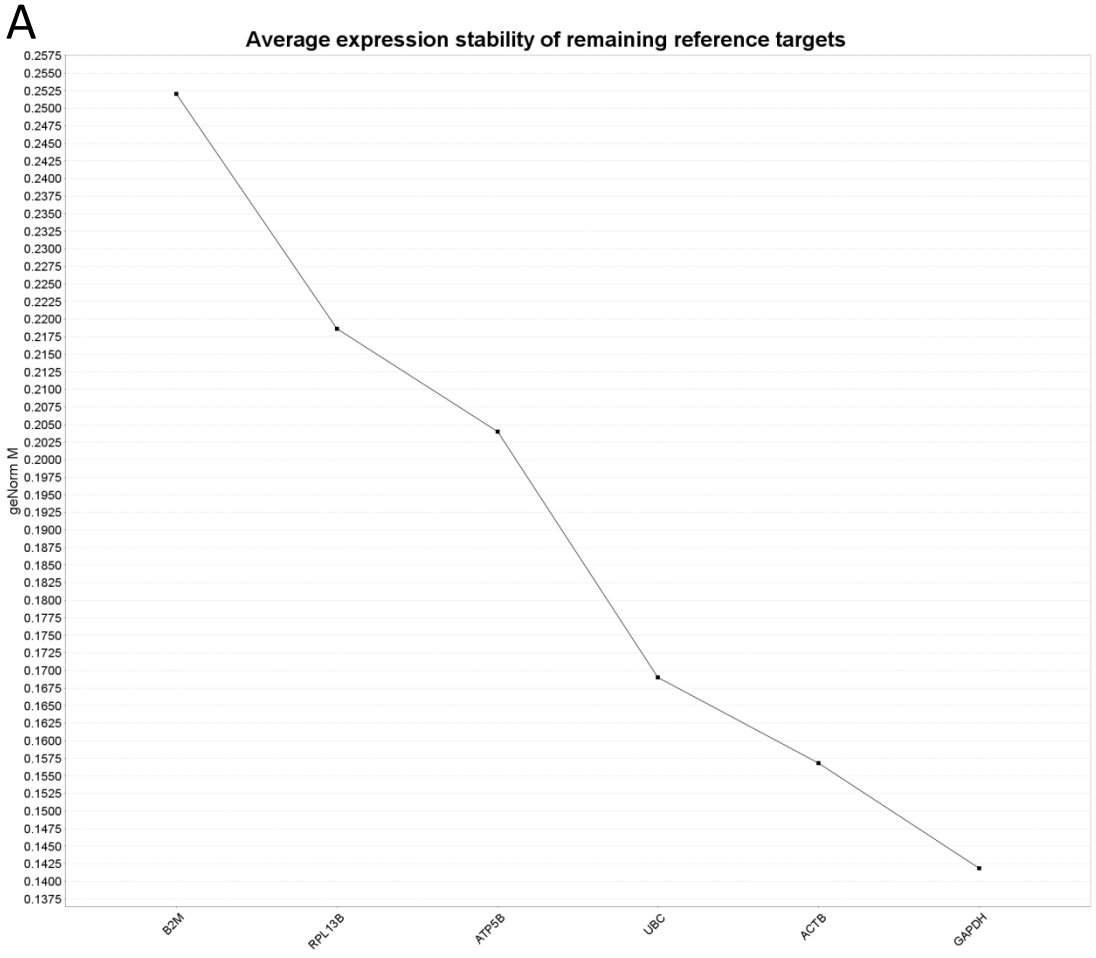
Average expression stability of remaining reference targets
geNorm M
0.2575
0.2550
0.2525
0.2500
0.2475
0.2450
0.2425
0.2400
0.2375
0.2350
0.2325
0.2300
0.2275
0.2250
0.2225
0.2200
0.2175
0.2150
0.2125
0.2100
0.2075
0.2050
0.2025
0.2000
0.1975
0.1950
0.1925
0.1900
0.1875
0.1850
0.1825
0.1800
0.1775
0.1750
0.1725
0.1700
0.1675
0.1650
0.1625
0.1600
0.1575
0.1550
0.1525
0.1500
0.1475
0.1450
0.1425
0.1400
0.1375
B2M
RPL13B
ATP5B
UBC
ACTB
GAPDH

B

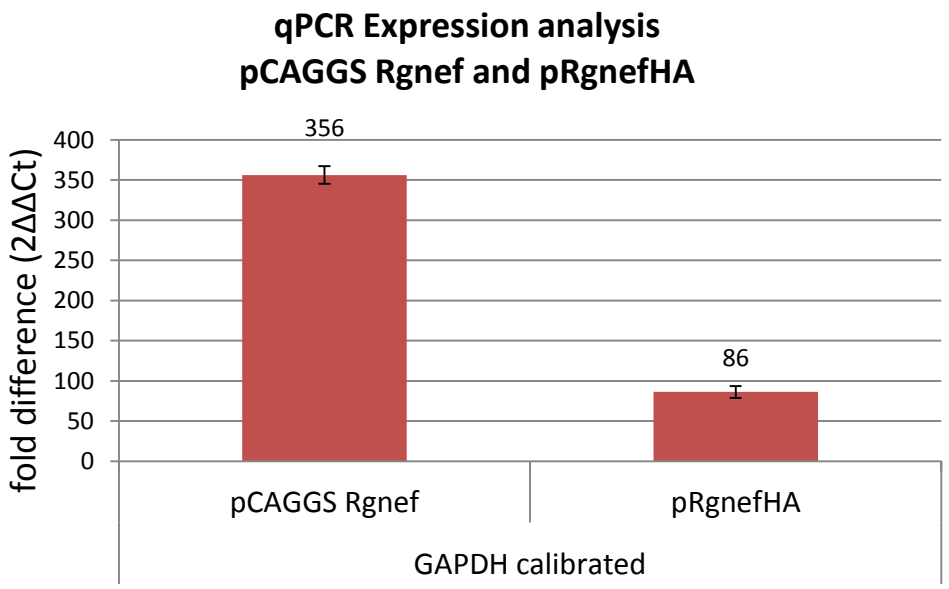
qPCR Expression analysis
pCAGGS Rgnef and pRgnefHA
fold difference (2ΔΔCt)
400
350
300
250
200
150
100
50
0
356
86
pCAGGS Rgnef
pRgnefHA
GAPDH calibrated

Figure 3-08 RT-qPCR validation of over-expression and from pCAGGS Rgnef and pRgnefHA transfection in Shh-LIGHT2 cells

(A) Results of RT-qPCR G-norm analysis for stability of 6 reference genes; GAPDH, β2-Microglobulin (B2M), ribosomal protein L13a (RPL13A) ubiquitin C (UBC), ATP synthase subunit (ATP5B) and β-Actin (ACTB). Expression changes relate to the Shh-LIGHT2 assay of Rgnef overexpression experiments (n=2). The stability of the reference genes were assessed by comparison with each other under the specific experimental conditions (Vandesompele et al., 2002). GAPDH and ACTB were identified as the most stable reference genes. (B) Results of RT-qPCR expression change analysis of Shh-LIGHT2 cells transfected with pCAGGS Rgnef and pRgnefHA. On average, Rgnef expression was increased 356 fold (n=4) and 86 fold (n=2) in response to pCAGGS and pRgnefHA transfection respectively. Expression change was calculated using the 2ΔΔCt method calibrated by GAPDH reference gene expression.

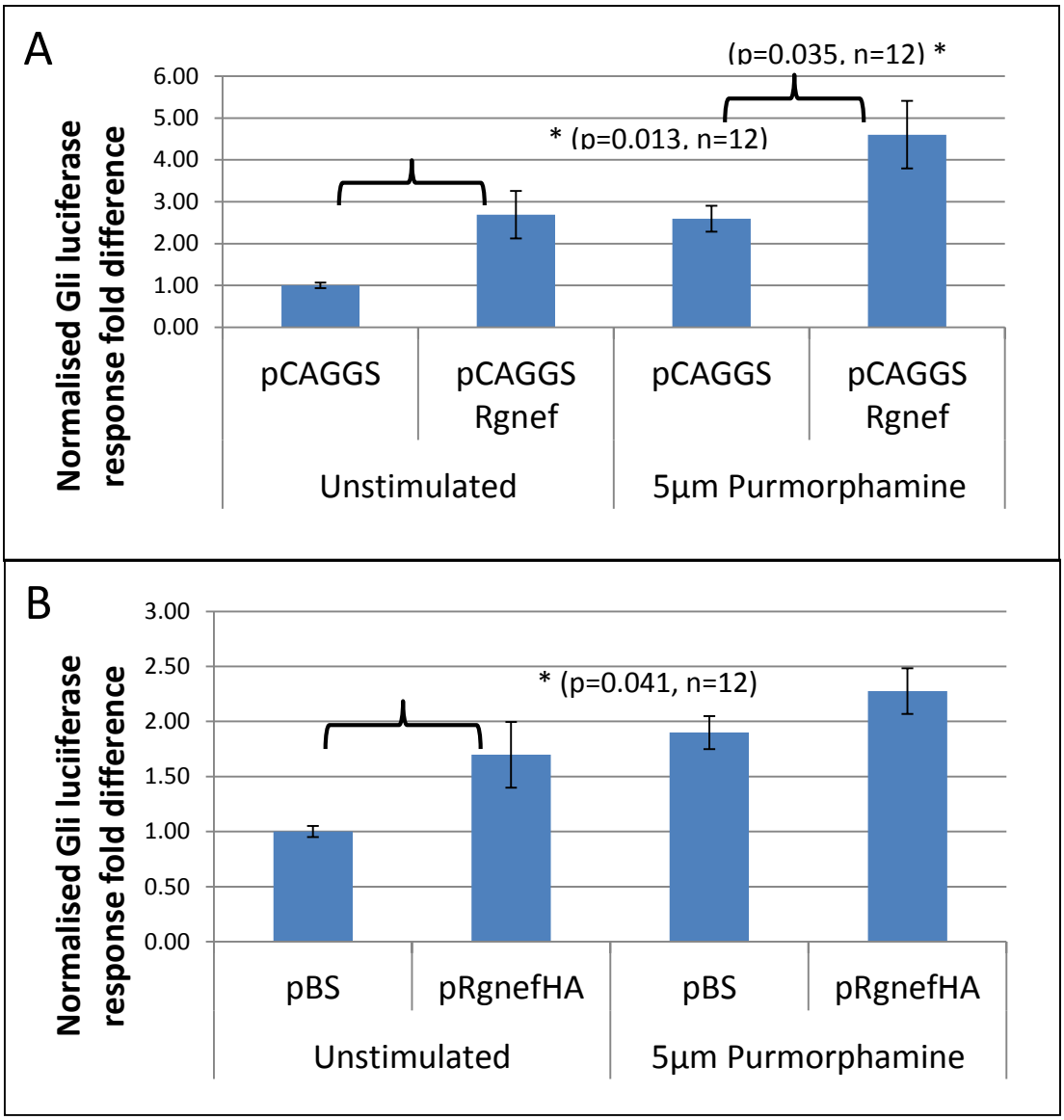
A
Normalised Gli luciferase response fold difference
6.00
5.00
4.00
3.00
2.00
1.00
0.00
(p=0.035, n=12) *
* (p=0.013, n=12)
pCAGGS
pCAGGS Rgnef
pCAGGS
pCAGGS Rgnef
Unstimulated
5µm Purmorphamine
B
Normalised Gli luciferase response fold difference
3.00
2.50
2.00
1.50
1.00
0.50
0.00
* (p=0.041, n=12)
pBS
pRgnefHA
pBS
pRgnefHA
Unstimulated
5µm Purmorphamine

Figure 3-09 Rgnef over-expression results in Shh pathway activation

(A and B) Shh-LIGHT2 cells are transfected with (A) pCAGGS Rgnef and (B) pcDNA3-HA-p190RhoGEF (pRgnefHA) prior to being serum starved to induce ciliogenesis. A comparison is also established between unstimulated cells and cells stimulated with 5µM purmorphamine. (A) Shh-LIGHT2 assay results show that pathway stimulation is significantly increased in cells transfected with pCAGGS Rgnef when pathway unstimulated and further increased in cells already stimulated (B) Shh pathway stimulation is also observed in pRgnefHA transfected cells. The results identify Rgnef as a positive regulator of the Shh signalling pathway.

3-07 Rgnef over expression inhibits primary ciliogenesis

In identifying Rgnef as Shh signalling pathway activator the aim was to investigate Rgnef subcellular localisation, particularly in relation to primary cilia. Experiments to assess Rgnef localisation were conducted in NIH 3T3 cells as they are the same cell line as Shh-LIGHT2 cells before stable transfection of reporters (section 3-02). Ciliogenesis was induced in NIH 3T3 cell by culturing in serum free media and transfection was performed using the same conditions as used to demonstrate Shh pathway activation in Shh-LIGHT2 cells. The cells were then fixed (4% Formaldehyde 0.2% Triton-X PBS) and immunostained with anti-acetylated tubulin antibody to identify each cell's primary cilium. The N-terminal HA tagged Rgnef protein synthesised from pcDNA3-HA-p190RhoGEF construct enabled HA-Rgnef detection by anti-HA antibody. Secondary antibodies Alexa Fluor® 594 (red) and 488 (green) were used for fluorescent detection of primary cilia and Rgnef respectively. Finally the cells were mounted using fluorescent signal guard, Vectashield™ with DAPI nuclear stain to identify each individual cell nucleus.

In untransfected NIH 3T3 cells the nuclei and primary cilia were clearly identified however there was a degree of general nonspecific background fluorescence relating to the use of the anti-HA rabbit polyclonal antibody (Figure 3-10 A, B and E). The anti-HA antibody detected basal body proteins at the base of each cilium, even in the cells without the HA-tagged protein construct transfected (Figure 3-10 E). Although basal body co-localisation evidence would be required to confirm this, the evidence does sufficiently show that that this antibody would interfere with any basal body protein co-localisation results.

Transfected NIH 3T3 cells overexpressing Rgnef protein were clearly identified by high intensity fluorescence (Figure 3-10 A). This is consistent with the high *Rgnef* gene expression detected by RT-qpcr results (Section 3-06). The most evident finding was the lack of primary cilia in cells identified as over-expressing Rgnef (Figure 3-10 A). The control un-transfected cells and even surrounding un-transfected cells were clearly able to ciliate (Figure 3-10 A). The same prepared slides were examined further using confocal microscopy without fluorescent identification of nuclear stain DAPI (Figure 3-10 G). This test was conducted to ensure against the possibility of primary cilium being

masked by the combination of high intensity Rgnef expression, nuclear staining and cell rounding. These high resolution stacked images were able to confirm the absence of primary cilia in Rgnef-over-expressing cells (Figure 3-10 G).

A HA-Rgnef in NIH 3T3 cells

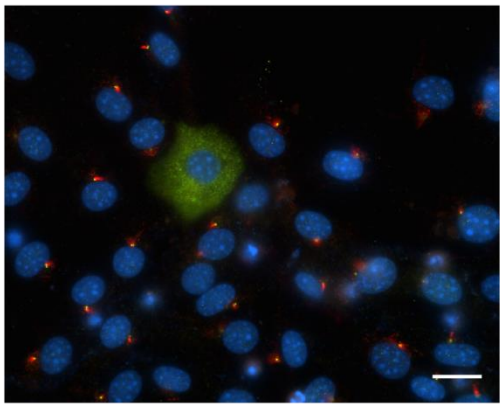

B Anti-HA antibody

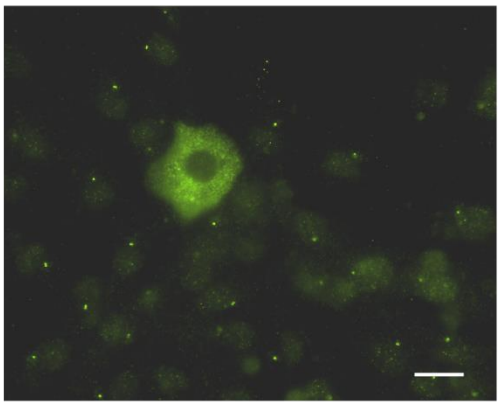

C DAPI (blue)

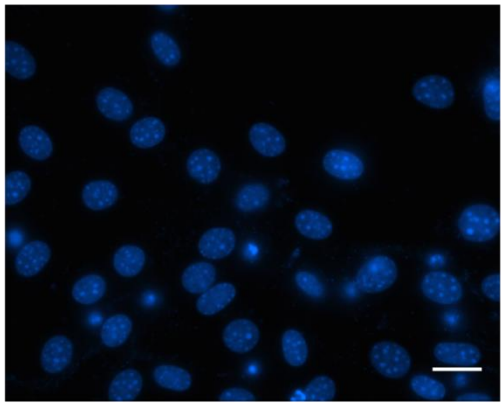

D AC-tubulin (red)

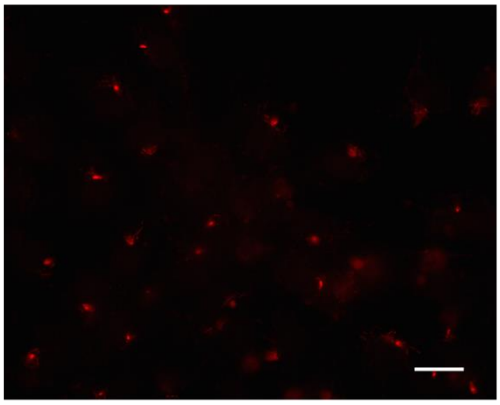

E Untransfected control

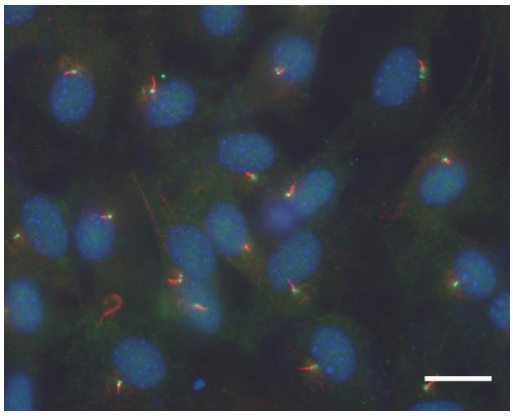

F

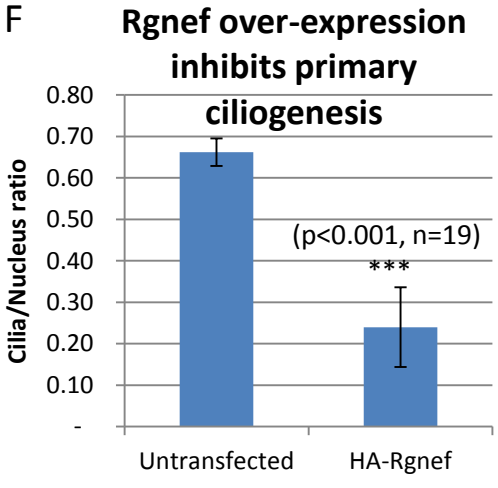

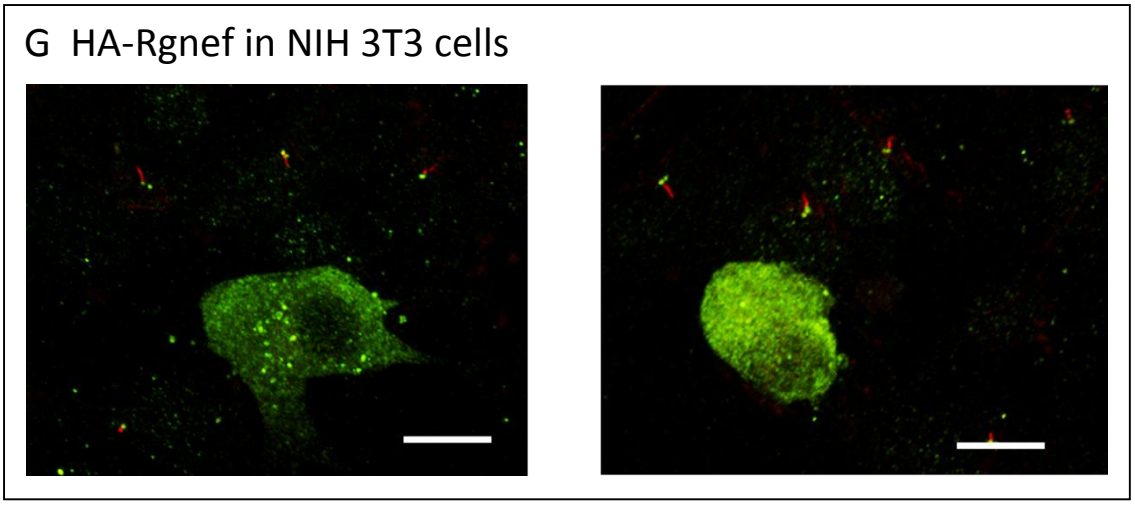

Figure 3-10 Rgnef overexpression inhibits ciliogenesis

(A-D) NIH 3T3 cells are transfected with pcDNA3-HA-p190RhoGEF for tagged HA-Rgnef expression prior to being serum starved to induce ciliogenesis. (A) Merged overlay of cell staining with (B) immunostained for HA tag protein (green), (C) counterstained with DAPI (blue) and (D) immunostained for acetylated tubulin (red). (E) Testing the specificity of antibodies revealed a degree of unspecific binding of basal body proteins by rabbit anti-HA antibody, this did not however deter from detecting Rgnef overexpressing cells. (F) The average primary cilia to nucleus ratio of cells overexpressing HA-Rgnef was significantly reduced compared to the average cilia to nucleus ratio of 739 untransfected cells expressing primary cilia ($p<0.001$, $n=19$). (G) Maximum projection of Z stacks from confocal microscopy to provide further evidence that cells overexpressing Rgnef lack primary cilia. (A-G) Scale bars = 20 µm

3-08 The effect of Rgnef overexpression on Rho activation

The activation of Shh signalling pathway observed by over-expression of Rgnef and HA-Rgnef was investigated in relation to RhoA activation. The aim was to determine if Rgnef overexpression also resulted in the activation of RhoA to help elucidate the mechanism by which the Shh signalling pathway was activated. A preliminary study was undertaken using an active Rho pull-down and detection kit (Thermo Scientific 16116), able to monitor small GTPase activation. The procedure involves column binding activated Rho-GTP moieties and then eluting for immunoblotting that detect the relative levels of activated RhoA, RhoB and RhoC. To ensure the pull down was working effectively, immunoblotting was also conducted using lysate treated with GTPYS (positive control) compared with lysate treated with GDP for negative control (Figure 3-11 A). The results show comparable levels of Rho activation detected in all three transfected cell sample preparations (Figure 3-11 B). The levels of activation were not significantly different in the cells transfected with pCAGGS-Rgnef or HA-Rgnef, compared to cells transfected with pCAGGS alone, showing that increasing Rgnef expression in these cells did not detectably induce Rho activation (Figure 3-11 C).

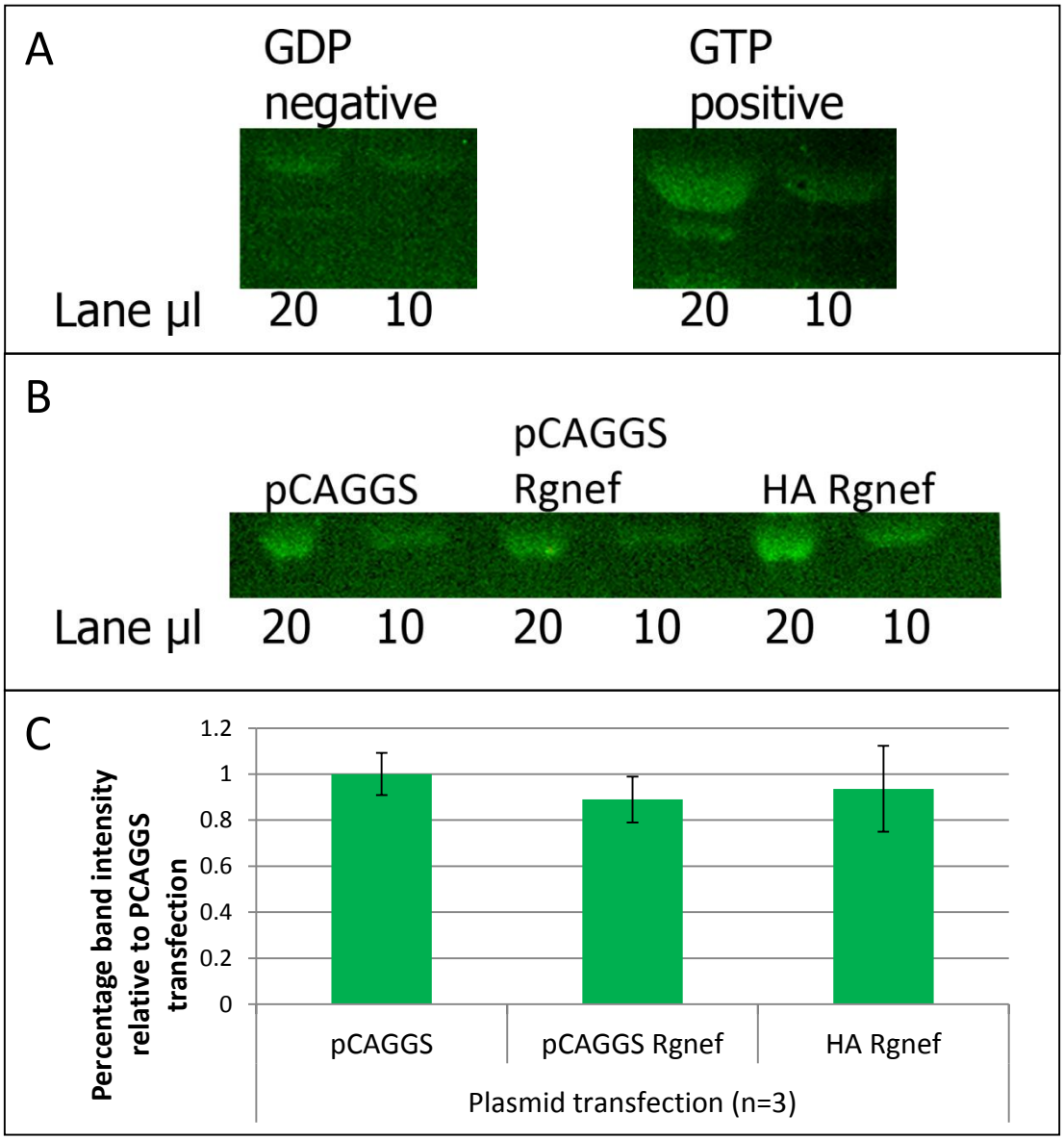
A
GDP
negative
GTP
positive
Lane µl
20
10
20
10
B
pCAGGS
pCAGGS
Rgnef
HA Rgnef
Lane µl
20
10
20
10
20
10
C
Percentage band intensity relative to PCAGGS transfection
1.2
1
0.8
0.6
0.4
0.2
0
pCAGGS
pCAGGS Rgnef
HA Rgnef
Plasmid transfection (n=3)

Figure 3-11 The effect of Rgnef overexpression on Rho activation

(A) Results of positive and negative controls from Active Rho pull-down and detection kit (Pierce Cat 16116). The addition to cell lysate of GTPγS for positive control and GDP for negative control enabled pull down and detection enabled validation of Rho activation assay window. (B) Representative immunoblot showing levels of activated Rho from three transfected NIH 3T3 mouse fibroblast cell samples, cultured in T75 cell culture flasks. The three transfection comparisons were pCAGGS, pCAGGS Rgnef and pcDNA3-HA-p190RhoGEF (HA-Rgnef). As per manufacturer's instructions, lysate was extracted and tested to identify levels of activated Rho through immunoblot band intensity comparison by the Odyssey fluorescent reader (Licor). Two lane volumes, 20 µl and 10 µl were loaded to allow a choice for optimal band intensity for comparison. (C) Results show no significant difference between levels of activated Rho in cells over-expressing Rgnef or tagged HA-Rgnef, compared to cells transfected with pCAGGS (n=3).

3-09 Discussion

3-9-01 The Shh-LIGHT2 assay as a reporter of Shh signalling pathway activation states

The Shh-LIGHT2 cell based assay was widely used in this thesis as a means to investigate the activation state of the Shh signalling pathway. It is a cell line that has been extensively used in many other studies (Taipale et al., 2000). Initial tests were made to test the robustness of this assay system, in our hands. For example, it was established that at least a 50% cell confluence was required in order to ensure the integrity of the assay window. The main limitation with the assay, identified in this thesis, was reduction of the assay window due to treatment by the transfection reagent Dharmafect. In the presence of Dharmafect, the extent of pathway activation was much reduced. However, it was still possible assess different activation states using this system despite this activation suppression. Further investigation revealed that Dharmafect does not detectably reduce the number of cells producing primary cilia. This is important, as the primary cilium is an organelle essential for Shh signal transduction and its loss would invalidate the integrity of the assay. An important conclusion to these results is the need to thoroughly identify potentially compromising factors of the Shh-LIGHT2 assay and conduct appropriate case by case controls. It is however still not known why this suppressive effect occurs with Dharmafect treatment. Hence future uses of Dharmafect, or indeed any transfection reagent should be carefully assessed for effects on pathway activation as well as cell structure and morphology.

A further consideration is the extent at which signalling cross-talk from other pathways can cause Shh pathway activation in Shh-LIGHT2 cells. This is well demonstrated by the first study of its kind, where Shh pathway activation changes were monitored against 90% of individually overexpressed human kinases (Varjosalo et al., 2008). In total 380 kinases significantly affected pathway activation, although clearly the degree of change was far less than any of the known effectors of the Shh signalling pathway (Varjosalo et al., 2008). It is not clear whether these results represent signalling crosstalk, as proposed in the study or effects on other systems due to kinase over expression. The results do however emphasise the importance of considering the viability of solely

using overexpression as a means to define pathway activation states in the Shh-LIGHT2 assay.

Therefore the Shh-LIGHT2 assay does provide an effective measure to broadly assess Shh signalling pathway activation. It is nevertheless important to consider its limitations in the context of the molecular complexity of all signalling pathways. Questioning such limitations will better help establish the extent to which cellular and molecular mechanisms in Shh-LIGHT2 cells represent an endogenous setting for the Shh signalling pathway.

3-9-02 Rgnef as a positive regulator of the Shh signalling pathway

The results in this chapter demonstrate a correlation between *Rgnef* expression levels and the extent of Shh signalling pathway activity. Increases or decreases in *Rgnef* expression were shown to activate or suppress pathway activation, respectively, in Shh-LIGHT2 cell based assay experiments. Expression analysis in E10.5 mouse embryos demonstrated *Rgnef* expression along the length of the neural tube. In transverse sections, *Rgnef* expression was seen ventrally in the floor plate, comparable to *Shh* expression. A notable difference is that *Shh* expression is also seen in the notochord wheras *Rgnef* was not. *Shh* expression originates from the notochord and the high ventral concentration induces *Shh* floorplate expression (Placzek et al., 1990, Echelard et al., 1993, Roelink et al., 1995). In Shh-LIGHT2 assay experiments, increased *Rgnef* expression was able to significantly increase Shh pathway activation even when the pathway was activated using potent agonist purmorphamine. This observation proposes the possibility that the extent or threshold of pathway activation is increased by Rgnef. Conversely, reducing *Rgnef* expression resulted in reduced Shh pathway activation, following purmorphamine treatment. From our results, we would predict that, in *Rgnef* mouse mutants, there would be reduced activation of the Shh pathway. This would be expected to lead to altered DV patterning in the neural tube. The patterning of the neural tube in *Rgnef* mouse mutants has not been reported. However, the *Rgnef* knockout mice are smaller than their littermates (Miller et al., 2012) which is intriguing given the role of the Shh pathway in regulating cell proliferation (Chiang et al., 1996, Epstein et al., 1996, Goodrich et al., 1997, Rowitch et al., 1999, Hynes et al., 2000, Litingtung and Chiang, 2000a, Litingtung and Chiang,

2000b, Wijgerde et al., 2002, Kenney et al., 2003, Cayuso et al., 2006). Otherwise the *Rgnef* mutants are reported as exhibiting normal development at E13.5, and there was no investigation as to why litters were reported as smaller than expected (Miller et al., 2012). It would be interesting to examine the mutants for subtle defects in embryonic development, particularly in relation to perhaps minor changes in DV patterning.

The results in this chapter also demonstrate a lack of primary cilia in cells over-expressing *Rgnef.* Primary cilia are involved in regulatory mechanisms that determine the balance between Gli activators and Gli repressors of transcription in Shh signal transduction. Primary cilia are required for both creation of Gli activator and processing of Gli3 to the repressor protein as regulators of pathway activity (Haycraft et al., 2005, Tran et al., 2008). The Gli repressor/Gli activator ratio is influenced by the rates of anterograde and retrograde intraflagellar transport, and disruption of specific IFT proteins can lead to either an overall increase or an overall decrease in Shh pathway activity (Huangfu and Anderson, 2005, Goetz and Anderson, 2010).

For instance, increased Shh signalling is observed in IFT-A mutant mice with cilia that are not lost but disrupted, shortened and bulged (Tran et al., 2008, Cortellino et al., 2009). This is in contrast to IFT complex B mutants which again display compromised or even absent cilia that instead leads to reduced Shh pathway activation (Huangfu et al., 2003, Tay et al., 2005). In our experiments, we have observed that *Rgnef* overexpression has caused a reduction in cilia in transfected cells, while also causing an overall increase in the activity of the Shh pathway. Therefore our results seem to show that *Rgnef* overexpression has shifted the balance of Gli repressor transcription factor processing in preference to Gli activator. It would be interesting to ascertain whether this occurs as a direct consequence of the transfected cells, or on some additional non-autonomous effect that extends beyond the proportion of transfected cells.

In Hek 293 cells, Shh treatment results in increased activation of RhoA, an effect that is suppressed by addition of Smo antagonist cyclopamine (Chen et al., 2002, Kasai et al., 2004). In this chapter, I have shown that increased *Rgnef* expression, while sufficient to lead to Shh pathway activation, did not cause a detectable increase in the level of activated Rho. A limitation of my study is that it did not distinguish between

the three Rho proteins, RhoA, RhoB and RhoC, and instead reported on the overall levels of activation from all three Rho proteins. It is therefore possible that net activation of Rho proteins remains constant in the assay only because relative differences between RhoA, B and C are offsetting each other. Alternatively, it is possible that Rgnef is affecting Shh pathway activation through another mechanism, not involving RhoA. Interestingly, investigations into endothelial cell lines have discovered that Shh induced cell activity in these cells is mediated by Rho in a process that does not involve Gli transcription factors (Renault et al., 2010). In fibroblast cells, Shh induction of RhoA GTPase activity has also been shown to involve a non-canonical Gli-independent Shh pathway activity (Polizio et al., 2011). Therefore the evidence from the literature suggest that there are two pathways downstream of Shh: a RhoA-dependent but Gli-independent pathway, in addition to the Rho-independent canonical Gli-dependant Shh pathway activation. Of course, the Shh-LIGHT 2 cell based assay will only detect Gli-dependent activity. However, the findings reported in my thesis support a role of Rgnef in the Rho-independent, Gli-dependent mechanism. This extends the involvement of Rgnef within cell signalling pathways.

Chapter 4: Investigation of Trim71 in regulation of the Shh signalling pathway

Heterochronic gene *Trim71* is an E3 ubiquitin ligase, negatively regulated by *Let7* miRNA pathway regulation and a system well conserved across many organisms. The role of Trim71 was first defined in *C.elegans* (Reinhart et al., 2000, Slack et al., 2000, Vella et al., 2004) and is broadly assumed across all organisms as providing temporal cues to prevent premature development of adult phenotypes (Pasquinelli et al., 2000, Kloosterman et al., 2004, Lancman et al., 2005, Schulman et al., 2005, Kanamoto et al., 2006, Chang et al., 2012). In mice, a lack of Trim71 results in NTD and in chick, inverse correlations have also been detected with Gli3 expression, both findings that relate to possible involvement in the Shh signalling pathway (Lancman et al., 2005, Maller Schulman et al., 2008). In our laboratory Trim71 was identified as a Tulp3-interacting protein a negative regulator of the Shh Signal pathway.

In this chapter I attempt to identify and investigate the possible role of Trim71 in Shh signal transduction. My investigations centre on using Shh Light-II cell based assay to monitor states of Shh pathway activation in relation to changes in Trim71 expression. Using siRNA transgenic suppression, I show *in vitro* that reducing Trim71 expression reduces the extent of induced Shh pathway activation. However through validation tests I discover a lack or already very low level of Trim71 expression in the NIH 3T3 cell line, used to construct the Shh-LIGHT2 cell based assay. In discovering my results to be a false positive, I endeavour to investigate possible causes and identify the result to be from a single siRNA amongst the total mix used for the experiments. I also successfully express GFP-Trim71 in NIH-3T3 cells and observe cell localisation patterns akin to published endogenous Trim71 cell localisation.

4-01 Suppression of Shh pathway activation by Trim71 siRNA transfection

The Shh-LIGHT2 cell based assay can provide a means to monitor Shh pathway activation (Section 3-03). To evaluate the effect of Trim71 on pathway activity, the aim was to knockdown *Trim71* gene expression with specific siRNA oligonucleotides. Shh-LIGHT2 cells were transfected with a 20 nM pool of four different *Trim71* siRNA sequences aimed at silencing gene expression. The results were compared with transfection with a control non-silencing siRNA oligonucleotide to ensure the results were based only on the effects of *Trim71* siRNA targeted knockdown. Shh pathway

activation was induced by 5 µM purmorphamine and luminescence measured using the Promega Dual-Glo Luciferase assay.

The results show a significant 22% suppression ($p=0.008$, $n=35$) in activation compared to non-target siRNA transfected cells (Figure 4-01 A). Qualification of these results was therefore made by separately examining the independent effects for each of the four siRNA oligonucleotides in the pool. The results revealed an inconsistent pattern of effect from the individual siRNA species (Figure 4-01 B). Only siRNA(1) was able to show a significant 64% suppression ($p=0.04$, $n=4$) of pathway activation compared to all other individual siRNAs tested. In further tests siRNA(1) transfected at 20 nM and 100 nM concentrations suppressed purmorphamine pathway activation by 31% ($p=0.009$, $n=12$) and 54% ($p<0.001$, $n=12$) respectively (Figure 4-01 A). The results show that the suppression induced collectively by a pool of 4 siRNAs was able to be repeated by using only one of the four siRNA species included in the pool. This result raises the possibility that the suppression of pathway activity was induced by an off-target effect by *Trim71* siRNA(1) and not by suppression of *Trim71* expression.

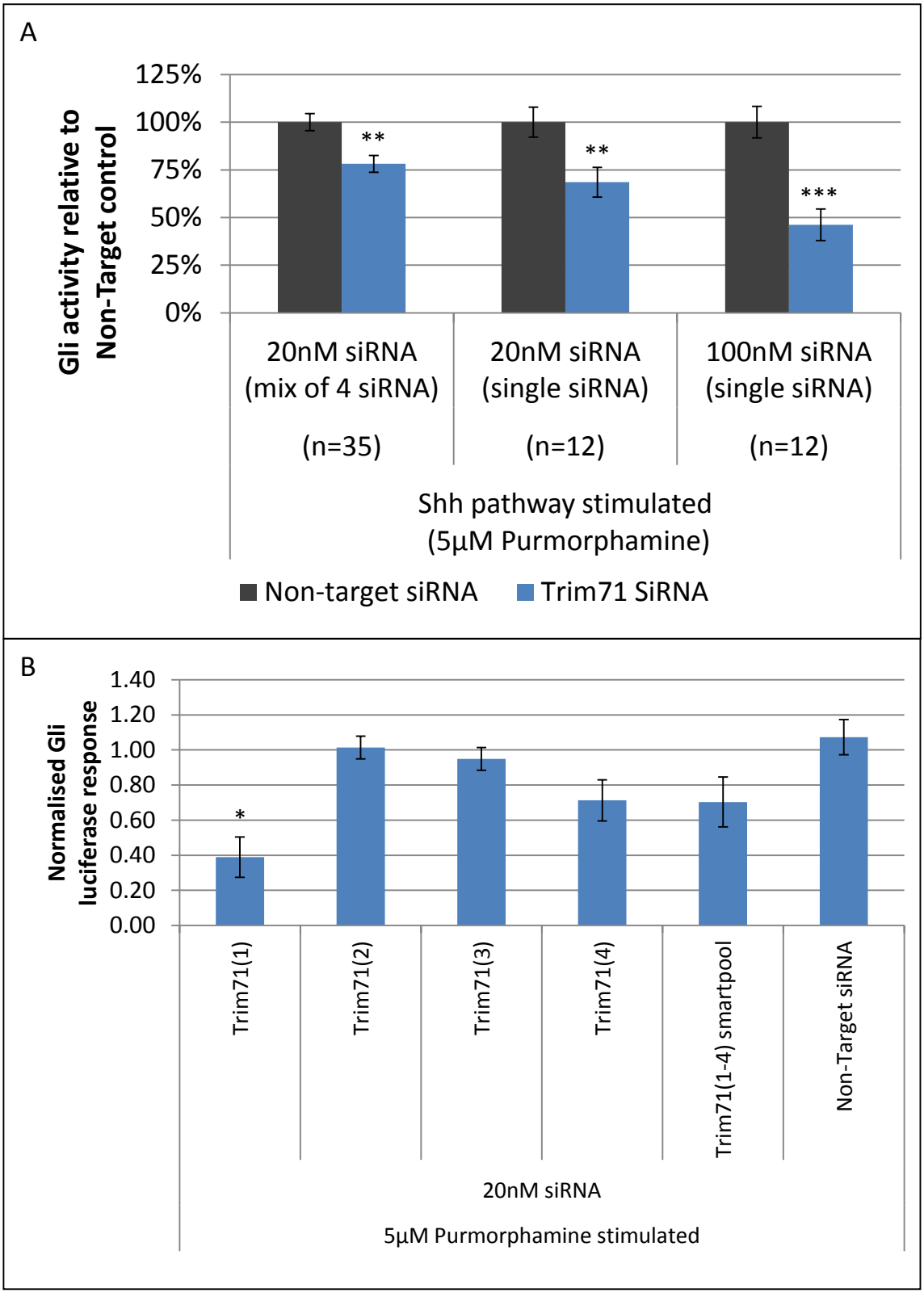
A
Gli activity relative to Non-Target control
125%
100%
75%
50%
25%
0%
**
**
***
20nM siRNA (mix of 4 siRNA)
(n=35)
20nM siRNA (single siRNA)
(n=12)
100nM siRNA (single siRNA)
(n=12)
Shh pathway stimulated (5µM Purmorphamine)
Non-target siRNA
Trim71 SiRNA
B
Normalised Gli luciferase response
1.40
1.20
1.00
0.80
0.60
0.40
0.20
0.00
*
Trim71(1)
Trim71(2)
Trim71(3)
Trim71(4)
Trim71(1-4) smartpool
Non-Target siRNA
20nM siRNA
5µM Purmorphamine stimulated

Figure 4-01 Suppression of Shh pathway activation by Trim71 siRNA transfection

(A) The results show the effects of Shh pathway activation from 20 nM pool of four different Trim71 siRNA sequences transfected to Shh-LIGHT2, aimed at silencing *Trim71* gene expression. The results were compared with non-target siRNA transfected cells. Shh pathway activation was induced by 5 µM purmorphamine and luminesce measured using the Promega Dual-Glo Luciferase assay. Results show a significant 22% suppression (P=0.008, n=35) in activation compared to non-target siRNA transfected cells. In the smartpool the concentration of just siRNA(1) was 5 nM, as 15nM consisting of the other three siRNA sequences. In further tests siRNA(1) transfected at 20 nM and 100 nM concentrations suppressed purmorphamine pathway activation by 31% (p=0.009, n=12) and 54% (p<0.001, n=12) respectively . The results show that the suppression induced collectively by a pool of 4 siRNA was able to be repeated by using only one of the four included in the pool.

(B) Prliminary result leading to further examination of siRNA(1) figure (A). Result compares each of the four siRNA oligonucleotide tested independently by Shh-LIGHT2 assay as well as collectively in the pool. The results revealed an inconsistent result pattern of effect from all the individual siRNA. Only 20 nM siRNA(1) was able to show a significant 64% suppression (p=0.04, n=4) of pathway activation compared to all other individual siRNA's tested, including the smartpool.

4-02 Trim71 expression in Shh-LIGHT2 cells

The results from the Shh-LIGHT2 cell experiments indicated that some, but not all, Trim71 siRNA species caused a suppression of Shh pathway activity. In order to assess the effects of the siRNA transfection on Trim71 expression, PCR assays were developed to analyse endogenous *Trim71* expression in Shh-LIGHT2 cells. Total RNA was extracted from cells cultured in media with and without fetal bovine serum. This was to ensure *Trim71* expression was assessed across all media conditions required during Shh-LIGHT2 cell assay experiments. PCR with primers designed to span an intron did not produce an expected 587 bp product from cDNA synthesised from Shh-LIGHT2 cells cultured in either serum containing or serum free media (Figure 4-02 A). Yet even at lower relative amounts of template, these *Trim71* primers amplified the expected product from E10.5 mouse embryo cDNA (Figure 4-02 A). PCR products were not detected from the negative control reactions without reverse transcriptase (Figure 4-02 A), confirming the amplification is not from contaminating genomic DNA. The *Trim71* primers did however consistently produce 2 bands in close proximity, marginally under and over 200 bp in size (Figure 4-02 A). As the primer sets were intron spanning, from exon 1 to exon 4, consideration was made for possible *Trim71* splice variation. Loss of exons 2 and 3 would bring the primer sites closer to deliver a 285 bp product (Figure 4-02 B). Yet both products detected were clearly smaller than 285 bp and rejects the hypothesis that a *Trim71* exon 1 and 4 splice variant was detected. In conclusion, *Trim71* expression was unable to be detected in Shh-LIGHT2 cells. Furthermore, since these experiments were conducted, the lack of *Trim71* expression in NIH 3T3 mouse fibroblasts (Shh-LIGHT2 cells were initially derived from NIH 3T3 cell line) has been reported (Chang et al., 2012). Despite the conclusion of the authors that there is no *Trim71* expression, the qPCR data of Chang et al (2012) appear to show a very low level of *Trim71* expression rather than a complete absence of expression. We note also the apparent positive identification of Trim71 protein from NIH 3T3 cells using commercially available antibody ab99487 from Abcam (http://www.abcam.com/trim71-antibody-ab99487.html). It therefore remains possible that *Trim71* is expressed at low level with some functional effect in Shh-LIGHT2 cells.

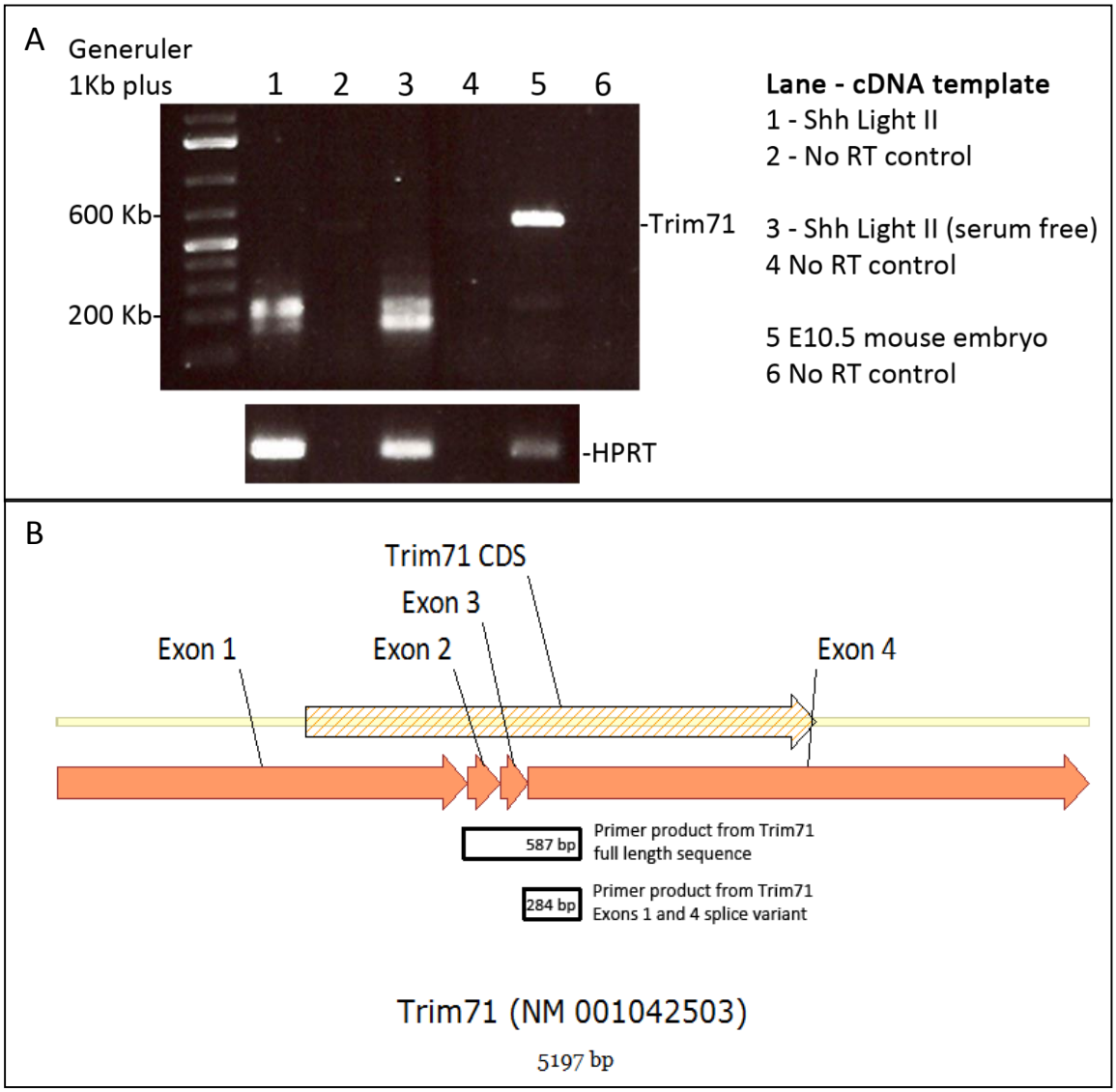

Figure 4-02 Trim71 expression is undetected in NIH 3T3 cells

(A) *Trim71* primer PCR products after electrophoresis through a 2% agarose gel. The expected 587 bp product was observed using the positive control E10.5 mouse embryo cDNA (lane 5). This was not detected in Shh-LIGHT2 cells (lanes 1 and 3) and instead two bands were resolved in close proximity, marginally under and over 200 bp in size. There were no bands in negative control reactions without reverse transcriptase enzyme (lanes 2 and 4). (B) A schematic representation of *Trim71* sequence showing positions of all four exons. The position and size of the 587 bp product is shown from intron spanning primers. Also shown is a hypothesised 284 bp product expected from an Exon 1 and 4 Trim71 splice variant. Overall results shows that the products detected were not from Trim71 or any splice variant of Trim71.

4-03 Over-expression of GFP-Trim71 in NIH 3T3 cells

NIH 3T3, the cell line used to create Shh-LIGHT2 assay, is investigated in respect to overexpression of *Trim71*. The overall aim was to determine the possibility of using Shh-LIGHT2 assay to assess the effect of Trim71 overexpression on Shh pathway activity. Furthermore, by using RT-qPCR techniques detection of endogenous *Trim71* could be re-attempted and assessed in contrast with Trim71 overexpression by plasmid construct transfection.

Trim71 expression in NIH 3T3 cells was increased, using a GFP-tagged *Trim71* expression construct. Transfection was achieved by reagent Lipofectamine 2000® complexed with pEGFP-N1-Trim71; an N-terminal eGFP tagged Trim71 expression construct obtained from Professor G. Wulczyn at the Charite Hospital in Berlin. Determination of *GFP-Trim71* expression after transfection was validated by quantitative RT-PCR using $2^{-\Delta\Delta C_T}$ method and calibrated by reference genes GAPDH and β2 Microglobulin. Total RNA extracted from cells was quantified to ensure equal amounts were added as templates for cDNA synthesis.

The $2^{-\Delta\Delta C_T}$ method depends on the presence of endogenous *Trim71* as it reports increases in GFP-*Trim71* from the pEGFP-N1-Trim71 transfection relative to the level of detectable *Trim71* without transfection. On two attempts, increases in expression were found to be as much as 4000 and 8000 fold, respectively. These high fold calculations represent the difference in the induced GFP-*Trim71* expression relative to any detected endogenous *Trim71* expression. However, given previous findings and the inconsistent reports regarding *Trim71* expression in these cells, detection of endogenous *Trim71* requires further investigation.

The first observation was that when detecting endogenous Trim71 in un-transfected cells, Ct values were over 30 cycles. Such late detection increases the probability of detecting unspecific binding. Melt curve analysis results in a single peak average of 87.9 ˚C for cells over-expressing GFP-Trim71. However, the same primer set instead detected 2 peaks in NIH 3T3 cells transfected with plasmid alone. Statistical comparison of melt curve peaks found that the peak with highest average temperature of 87.6 ˚C from endogenous Trim71 expression analysis, was not significantly different to the 87.9 ˚C single temperature peak for GFP-Trim71 detection (Figure 4-03 A).

An analysis using uMelt (Utah University) was conducted, to assess the predicted amplicon melt curve expected from the Trim71 primer set used. uMelt predictions are based on nucleotide content and pattern, as well as concentration of monovalent cations and free Mg++ present in the reaction (Dwight et al., 2011). The 92 bp amplicon sequence (60% GC content) expected from Trim 71 primer set predicted a single melt curve peak of 88 ˚C (Figure 4-03 B). Concentration of monovalent cations and Free Mg++ was 0.69 mM and 26 mM respectively. The results therefore present a case of corresponding predicted and actual melt curves, with single primer products, consistent with positive Trim 71 detection (Figure 4-03 A and B). The production of the second lower temperature amplicon is possible when low endogenous *Trim71* levels increase the probability of unspecific primer binding, or primer dimers (Figure 4-03 A). This is not observed in cells overexpressing GFP-Trim71 due to the abundance of template, shown by the early Ct values of between 18 and 20 cycles and the single peak melt curve (Figure 4-03 A).

Fluorescent microscopy of pEGFP-N1-Trim71 transfected NIH 3T3 cells shows distinct points of GFP-Trim71 within the cytoplasm (Figure 4-03 E). This is consistent with images of endogenous Trim71 localized to cytoplasmic foci, shown to be RNA processing structures called p-bodies (Rybak et al., 2009). It therefore qualifies protein abundance as the result of increased *Trim71* expression reported by RT-qPCR.

A

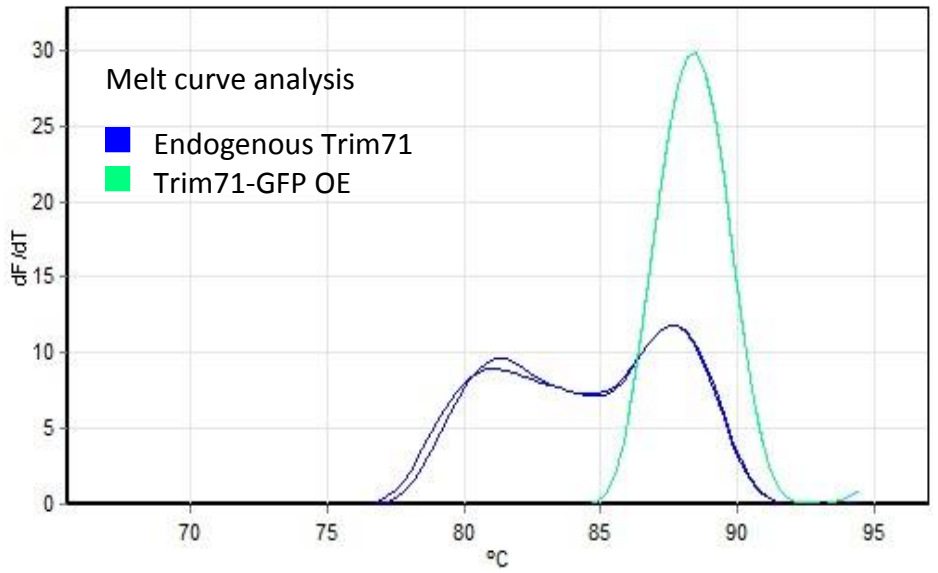
Melt curve analysis
Endogenous Trim71
Trim71-GFP OE
dF /dT
°C
30
25
20
15
10
5
0
70
75
80
85
90
95

B

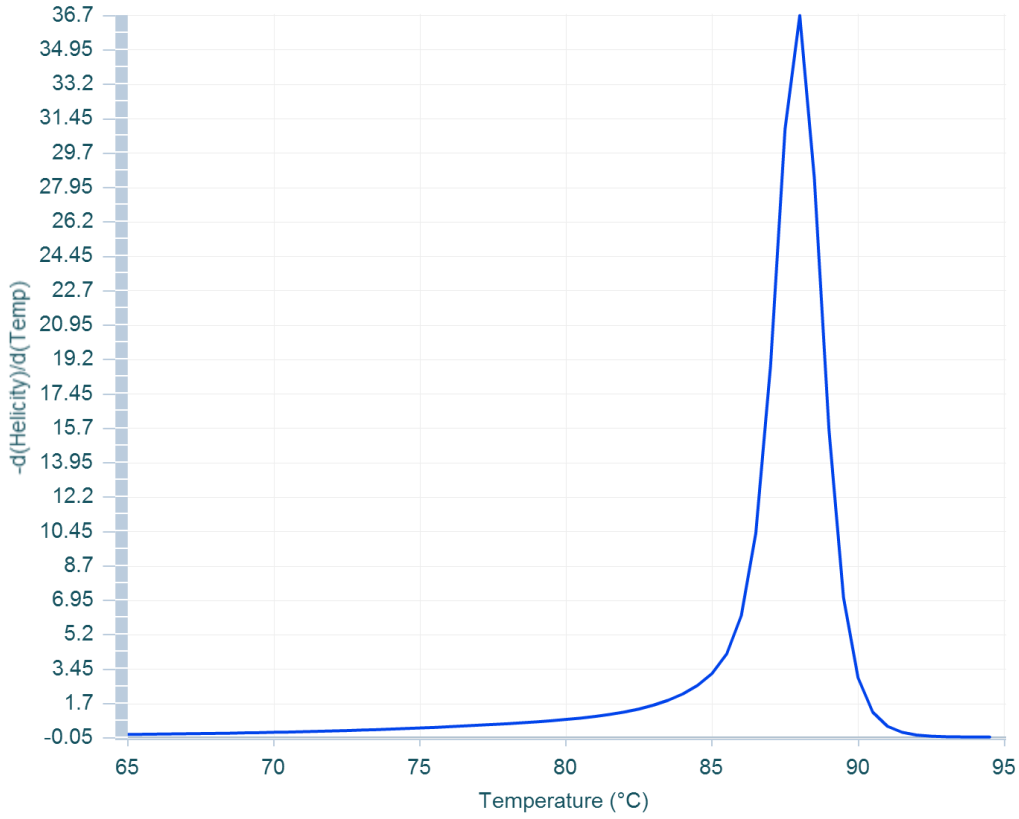
-d(Helicity)/d(Temp)
Temperature (°C)
36.7
34.95
33.2
31.45
29.7
27.95
26.2
24.45
22.7
20.95
19.2
17.45
15.7
13.95
12.2
10.45
8.7
6.95
5.2
3.45
1.7
-0.05
65
70
75
80
85
90
95

C – Brightfield

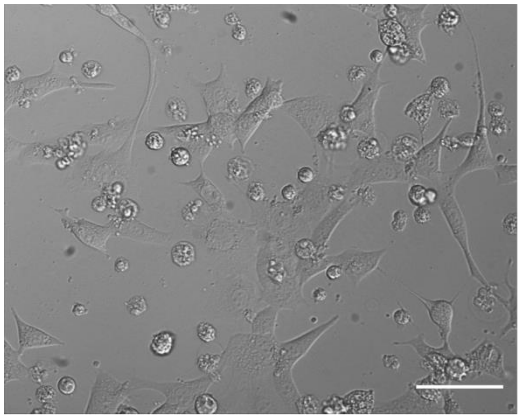

D – Trim71- GFP

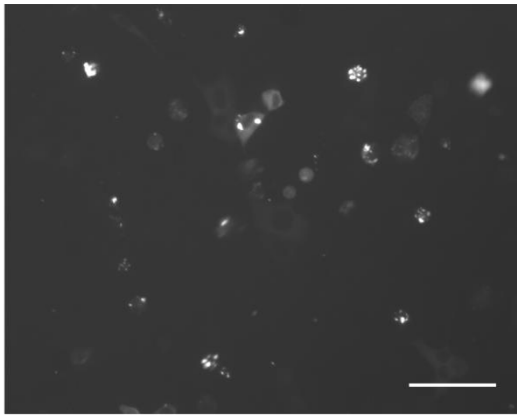

E – Merged

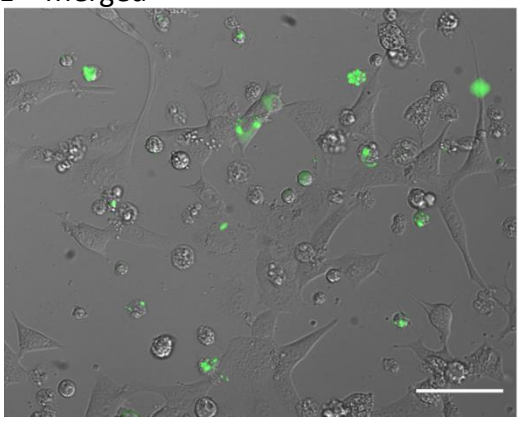

F – Merged (enlarged cells from E)

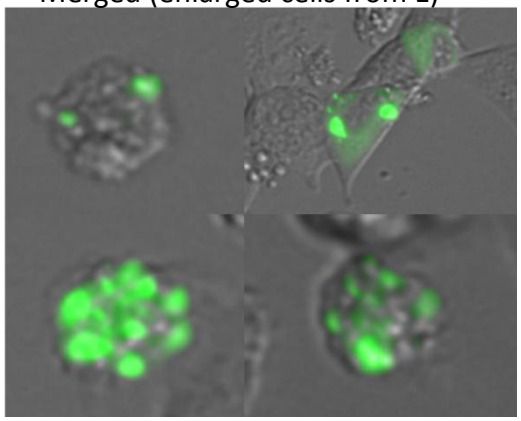

Figure 4-03 Over-expression of GFP-Trim71 in NIH 3T3 cells

(A) Representative melt curve analysis result showing temperature peaks that identify PCR products. In cells over expressing *Trim71* a single 87.9 ˚C peak is observed consistent with a single PCR product. Double temperature peaks were found when attempting to detect endogenous *Trim71* in untransfected cells and an indication of multiple PCR products. In both melt curves examined, the higher temperature 87.6 ˚C peak was found to not be significantly different to the single peak detection resulting from GFP-*Trim71* expression (p=0.2, n=5). (B) Graph derived from uMelt predictive software, showing the expected melt curve analysis with single 88 ˚C peak expected from the amplicon expected from the Trim71 primer set used.(C - F) Representative images of NIH 3T3 cells transfected with pEGFP-N1-Trim71. (C) Shown as single channel, live cell brightfield image of NIH 3T3 cells and (D) identified transfected GFP-Trim71 expression. (E) Merged image of live cell and GFP-Trim71 with (F) Enlarged examples to highlight GFP-Trim71 localized to cytoplasmic foci. This is consistent with reported localisation to RNA processing structures called p-bodies (Rybak et al., 2009). (C-F) Scale bars = 100 µm

4-04 Discussion

4-4-01 Investigating the false positive results from Trim71 siRNA

The results determined that Shh signalling Pathway suppression was induced by a single Trim71 siRNA(1) and not by the collective pool of four siRNAs used. The results conclude the effect to be an off target effect, particularly as a lack of *Trim71* expression in NIH 3T3 cells has since been reported elsewhere. The question therefore arises as to what this single siRNA was targeting to have induced pathway suppression and potentially identifying a known or novel positive regulator of the Shh signalling pathway. Further examination, using nucleotide BLAST searches (http://blast.ncbi.nlm.nih.gov/Blast.cgi), revealed a 15 bp sequence homology to glycogen synthase kinase 3 beta (GSK3β).

siRNA(1) G**AUCAUAGUGGCCGA**CAAA
GSK3β **ATCATAGTGGCCGA**

The results determined that Shh signalling pathway suppression was induced by a single Trim71 siRNA(1) and not by the collective pool of four siRNAs used. The results conclude the effect to be an off target effect, particularly as a lack of *Trim71* expression in NIH 3T3 cells has since been reported elsewhere (Chang et al., 2012).The question therefore arises as to what this single siRNA was targeting to have induced pathway suppression and potentially identifying a known or novel positive regulator of the Shh signalling pathway. Further examination, using nucleotide BLAST searches (http://blast.ncbi.nlm.nih.gov/Blast.cgi), revealed a 15 bp sequence homology to glycogen synthase kinase 3 beta (GSK3β).

siRNA(1) G**AUCAUAGUGGCCGA**CAAA
GSK3β **ATCATAGTGGCCGA**

However, GSK3β has already been identified as a negative, not positive, regulator of Shh signalling pathway. GSK3β is one of the kinases responsible for Gli3 phosphorylation that leads to the proteolytic processing of Gli3 to form the pathway repressor $Gli3^R$ (Jia et al., 2002, Kim et al., 2009b). Disruption of GSK3b would therefore be expected to reduce the phosphorylation of Gli3, leading subsequently to reduced formation of Gli3R which would be observed as increased pathway activation

in the Shh-LIGHT2 cell based assay. This robust model therefore opposes the possibility that pathway suppression was induced by a knock down of *GSK3*β by an off-target effect of Trim71 siRNA(1). It is however important to state that although this is a possibility, it cannot be positively stated that direct effect of *GSK3*β knock-down on Shh signalling pathway activation has occurred in this assay without further validation. At very least RT-qPCR validation would be required to demonstrate that *GSK3β* expression was altered. This finding therefore only proposes a hypothesis to further test the role of GSK3β using the Shh-LIGHT2 assay.

An assessment was made following the overexpression of GFP-Trim71 in NIH 3T3 in light of the absence of expression in this cell line. An increase in expression was achieved as well as a cell localisation pattern consistent with reported P-body localisation (Rybak et al., 2009). In order to further qualify P-body localisation, further co-localisation with P-body effectors, would be required, Ago2 for instance (Rybak et al., 2009). Future plans for *Trim71* expression changes on Shh signalling pathway activation could therefore involve using Shh-LIGHT2 assay in respect to *Trim71* overexpression. It is however an unsuitable assay for reducing *Trim71* expression, as the endogenous expression of *Trim71* in the Shh-LIGHT2 assay cell line is at best very low anyway.

Chapter 5: Gli2 protein characterisation

In previous chapters investigations were based on identifying two novel protein regulators of Shh signal transduction. Results in this chapter instead investigate the established effector Gli2, one of three transcription factors conserved in vertebrate Shh signalling. This study aims to help further understand pathway regulation in relation to the PTM of Gli2, the principle initiator of pathway activity.

Gli2 was characterised by mass spectrometry, attempted by both the MALDI-TOF and AmaZon ion Trap mass spectrometers. In characterising Gli2 I aimed to reveal sites of protein modification that would help to further understand its role. My results also detail the processes involved in identifying Gli2 by SDS PAGE and immunoblotting, as well as MS sample preparation techniques. The aim is an assessment of these processes in relation to effective and improved MS analysis and characterisation.

5-01 Endogenous Gli2 detection in NIH 3T3 cell lysate using ECL detection immunoblotting

To identify endogenous Gli2 protein abundance in NIH 3T3 cells, protein extracts were resolved from total cell lysate by use of SDS PAGE and detected by immunoblotting using anti-Gli2 antibody obtained from Dr Baolin Wang (Cornell University). Endogenous Gli2 is a 185 kDa protein that is also processed to a 78 kDa cleaved isoform (Pan et al., 2006). Due to its low abundance the shorter cleaved Gli2 isoform has been reported to be undetectable without enriching for Gli2 protein before immunoblotting (Pan et al., 2006). The enrichment method used was provided by Dr Baolin Wang. This was based on magnetic bead separation using biotinylated oligonucleotide Gli transcription factor binding sequences to bind and enrich Gli2. Control purification reactions were also prepared, using oligonucleotides with mutated Gli binding sequences (Pan et al., 2006), to evaluate if Gli2 enrichment was effective. Also, proteins that non-specifically bind the complex can be identified from the mutated Gli2 binding site oligo enrichments.

Results, demonstrated in a representative immunoblot, show a band detected in a region between 180 and 190 kDa (Figure 5-01 A). Based on the Invitrogen HiMark™ protein marker standard curve, this band was calculated to be 187 kDa, therefore close to the 185 kDa size expected for full length Gli2 (Figure 5-01 A). Bands in the region of the cleaved 78 kDa Gli2 repressor isoform were undetected in these examples

however proteins were detected at around 129 kDa, 70 kDa and 61 kDa, as calculated by comparison to the protein marker standard curve (Figure 5-01 A). The abundance of processed Gli2 has previously been reported to be low relative to full length Gli2 (Pan et al., 2006), which may explain why the cleaved isoform is not detected here. Moreover, the intensity of the 70 kDa protein relative to the proposed 187 kDa full length Gli2 makes this band an unlikely candidate for processed 78 kDa Gli2. However, the proteins detected still merit investigation as they did not appear in the control enrichments and may possibly be degraded Gli2 protein or indirectly enriched Gli binding partners.

The immunoblots were used as references for gel section extraction from equivalent silver stained SDS PAGE gels prepared in parallel (Figure 5-01 A). Sample preparation and SDS PAGE of the silver stained gels was executed using the same procedure as gels prepared for immunoblotting. Initial observations from silver stained gels revealed multiple protein bands without distinctive or conclusive differences between Gli2 binding sequence oligo and mutated oligo purification lanes (Figure 5-01 A). The silver staining demonstrates that during the Gli2 enrichment procedure, a considerable amount of protein was retained during the purification wash steps, and the enrichment does not generate pure Gli2 protein. The enrichment of Gli2 detected in the immunoblots was not observable as a distinct band amongst the protein detected in the silver stained gels (Figure 5-01 A).

Gel regions were excised relating to any bands detected in their paired immunoblots and in the precise region of the 185 kDa and 78 kDa protein migration expected for Gli2. All gel sections were fragmented, de-stained and incubated for tryptic digestion, before being prepared for MALDI-TOF mass spectrometry analysis. However, Gli2 was not detected in any of these preparations, concluding that endogenous Gli2 is was not abundant enough in these preparations for protein identification and protein extraction. Clearly the requirement is to be able to see a stained band in order to detect it in the mass spectrometer.

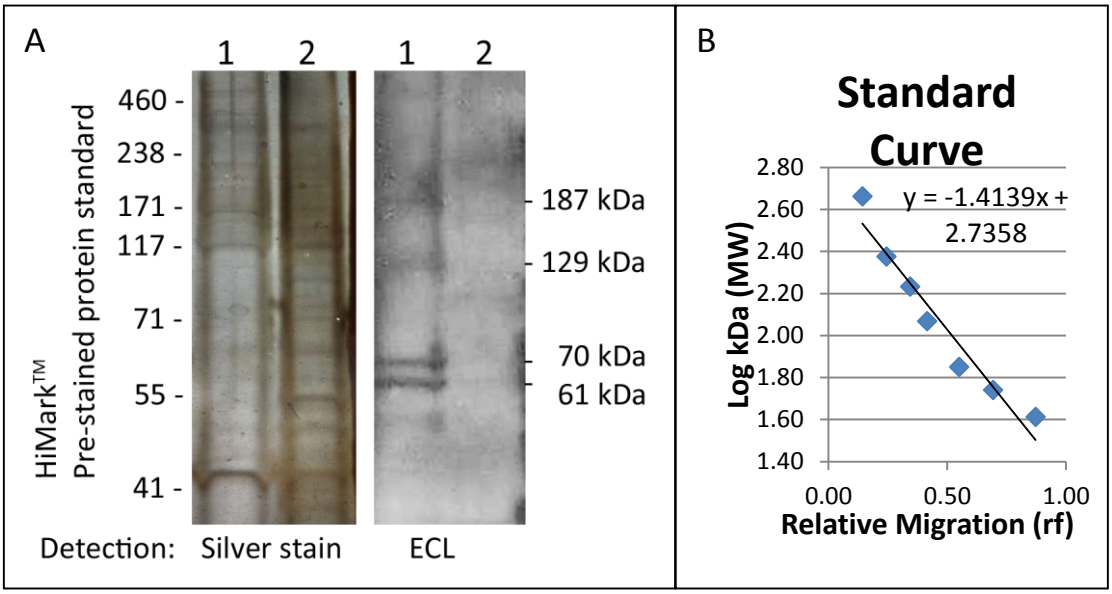

Figure 5-01 Endogenous Gli2 detection in following enrichment of NIH 3T3 cell lysate

(A) Representative example of silver-stained SDS PAGE gel and blot probed for Gli2, following oligo pull-down from NIH 3T3 cell lysates. Each 300 µl lysate preparation added to magnetic bead complex consisted of approximately 120 µg total protein. Lane 1 enriched Gli2 eluent based on magnetic bead separation of biotinylated oligonucleotide Gli transcription factor binding sequences. Lane 2 is a control purification reaction using oligonucleotides with mutated Gli binding sequences. Eluents from oligo pull-down reactions were resolved on SDS-PAGE gels and silver-stained to view total proteins, or electroblotted to nitrocellulose membrane for immunodetection using anti-Gli2 antibody. Sizes of HiMark protein standards are indicated on the left, and calculated size of observed bands on the blot are indicated on the right. Immunoblot detected bands were used to identify sections to remove in silver stained gels, prepared in parallel. Immunoblot protein bands were identified between 180 and 190 kDa. There was inconsistent detection of bands in the regions of 78 kDa and yet proteins of other sizes were detected after enrichment but not detected in control purifications. Based on these results gel sections were removed for protein mass spectrometry protein identification. (B) Protein molecular weight marker standard curve.

5-02 Endogenous Gli2 detection in NIH 3T3 cell lysate using fluorescent detection immunoblotting

In an attempt to improve upon previous ECL detection results, immunoblots were prepared using fluorescent immunodetection techniques. The aim was to better confirm identification of endogenous Gli2 and enable improved targeting of gel sections for MALDI-TOF analysis.

Total cell lysate from NIH 3T3 cells was prepared, without Gli2 enrichment, for SDS PAGE and electroblotting to PVDF membrane. In each experiment, changes in Shh signalling pathway activity were compared by preparing lysate from unstimulated and stimulated cells. Shh pathway stimulation was achieved by Smoothened-agonist purmorphamine. The pathway activation, using the same purmorphamine media preparation, was validated by Shh-LIGHT2 cell based assay (Figure 5-02 G).

Loading control, 220 kDa fatty acid synthase (FAS) was detected using Santa Cruz mouse anti-FAS primary antibody and fluorescent secondary anti-mouse (Licor 800CW). A single band was identified and estimated to run at 216 kDa (Figure 5-02 A – C; green band). Gli2 was identified by fluorescent secondary antibody anti-rabbit (Licor 680RD) that in turn identified rabbit anti-Gli2 primary antibody obtained from Dr Baolin Wang (Figure 5.02 A-C; red band). Two commercially available primary antibodies tested, failed to detect Gli2 (Figure 5-02 B and C).

Gli2 immunodetection on PVDF membrane was improved by a number of optimisation steps. This included doubling the amount of protein loaded per lane, a 5 fold reduction of primary antibody concentration used and 2 fold reduction of secondary antibody concentration used. Also the Licor anti-rabbit secondary antibody for Gli2 was changed from Licor 680RD to Licor 800CW as it provided more sensitivity with less background (Figure 5-02 D).

The two bands identified by Gli2 antibody were calculated to be 200 kDa and 78 kDa, based on Invitrogen Novex sharp protein marker standard curve estimates (Figure 5-02 E). NuPAGE® 7% tris acetate gel has an ideal separation of between 35 kDa and 180 kDa, so observing Gli2 at 200 kDa, instead of 185 kDa may simply reflect the sub-optimal resolution of the larger proteins on this gel. This would also explain why

processed Gli2 was still found at the expected 78 kDa, as it is within the gel's optimal separation range.

In Shh pathway stimulated and unstimulated cells both full length and cleaved Gli2 bands were detected (Figure 5-02 D). Compared to unstimulated cells, the 78 kDa Gli2 band intensity relative to full length 185 kDa Gli2 was 39% less in Shh pathway stimulated cells (Figure 5-02 F). The purmorphamine preparation used to stimulate NIH 3T3 was successfully tested using the Shh LIGHT2 assay (Figure 5-02 G).

ECL immunoblot detection of processed Gli2 using this antibody has been reported to require a protein purification step due to its low abundance (Pan et al., 2006). Processing of the 78 kDa repressor isoform is reported to reduce relative to Gli2 (Pan et al., 2006). In these experiments, 78 kDa Gli2 was detected without Gli2 enrichment. It continued to be detected after Shh pathway activation, although band intensity was reduced relative to full length Gli2. A possibility is that even at reduced abundance the 78 kDa Gli2 protein was detectable using immunofluorescence detection as opposed to ECL reagent detection. These preliminary results therefore may reflect an improved sensitivity of immunofluorescent detection compared to reported results using ECL reagent western techniques.

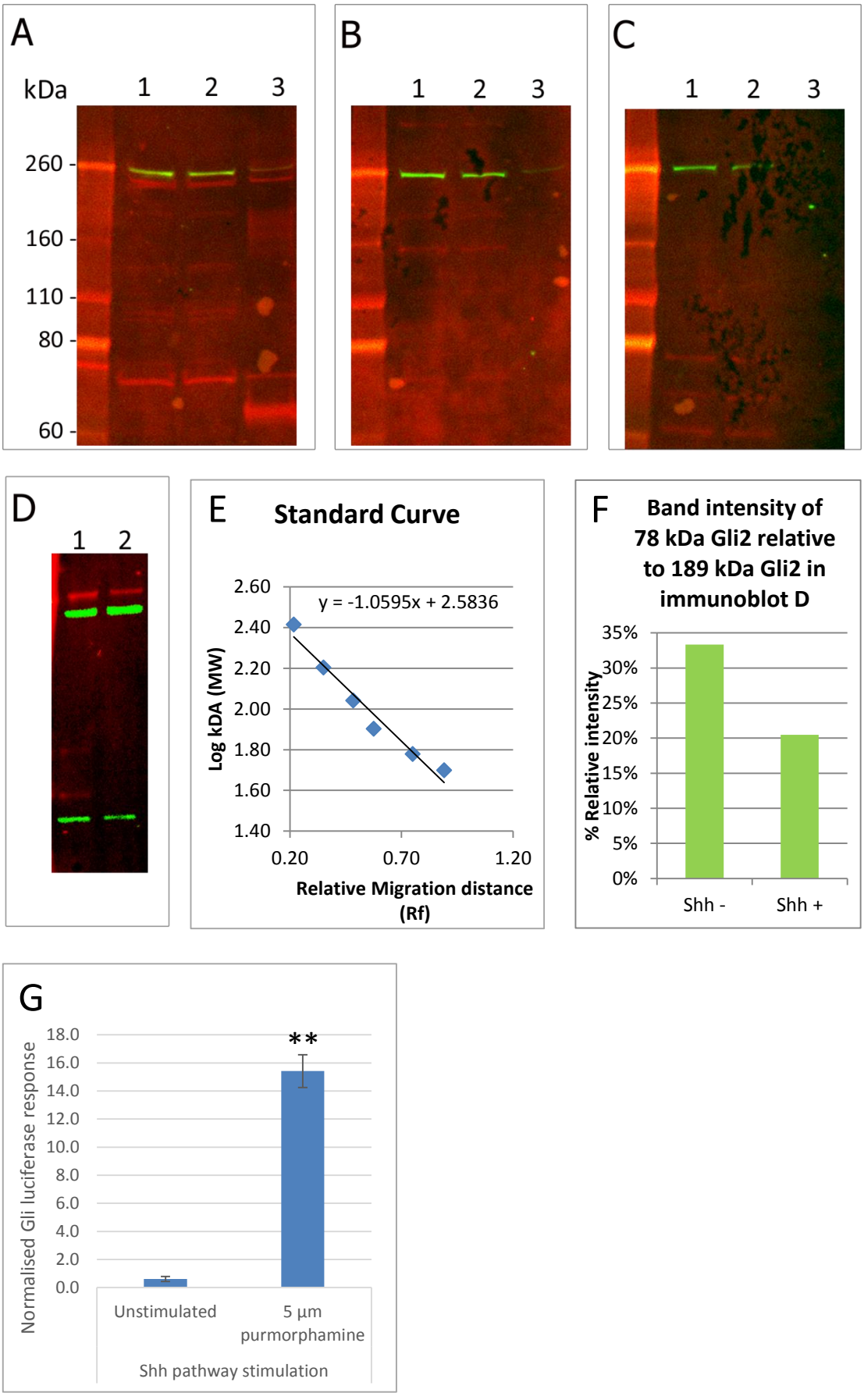
A
kDa
1
2
3
260
160
110
80
60
B
1
2
3
C
1
2
3
D
1
2
E
Standard Curve
y = -1.0595x + 2.5836
2.60
2.40
2.20
2.00
1.80
1.60
1.40
Log kDA (MW)
0.20
0.70
1.20
Relative Migration distance (Rf)
F
Band intensity of 78 kDa Gli2 relative to 189 kDa Gli2 in immunoblot D
35%
30%
25%
20%
15%
10%
5%
0%
% Relative intensity
Shh -
Shh +
G
18.0
16.0
14.0
12.0
10.0
8.0
6.0
4.0
2.0
0.0
Normalised Gli luciferase response
**
Unstimulated
5 µm purmorphamine
Shh pathway stimulation

Figure 5-02 Endogenous Gli2 detection in NIH 3T3 cell lysate using fluorescent detection immunoblotting

(A, B and C) Representative images of NIH 3T3 total cell lysate SDS PAGE, electro-blotted to PVDF membrane for immuno-detection of endogenous Gli2 protein. NIH 3T3 cells total cell lysate loaded in each well contained 5 µg total protein. Lane 1 unstimulated NIH 3T3 lysate whereas lane 2 contained lysate from Shh pathway stimulated cells.. Shh pathway stimulation was achieved by overnight incubation in 5 µm purmorphamine in 0.5% DMSO in serum free media and unstimulated control in 0.5% DMSO in serum free media. The purmorphamine used was directly tested in parallel with Shh-LIGHT2 cell based assay to ensure that it was able to induce pathway stimulated. Lane 3 contained unstimulated Shh-LIGHT2 cell lysate. Bands were identified by primary antibody provided Dr Baolin Wang and Licor anti-rabbit 680RD fluorescent secondary antibody.(A) Two clearly identifiable bands at 200 kDa and 78 kDa based on Invitrogen Novex Sharp protein standard curve estimates. The single band identified in green and estimated at 216 kDa was Fatty Acid Synthase (FAS) Santa Cruz mouse anti FAS primary antibody and Licor anti-mouse 800CW secondary antibody. Changes in Gli2 expression was compared between unstimulated and Shh pathway stimulated (lane 1 and lane 2 respectively). Gli2 was also probed and detected in total lysate from the Shh-LIGHT2 cells (lane 3). (B and C) Two commercially available secondary antibodies from Abcam Laboratories (Ab26056 and Ab7195) failed to detect Gli2, although loading control FAS was detected. (D) Continued use of primary antibody provided by Dr Baolin Wang with improved results due to optimisation. This was achieved by a number of changes, including increasing total protein loaded to 18 µg per lane and switching the fluorescent secondary antibody for Gli2 primary from Licor 680RD (red) to Licor 800CW (green). (E) The two bands identified by Gli2 antibody were calculated to be 200 kDa and 78 kDa, based on Invitrogen Novex sharp protein marker standard curve estimates. (F) Changes in Gli2 expression was compared in optimised immunoblot (D) between unstimulated and Shh pathway stimulated cells, lanes labelled “Shh-“ and “Shh +” respectively. In unstimulated and Shh pathway stimulated cells both full length and cleaved Gli2 bands were detected. Relative to full length 185 kDa, the Gli2 78 kDa Gli2 band intensity was 39% less in Shh pathway stimulated cells, compared to unstimulated. (G) Pathway activation was validated by Shh-LIGHT2 cell based assay ($p<0.01$, $n=4$). The same purmorphamine media preparation applied to the NIH 3T3 cells was used on Shh LIGHT2 cells cultured in parallel.

5-03 Gli2 protein abundance is increased by expression plasmid construct transfection

The aim was to increase the amount of Gli2 in cells by transfection of expression plasmid constructs. In the current model of Shh signal transduction, primary cilia are recognised as post translational processing centres for Gli2 and Gli3 (Price and Kalderon, 1999, Jia et al., 2002, Price and Kalderon, 2002, Jia et al., 2005, Pan et al., 2009).

The aim was to transfect NIH 3T3 cells with a plasmid to express GFP-tagged Gli2 protein in order to examine, in our hands, over-expressed GFP-Gli2 protein localisation. The construct used was purchased from Addgene pCEFLmGFP-Gli2 (Kim et al., 2009a). The increase in *Gli2* expression measured by RT qPCR detected a 184 fold increase in *Gli2* in transfected cells compared to endogenous *Gli2* expression in control transfected cells (Figure 5-03 A). To determine co-localisation with primary cilia, cells were stained with mouse anti-acetylated tubulin primary antibody, as tubulin acetylation is a post translational modification found predominately in primary cilia (Wloga and Gaertig, 2010). Results show co-localisation of GFP-Gli2 and primary cilia (Figure 5-03 B-G).

To increase Gli2 protein for mass spectrometry analysis NIH3T3 cells were replaced with HEK293Tcells. Easy to transfect, HEK293T are a ciliating human cell line with a high rate of growth and protein synthesis. Preliminary FACS analysis of GFP transfection in HEK293T cells revealed a 98% transfection rate (Figure 5-04 A). The Gli2 plasmid construct transfected for this purpose was HA-tagged mouse Gli2 plasmid construct, pCEFL3XHAmGli2 (Kim et al., 2009a). Plasmid construct pCEFL3XHAmGli2 is predominately the same as pCEFLmGFP-Gli2, instead replacing the GFP insert with a triplicate HA tag sequence (Kim et al., 2009a). Subsequent expression of HA-Gli2 in HEK293T can then be enriched by either oligo pull-down or HA tag immunoprecipitation. RT-qPCR analysis of pCEFL3XHAmGli2 transfected HEK293T cells detected a 6000 fold increase in *Gli2* expression compared to cells transfected with pCEFL plasmid alone (Figure 5-04 B).

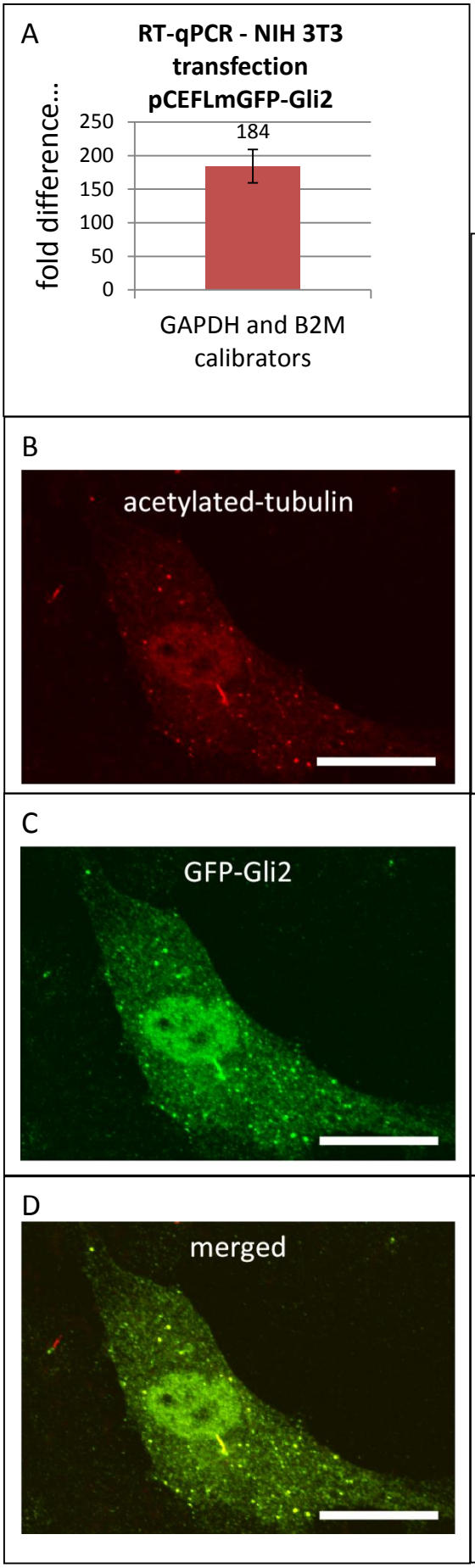
A
RT-qPCR - NIH 3T3 transfection pCEFLmGFP-Gli2
fold difference...
250
200
150
100
50
0
184
GAPDH and B2M calibrators
B
acetylated-tubulin
C
GFP-Gli2
D
merged
E
Intensity
4,000
3,800
3,600
3,400
3,200
3,000
2,800
2,600
2,400
2,200
2,000
1,800
1,600
1,400
1,200
1,000
800
600
0
1
2
3
4
5
6
7
Length (um)
F
G
untransfected

Figure 5-03 Gli2 protein abundance is increased by expression plasmid construct transfection

(A) RT qPCR results of NIH 3T3 cells transfected with pCEFLmGFP-Gli2 (Kim et al., 2009a). Normalised expression changes were calculated using the $2^{-\Delta\Delta C_T}$ method relative to the expression of reference genes *Glyceraldehyde 3-phosphate dehydrogenase* (*GAPDH*) and *Beta-2-microglobulin* (*B2M)*. A 184 fold increase in expression was detected in cells expressing GFP-Gli2 compared to endogenous *Gli2* expression. (B-D) Viewed by confocal microscopy, a representative example of GFP-Gli2 co-localisation with primary cilia in NIH 3T3 cells transfected with pCEFLmGFP-Gli2., (B) Cells were stained for acetylated tubulin (red), as tubulin acetylation is a post translational modification found predominately in primary cilia. (C) GFP-Gli2 localisation is shown in green. (D) Merged channels show GFP-Gli2 and primary cilia localisation.(E) Analysis of the observed co-localisation by quantitative comparison of the channels fluorescent intensities. (F) The 7 μm cross sectional line (in red) across the primary cilium depicts the area measured for fluorescent intensity analysis across the cilium shown in (E). (G) A representative confocal microscopy control image analysis of untransfected NIH 3T3 cells that are also stained for acetylated tubulin and viewed for GFP fluorescence. Scale bars = 20 μm.

A

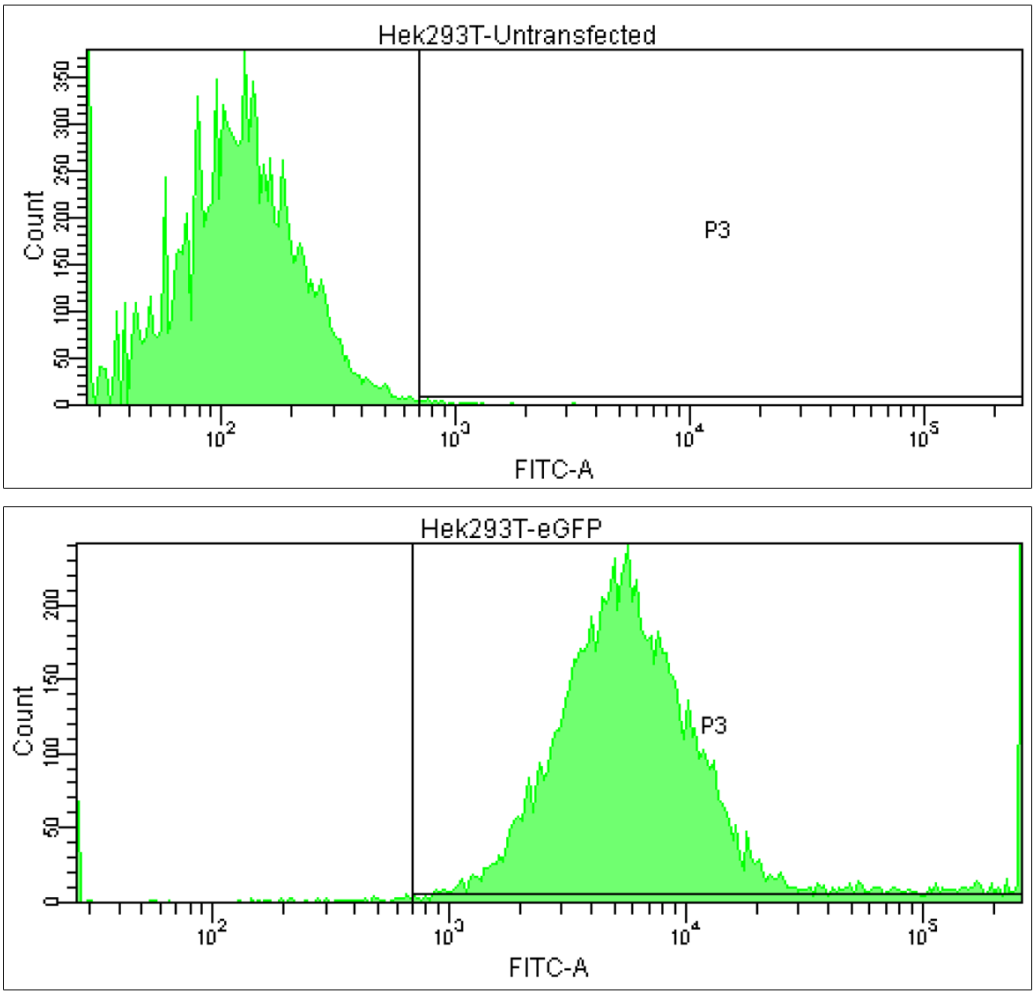
Hek293T-Untransfected
Count
P3
FITC-A
Hek293T-eGFP
Count
P3
FITC-A

B

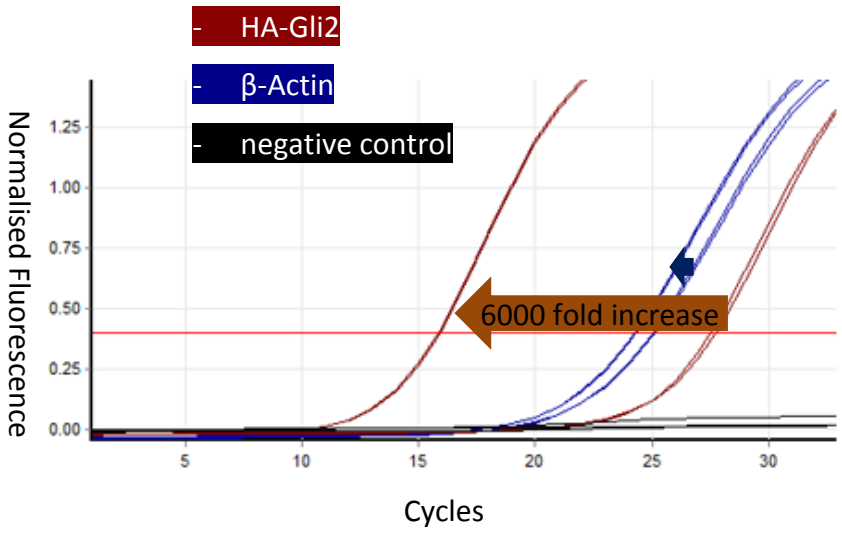
- HA-Gli2
- β-Actin
- negative control
Normalised Fluorescence
6000 fold increase
Cycles

Figure 5-04 Gli2 protein abundance is increased by expression plasmid construct transfection

(A) FACS population histogram for detected eGFP transfected cells HEK293T. Selected cells are counted based on level of GFP expression and the region P3 denotes levels that adequately detect GFP to confirm transfection. Results show a 98% transfection rate in HEK293T cells after overnight incubation.

(B) RT qPCR results of Hek293T cells transfected with pCEFL3XHAmGli2 (Kim et al., 2009a). Normalised expression changes were calculated using the $2^{-\Delta\Delta C_T}$ method relative to the expression of reference gene β-Actin. A 6000 fold increase in expression was detected in cells expressing HA-Gli2 compared to endogenous *Gli2* expression.

5-04 HA-Gli2 transfected and extracted from HEK293T cells is identified by MALDI-TOF mass spectrometry

The aim was to extract overexpressed HA-Gli2 from HEK293T cells for MALDI-TOF analysis. HA-Gli2 was enriched using binding oligonucleotide sequences for Gli transcription factors to perform oligo-binding pull-downs (Section 5-01). Control enrichments were also performed, using mutated binding site sequence oligonucleotides or magnetic beads alone, to detect unspecific binding (Section 5-01). The aim of continuing with the oligo pull-down method of enrichment was, firstly, to compare the results with earlier attempts at endogenous Gli2 enrichment. This method also provides a test to ensure transcription factor promoter binding is not impaired by the HA tag on HA-Gli2.

All results were normalised relative to 55 kDa β-tubulin abundance, a common protein used as a loading control but also referred to here as a marker to represent total protein after enrichment. The results show an increase in HA-Gli2 band intensity relative to controls (Figure 5-05 A). This increase shows that HA-Gli2 transcription factor binding is not blocked by the addition of an HA tag. After normalisation to β-tubulin intensity, the band intensity of binding site oligo-enriched Gli2 was approximately 2.5 fold greater than in mutated oligo or bead-only controls (Figure 5-05 B). Enriched HA-Gli2 was observed in silver stained SDS PAGE gels as a broad shaded band (Figure 5-05 A). Interestingly this was not observed in the controls for HA-Gli2 enrichments and suggests higher fold enrichment than the 2.5 fold increase calculated from the immunoblot band intensity comparisons. However this may simply be due to the sensitivity thresholds of both methods. Enrichment increases protein concentration above the minimum sensitivity for silver staining (0.1 ng of BSA/mm^2) allowing it to be visualised when otherwise it would not. Yet the high sensitivity of fluorescent immunodetection was able to detect Gli2 amongst any remaining total protein lysate in control enrichments. The silver stained gels also highlight the persistent amount of total protein in the purification eluents despite the numerous wash steps. It shows that to a large extent, the 2.5 fold increase would be improved if less total protein was retained after Gli2 enrichment.

The area of silver stained gel identified as Gli2 was excised and prepared for MALDI-TOF mass spectrometry. Three Gli2 peptides were discovered that together amounted to 2% coverage of the protein (Figure 5-05 C). Measures to increase the amount of protein for analysis focused on reducing loss during mass spectrometry sample preparation. There is a high rate of peptide loss inherent in the multi-step sample methodology of in-gel tryptic digestion. This includes 20 hours in-gel digestion at 37^0C, followed by extensive sonification and centrifugal evaporation. MALDI-TOF preparation further reduces the sample by its requirement for crystal matrix complex formation. Once matrix is formed, the sample is then not analysed in its entirety but instead selectively sampled by laser point ionisation.

In summary, although detection coverage was low, these results provided the first identification of Gli2, made possible by the steps taken to increase protein abundance and a means to identify it by fluorescent immunodetection. Further improvements in Gli2 purification were attempted by using the HA tag for enrichment, with highly optimised anti-HA immunoprecipitation techniques. This method should provide high yield and specificity benefits of high affinity antibody binding and does not require Gli2 to retain its structure. It is a method that fulfils the aims of ensuring optimal amount of Gli2 for protein characterisation.

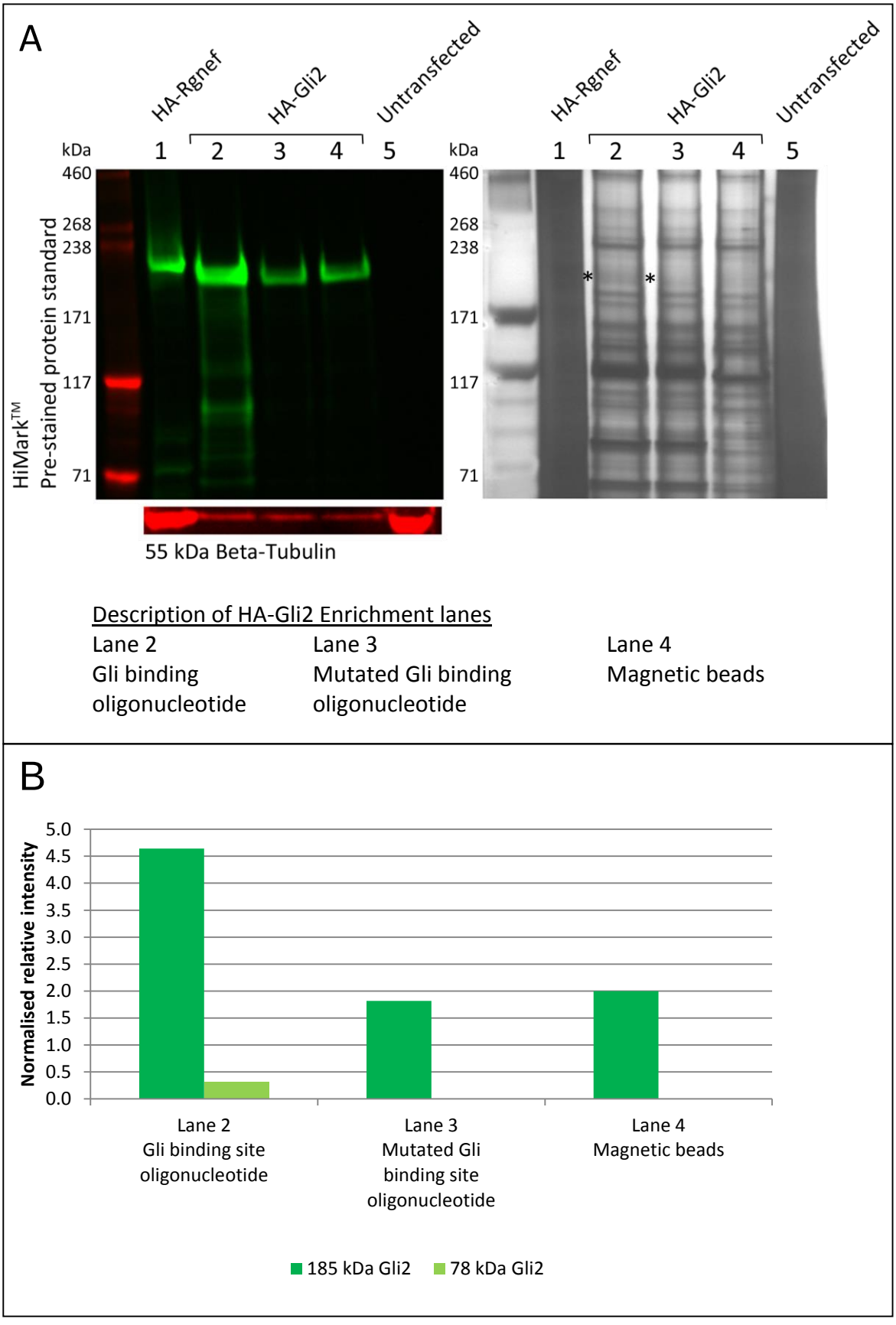

Description of HA-Gli2 Enrichment lanes

Lane 2	Lane 3	Lane 4
Gli binding oligonucleotide	Mutated Gli binding oligonucleotide	Magnetic beads

C

Protein View: GLI2_MOUSE

Protein sequence coverage: 2%

Matched peptides shown in ***bold red***.

```
   1 METSAPAPAL EKKEAKSGLL EDSSFPDPGK KACPLAVAAA VAAHGVPQQL
  51 LPAFHAPLPI DMRHQEGRYH YDPHSVHSVH GPPTLSGSPV ISDISLIRLS
 101 PHPAGPGESP FSAHHPYVNP HMEHYLRSVH SSPTLSMISA ARGLSPADVA
 151 HEHLKERGLF SLAAPGTNPS DYYHQMTLMA SHPTPYGDLL MQSGGAASAP
 201 HLHDYLNPVD ASRFSSPRVT PRLSRKRALS ISPLSDASLD LQRMIRTSPN
 251 SLVAYINNSR SSSAASGSYG HLSAGALSPA FTFPHPINPV AYQQILSQQR
 301 GLGSAFGHTP PLIQPSPTFL AQQPMTLTSI STMPTQLSSS SSNCLNDANQ
 351 NKQNSESAVS STVNPITIHK RSKVKTEAEG LRPASPLGLT QEQLADLKED
 401 LDRDDCKQEA EVVIYETNCH WADCTKEYDT QEQLVHHINN EHIHGEKKEF
 451 VCRWQACTRE QKPFKAQYML VVHMRRHTGE KPHKCTFEGC SKAYSRLENL
 501 KTHLRSHTGE KPYVCEHEGC NKAFSNASDR AKHQNRTHSN EKPYICKIPG
 551 CTKRYTDPSS LRKHVKTVHG PDAHVTKKQR NDVHVRAPLL KENGDNEASA
 601 EPGGRGPEES VEASSTSHTV EDCLHIKAIK TESSGLCQSS PGAQSSCSSE
 651 PSPLGSAPNN DSGMEMPGTG PGSLGDLTAL ADTCPGADTS ALAAPSTGGL
 701 QLRKHMSTVH RFEQLKREKL KSLKDSCSWA GPAPHTRNTK LPPLPVNGSV
 751 LENFNNTGGG GPAGLLPSQR LPELTEVTML SQLQERRDSS TSTMSSAYTV
 801 SRRSSGISPY FSSRRSSEAS PLGGLRPHNA SSADSYDPIS TDASRRSSEA
 851 SQCSGGGPGL LNLTPAQQYN LRAKYAAATG GPPPTPLPGL DRVSLRTRLA
 901 LLDAPERALP GACPHPLGPR RGSDGPTYSH GHGHGYAGAA PAFPHEGPNS
 951 STRRASDPVR RPDPLILPRV QRFHSTHNMN PGSLPPCADR RGLHVQSHPS
1001 VDSNLTRNAY SPRPPSINEN VVMEAVAAGV DGPGLECDLG LVEDELVLPD
1051 DVVQYIKAHT GGTLDDGIRQ GYPTEGTGFP ENSKLPSPGL QGHRRLAAAD
1101 SNMGPSAPGL GGCQLSYSPS SNLNKSNMPV QWNEVSSGTV DALPTQVKPP
1151 PFPHSNLAVV QQKPAFGQYP GYNPQSVQSS SGGLDSTQPH LQLRGAPSAS
1201 RGSYTQQPRQ PAAGSQCLGM SAAMSPQASY SQAHPQLSPN IVSGSLNQFS
1251 PSCSNMAAKP SHLGLPQQME VVPNATIMNG HQREHGVPNS SLAAVSQPHP
1301 VLSYPQQDSY QQGSNLLSSH QPGFMESQQN AGFGLMQPRP PLEPNTASRH
1351 RGVRSGQQQL YARTTGQAMV TSANQETAEA MPKGPAGTMV SLAPQPSQDT
1401 GRAQDQNTLY YYGQIHMYEQ NGGCPAVQPQ PPQPQACSDS IQPEPLPSPG
1451 VNQVSSTVDS QLLEPPQIDF DAIMDDGDHS SLFSGALSPT LLHNLSQNSS
1501 RLTTPRNSLT LPSIPAGISN MAVGDMSSML TSLAEESKFL NMMT
```

Figure 5-05 HA-Gli2 transfected and extracted from Hek293T is identified by MALDI-TOF mass spectrometry

(A) 4-12% Tris Acetate SDS PAGE of HEK293T lysate from cells transfected with constructs pcDNA3-HA-p190RhoGEF in lane 1, pCEFL3XHAmGli2 in lanes 2-4 and un-transfected in lane 5. Lanes 2-4 are loaded with eluents from Gli2 pull-down purification procedure. (Lane 2) Gli2 was selected by binding to oligonucleotide sequence that corresponds to Gli2 transcription factor binding regions. (Lane 3) Prepared lysate controls for nonspecific binding using a mutated Gli2 binding sequence oligonucleotide. (Lane 4) Control enrichment with only magnetic bead. Proteins were electroblotted to PVDF membrane and probed by rabbit anti-HA and mouse anti-Beta Tubulin primary antibodies. Secondary antibodies 800CW (shown in green) anti-mouse reveals Rgnef in lane 1 and Gli2 in lanes 2 to 4. Secondary 680RD (shown in red) reveals Beta-Tubulin in all lanes. Lane 5 provides a negative control for background nonspecific binding. Silver staining SDS PAGE also reveals this band of HA-Gli2 pull-down detected in lane 2 and is absent from lanes 3 and 4 controls. The total protein lysates are over developed in Lanes 1 and 5 in order to allow time to develop the HA tag pull-downs in lanes 2-4. HA-Gli2 purification is observed by the increase in HA-Gli2 band intensity relative to control bands and in light of the decrease in total protein, demonstrated by the loss of intensity of the 55 kDa Beta tubulin. (B) After beta tubulin intensity normalisation in each lane, the Gli2 band intensity from the lane 2 pull-down is 2.5 times higher than controls in lane 3 and 4. Fluorescent band intensity for 78 kDa Gli2 is only observed after Gli2 enrichment. (C) A representation of Gli2 protein sequence with MALDI-TOF identified trypsinised sequences in red. The total sequence coverage amounted to 2%.

5-05 HA-Gli2 and HA-Rgnef protein enrichment by HA tag immunoprecipitation

The aim of these experiments was to improve on HA-Gli2 protein enrichment for Gli2 mass spectrometry characterisation. The method of enrichment was immunoprecipitation (IP) using an anti-HA magnetic beads complex. Pre-optimised and tested, this immunoprecipitation binding complex provides the high yield and specificity benefits of high affinity antibody binding. Unlike enrichment by target oligonucleotide binding (section 5-01) it captures Gli2 irrespective of the state of its tertiary protein structure. Removal of captured Gli2 from the complex was tested by two elution buffers; a basic (pH 8) 50 mM NaOH buffer and an acidic (pH 2) 100 mM glycine buffer.

A positive control measure was also prepared by overexpressing HA-Rgnef in HEK293T cells. Details of the transfected plasmid construct pcDNA3-HA-p190RhoGEF can be found in Section 3-01. In these experiments HA-Rgnef solely provides a similar sized (190 kDa) HA-tagged protein to use as a positive control.

Immunodetection for HA-Gli2 reveals bands from both basic and acidic elution buffers (Figure 5-06 A). In terms of migration and shape, the protein bands from the basic buffer were comparable to those detected in the lysate before purification. The protein band from the acidic buffer elution appears to have migrated less, appears fainter and seems more coalesced. In comparison, Rgnef HA immunoprecipitation also produced a band using the basic buffer and no band at all with the acidic buffer (Figure 5-06 A). This may not be the result of protein degradation as the low pH may have simply compromised SDS PAGE loading buffer. Nevertheless the basic buffer was clearly providing better results and chosen for protein elution prior to MS preparation and analysis. Yet one consideration to take forward is that the stringency of the basic buffer is reported to cause HA antibody leaching from the beads (Pierce™ Anti-HA Magnetic Beads protocol 88836). This would therefore be a contamination to factor in for subsequent mass spectrometer analysis.

Detected HA-Gli2 bands in relation to HiMark protein standard curve were calculated to be 216 kDa and 101 kDa, far larger than 185 kDa and 78 kDa published for Gli2. The 190 kDa Rgnef protein detected in lane 1 was also found to be larger at 230 kDa. This

40 kDa increase in Rgnef detected was used to proportionally re-calibrate the standard curve. Upon recalculation, Gli2 was approximated to 175 kDa and 82 kDa, within range of expected molecular weights. The comparison to Rgnef provides evidence that Gli2 is detected despite the discrepancy measured by the protein standard. Further evidence is the reported high specificity of the antibody used for Gli2 when overexpressing in HEK293T (Pan et al., 2006), and the lack of detected protein in control un-transfected lysate lane (Figure 5-06 A (lane 5)). Furthermore, Gli2 detection using anti-Gli2 antibody instead of anti-HA, also detected a larger 200 kDa band for Gli2 (Section 5-02).

Also observed in this and previous experiments is how Gli2 protein bands appear vertically broader than would be expected for a single protein (Figure 5-06 A). Rgnef-HA provides an example of a clearly defined band, as usually expected in western detection of a single protein (Figure 5-06 B). Protein degradation is a possible reason for the broader Gli2 band; however this seems unlikely as degradation would also be expected to be seen with Rgnef-HA and involve a wider and less consistent spread of detected protein. The broad band may therefore represent a range of PTM, ranging from a higher to low number of modifications to Gli2. To explain; the increased molecular weight of the highly modified Gli2 proteins would migrate less than their low or unmodified versions, resulting in a thickened band.

Paired SDS PAGE gel followed by protein silver staining also detected the over expression bands of both HA-Gli2 and HA-Rgnef amongst surrounding total protein bands. The respective bands for HA-Gli2 and HA-Rgnef are not seen in each other lanes amongst the numerous comparable total protein bands detected. It provides early indication of adequate protein available for mass spectrometry analysis amongst the total protein retained during the purification step (Figure 5-06 A and B).

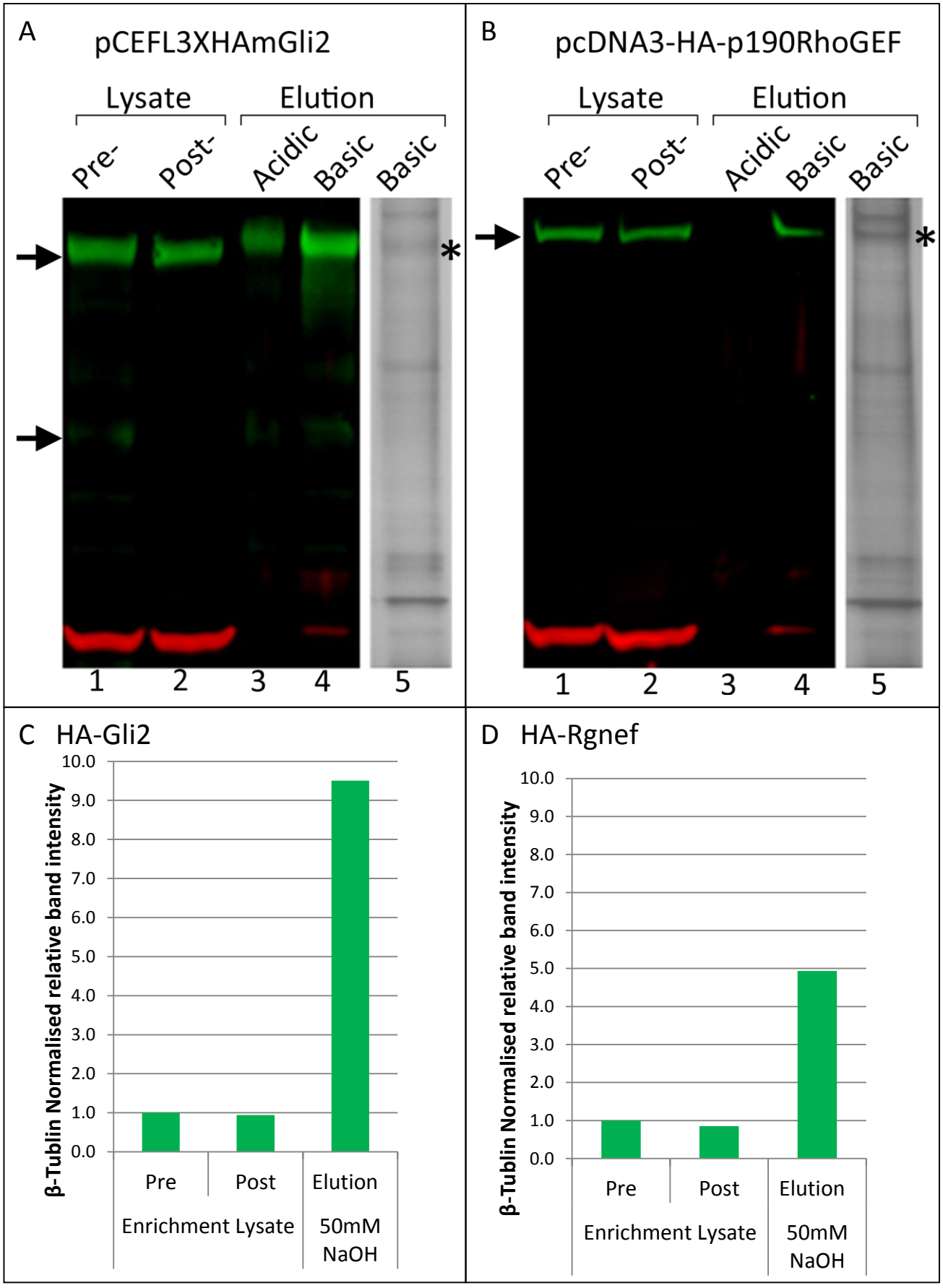
A
pCEFL3XHAmGli2
Lysate
Elution
Pre-
Post-
Acidic
Basic
Basic
*
1
2
3
4
5
B
pcDNA3-HA-p190RhoGEF
Lysate
Elution
Pre-
Post-
Acidic
Basic
Basic
*
1
2
3
4
5
C HA-Gli2
β-Tublin Normalised relative band intensity
10.0
9.0
8.0
7.0
6.0
5.0
4.0
3.0
2.0
1.0
0.0
Pre
Post
Elution
Enrichment Lysate
50mM NaOH
D HA-Rgnef
β-Tublin Normalised relative band intensity
10.0
9.0
8.0
7.0
6.0
5.0
4.0
3.0
2.0
1.0
0.0
Pre
Post
Elution
Enrichment Lysate
50mM NaOH

Figure 5-06 HA-Gli2 and HA-Rgnef protein enrichment by HA tag immunoprecipitation

(A and B) Immunoblots showing anti-HA immunoprecipitation enrichment of (A) HA-Gli2 and (B) HA-Rgnef. SDS PAGE and immunoblot were prepared to analyse lysate before (lane 1) and after (lane 2) enrichment by incubation with anti-HA antibody conjugated magnetic bead complex. Two elution methods were tested; (lane 3) an acidic pH 2 glycine buffer and (lane 4) a basic pH 8 NaOH buffer. Highlighted by arrows are respective bands for (A) HA-Gli2 and (B) HA-Rgnef, detected by mouse anti-HA primary antibody and secondary anti-mouse 800CW in green (Licor). Also detected was β-Tubulin by rabbit anti-β Tubulin primary antibody and secondary anti-rabbit 680RD in red (Licor). (Lane 3) Acidic glycine buffer did not elute protein bands comparable to HA-Gli2 detected in lysate and HA-Rgnef elution was undetected. (Lane 4) In contrast, 50 mM NaOH elution buffer performed better for both Gli2 and Rgnef having maintained the migration, shape and intensity detected in total lysate prior to purification step. (Lane 5) Silver stained SDS PAGE gels corresponding to basic buffer elution of Gli2 HA and Rgnef HA also detected protein bands as highlighted by (*). As a result the eluent derived from NaOH buffer was subject to, tryptic digest and subsequent peptides resolved by nano-flow high performance liquid chromatography for MS analysis.

(C and D) Measurement of band intensity in immunoblots for HA-Gli2 bands in (A) and HA-Rgnef in (B) respectively. Intensity was normalised against detected β Tubulin as it was still observed to persist after purification of HA-tagged proteins. Band intensities in protein lysate prior to (pre) and after (post) immunoprecipitation were compared, along with final eluent. Hence compared to lysate, the result highlights the enrichment of HA-tagged proteins in eluent by using β Tubulin as a marker for total protein.

5-06 HA-Gli2 transfected and extracted from HEK293T cells is identified by Amazon Ion-Trap mass spectrometry

The aim was to improve upon the preliminary MALDI-TOF identification of Gli2 by reducing the high peptide loss required for sample preparation (Section 5-04). Hence a new mode and method was employed using Ultimate™ 3000 RSLCnano HPLC system (Thermo Scientific Dionex) coupled to an Amazon ion trap mass spectrometer (Bruker). This enabled a direct route to protein analysis as the procedure does not require SDS PAGE followed by in-gel tryptic digest. Rather, the entire sample eluent can be analysed, providing a more rapid and more comprehensive analysis.

The results of six independent peptide preparations showed that each significantly identified Gli2 and together provided a reproducible 28% sequence coverage (Figure 5-07). Mapped out along Gli2's protein sequence, the identified peptides were not randomly distributed and instead were found in localised regions of the Gli2 sequence. Hence peptides identified 6 times would normally be flanked by those identified 4 or 5 times. This was effectively a Gaussian distribution pattern, as the frequency would reduce further from central well-defined regions, until there were sections of unidentified protein (Figure 5-07). It is a pattern that could reflect the exposed regions in the tertiary structure of Gli2. These regions identified are therefore hypothesised to be areas not hidden by protein folding or were at least easily exposed by reducing agents used. These regions would therefore be more responsive to trypsin enzyme digestion. As Gli2 is a large 185 kDa protein, the results suggest that more extensive protein degradation is required to achieve higher protein coverage.

Two peptides characterised; aa788-aa803 (n=4) and aa804-aa814 (n=1) were identified as modified by multiple phosphorylation sites (Figure 5-07). The areas covered by these peptides correspond to region aa784-aa855, reported to be PKA, CK1 and GSK3 phosphorylated sites (Pan et al., 2006). This was also an area that Prosite (de Castro et al., 2006) predicted to have multiple phosphorylation sites (Figure 5-07). Adjacent to this region, 73 amino acids downstream towards the C termini, a region aa873-aa1007 was also readily identified by six peptide sequences, however phosphorylation in this region was undetected (Figure 5-07).

MS coverage of the zinc finger domain between aa493-aa578 identified two serine phosphorylation sites (aa560 and aa559) that also corresponded to the Prosite predicted cAMP phosphorylation sites (Figure 5-07). Also a total of five phosphorylated peptides were also identified near the N-terminus and eight C-terminus (Figure 5-07). These sites were however unpredicted by Prosite. These specific “zinc finger”, N-terminus and C-terminus sites of phosphorylation represent potentially new sites of Gli2 regulation.

In blue: MS detected fragments

In red: MS detected phosphorylation site

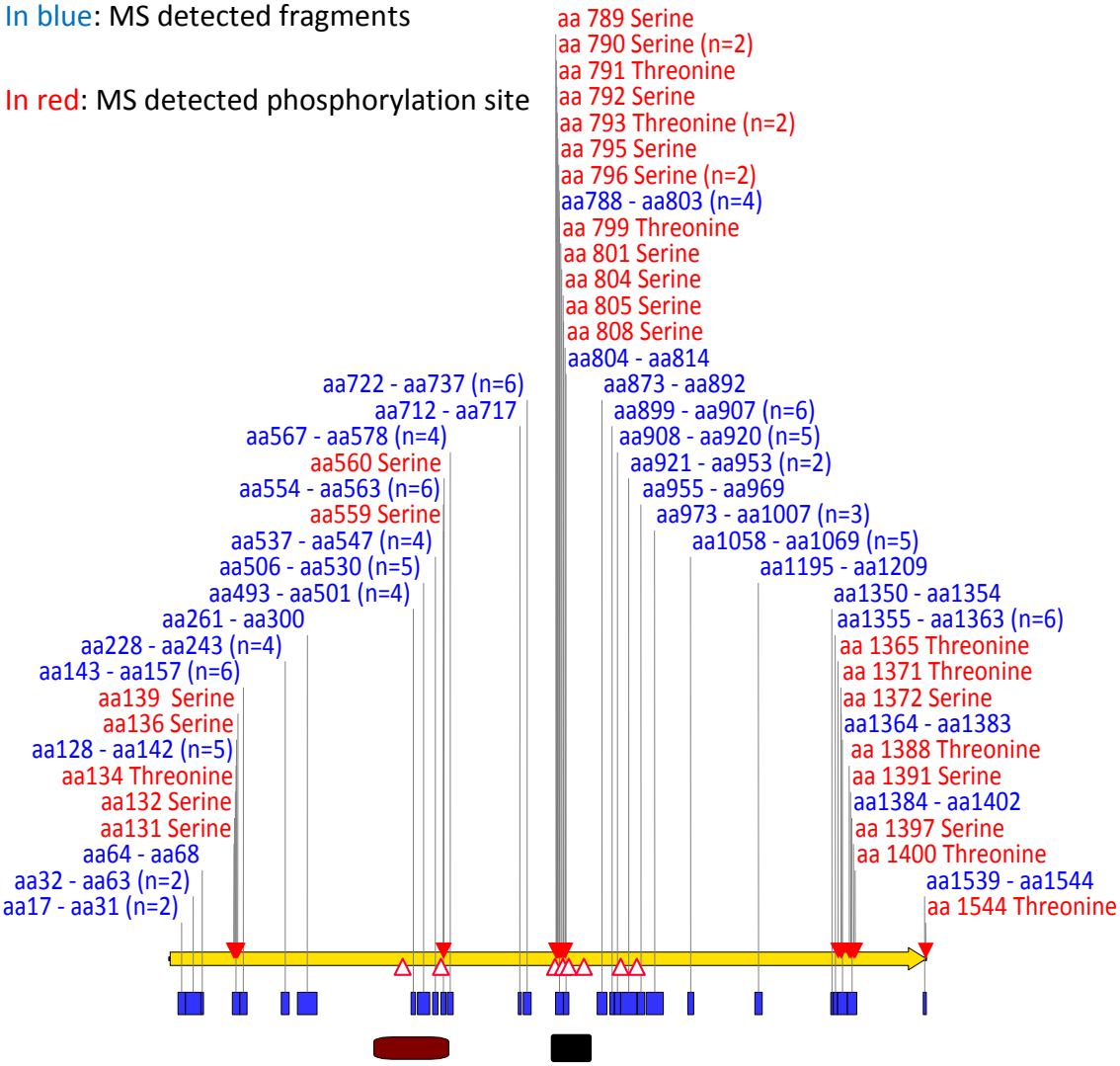

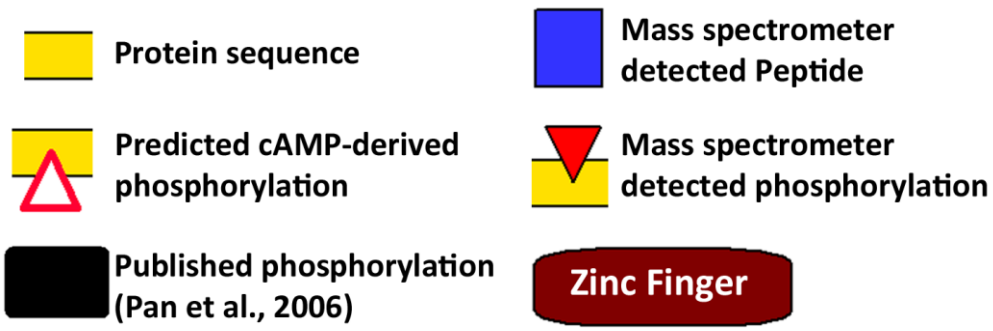

Figure 5-07 HA-Gli2 transfected and extracted from Hek293T is characterised by Amazon Ion-Trap mass spectrometry

Results of LC-MS Dionex 3000 Nano HPLC in conjugation with Amazon Ion-trap MS Analysis of protein extract from HEK293T cells transfected with pCEFL3XHAmGli2 (Kim et al., 2009a). The results are a summary of Gli2 identified from six independent peptide preparations that together provide 28% sequence coverage. Two peptide sequences identified in a region reported to have Gli2 phosphorylation sites (Pan et al., 2006). These were aa788-aa803 and aa804-aa814 and within this sequence a combination of eight Serine and Threonine peptides were detected as modified by phosphorylation. Adjacent to this region, 73 amino acids downstream towards the C terminus side between aa873 and aa1007 was also readily identified by six peptide sequences but without any detected phosphorylation. Phosphorylation was detected in the zinc finger domain of Gli2 as well at either end of Gli2 sequence at the N and C termini. These terminal end phosphorylation were not predicted by the ScanProsite (http://www.expasy.org/tools/scanprosite/), whereas predictions were made that corresponded to the other sites of detected phosphorylation.

5-6-01 Phosphorylation of Gli2

In these experiments HA-Gli2 was extracted from HEK293T cells during Shh signalling pathway inactivation for direct MS analysis of PTM. Direct MS sequencing of Gli2 provides an independent assessment of potential PTMs that can be compared and contrasted against current findings. Table 5-01 provides a list of each Gli2 PTM identified along with any previous findings or related Prosite predictions. A region of particular interest for Gli2 is between amino acids 784-855, identified as PKA, CK1 and GSK3 phosphorylation sites for transcription factor regulation (Pan et al., 2006). In Gli2, phosphorylation of this region relates to negative regulation of the Shh signalling pathway (Pan et al., 2006). In confirmation, the MS analysis of the aa788-803 peptide fragment identified within this region of Gli2 detected multiple phosphorylated residues. This includes all the predicted PKA, CK1 and GSK3 phosphorylated sites identified as either primary or secondary sites of phosphorylation (Pan et al., 2009). This region also occurs in Gli3 and is subject to the same PTM (Pan et al., 2009). There is therefore very strong sequence homology between these two regions in Gli2 and Gli3 (Figure 5-08 C). These results therefore provide the first mass spectrometer derived evidence to confirm the active phosphorylation of this region.

Prior to MS analysis, my Prosite analysis of Gli2 also predicted two potential PKA phosphorylation sites corresponding to the second and fifth zinc fingers. The MS peptide coverage I achieved did not extend to the second zinc finger, but did discover two phosphorylated serine residues (Serine aa559 and aa560) in the fifth zinc finger, that corresponded to the Prosite prediction. There are no reports of phosphorylation within the Gli2 zinc finger domain. However phosphorylation of the second zinc finger of Gli1 has been reported by others to negatively regulate Gli1 in a process that does not involve proteolytic cleavage (Kaesler et al., 2000). Zinc finger domains are well conserved in all the Gli proteins, so that by association this identified region of PTM in Gli2 may also be a means of negative regulation (Figure 5-08 B). It also raises the question of whether Gli1 and Gli3 are also subject to the same PTM and regulation as they also share homology with Gli2 zinc finger regions (Figure 5-08 B). Interestingly, the zinc finger domains are also retained in Gli2 and Gli3 repressor forms. The possible regulation of this shared region could therefore potentially provide an overriding layer of regulation for all Gli proteins, including isoforms. This high Gli protein zinc finger

sequence homology also extends to *Drosophila* and human Gli2 protein orthologues (Figure 5-08 C).

The regions of PTM that bestow positive regulation of Gli1 and Gli2 by ULK3 phosphorylation are broadly defined as being at either ends of the proteins (Maloverjan et al., 2010b). However the specific regions were only deduced by investigating broad Gli1 segments between aa1-426 of the N-terminus and aa754-1126 of the C-terminus (Maloverjan et al., 2010b). Together these regions contain 125 potential serine and threonine phosphorylation sites (Maloverjan et al., 2010b). In my study, specific phosphorylated N and C terminal serine and threonine residues were identified in Gli2 that by alignment come within these broad regions of Ulk3 phosphorylation in Gli1 outlined by (Maloverjan et al., 2010b). Specifically these are five residues near the N-terminus between aa131-aa139 and a further eight near the C-terminus spanning between aa1365-aa1544 (Figure 5-08 A, E and F). In alignment with Gli1 there is almost no specific residue homology, it is however fair to hypothesise that although specific residue may differ in this broad region the function may be the same. There is certainly better homology in these regions with Gli3, particular in the N-terminal regions (Figure 5-08 A, E and F). These regions are also retained in cleaved Gli2 and Gli2 repressor isoforms (Figure 5-08 A, E and F).

Table 5-01 Related evidence for MS detected Gli2 phosphorylation

residue position and type	Evidence for each Gli2 phosphorylation site. Grey shading denotes novel MS PTM detected
aa131 Serine	
aa132 Serine	
aa134 Threonine	
aa136 Serine	
aa139 Serine	
aa559 Serine	
aa560 Serine	
aa789 Serine	Predicted as cAMP phosphorylation site by Prosite* Identified as PKA site (Pan et al., 2006)
aa790 Serine	
aa791 Threonine	Identified as GSK3 and CK1 site (Pan et al., 2006)
aa792 Serine	Identified as CK1 site (Pan et al., 2006)
aa793 Threonine	
aa795 Serine	Identified as GSK3 and CK1 site (Pan et al., 2006)
aa796 Serine	
aa799 Threonine	
aa801 Serine	Predicted as PKC site by Prosite* Identified as GSK3 site (Pan et al., 2006)
aa804 Serine	Identified as GSK3 site (Pan et al., 2006)
aa805 Serine	Predicted as cAMP site by Prosite* Identified as PKA site (Pan et al., 2006)
aa808 Serine	Identified as CK1 site BW (Pan et al., 2006)
aa1365 Threonine	
aa1371 Threonine	
aa1372 Serine	
aa1388 Threonine	
aa1391 Serine	
aa1397 Serine	
aa1400 Threonine	
aa1544 Threonine	

* ScanProsite - http://www.expasy.org/tools/scanprosite/ (de Castro et al., 2006)

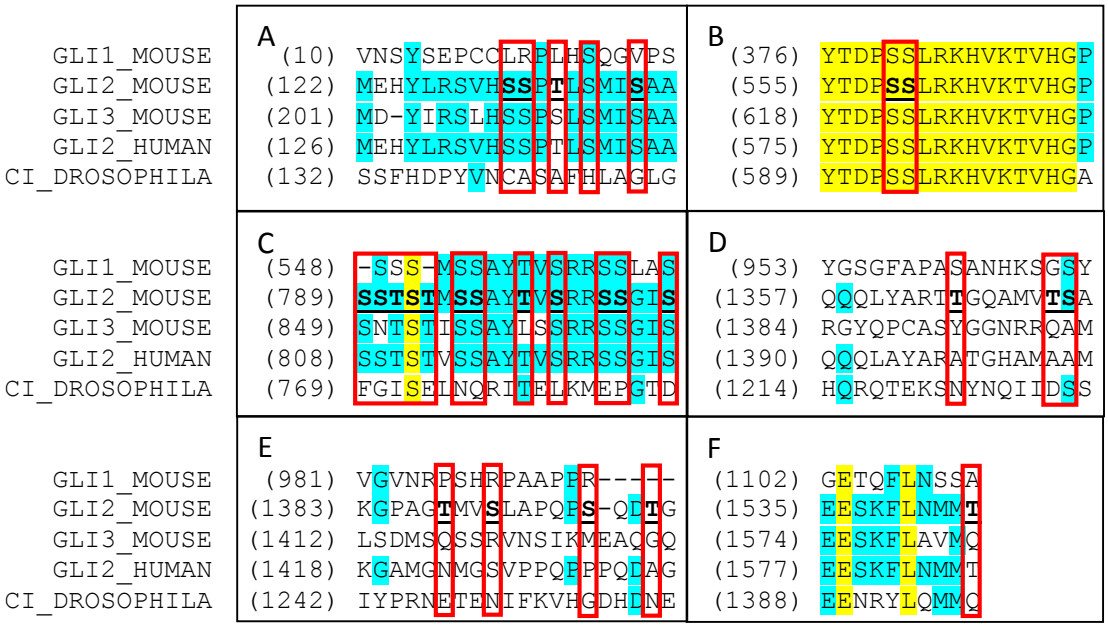

Figure 5-08 Sequence alignment with Gli1 and Gli2 against MS detected GLI2 phosphorylation sites and with human and *Drosophila* Gli2 protein homologues.

Vector NTI-AlignX derived alignments based regions of MS detected Gli2 serine and threonine amino acid sequences (bold and underlined). Alignments were made with the other two mouse Gli protein family members (Gli1 and Gli3) as well as human GLI2 and *Drosophila* Ci protein orthologues. Colour coding summarises collective amino acid similarities: black on white - non-similar residues, black on cyan - the occurrence of greater than 50% of a single residue; red on yellow - completely conserved residue in all sequences aligned. (A) N-terminal region of proteins alignment where 6 serine Gli2 protein residues were MS detected for phosphorylation. All these residues share homology with Gli3 and human Gli2 and some with Gli2, although no similarity is detected with drosphila Ci. (B) Two MS detected Gli2 serine residues within the zinc finger in a region with complete sequence homology with all sequences in alignment. (C) This region produced a high number of MS detected Gli2 phosphorylation sites and incorporates a region of Gli2 and Gli3 that has been identified as PKA, CK1 and GSK3 phosphorylation sites for transcription factor regulation (Pan et al., 2006). (D-F) Three C-terminal regions showing MS detected phosphorylated residues in Gli2. Overall sequence homology is these regions are not high amongst all the sequences, although specific residue matches do occur.

5-07 Discussion - Mass spectrometer characterisation of Gli2

The main strengths of the 28% coverage of Gli2 sequence by Amazon ETD analysis was the reproducibility of the regions identified. A strategy to improve sequence coverage requires a review of all steps involved in the process. At 185 kDa, Gli2 is a large protein to optimally denature and fragment. This particularly highlights the importance of sample preparation and as such is the focus of the next section as it provides the highest potential to improve Gli2 characterisation.

Following on from sample preparation is the process of nano-HPLC and the aim here is to provide the optimal resolution of peptide fragments for mass spectrometry analysis. The time and gradient increase of the non-polar solvent is required to be uniquely defined for every protein analysed. Furthermore the nano HPLC flow rate of 0.25 µl min^{-1} is highly susceptible to even precise changes in set-up. Factors to consider include the precise integrity of the 20 µm internal diameter of silica tubing, to ensure samples are not dispersed causing broad chromatogram peaks. Care also needs to be taken to ensure the continuous quality of reagents. Peptides can then enter the MS by optimising the very fine process of sample nano-spray ionisation.

One of the main processes of this study was mass spectrometer fragmentation of peptides (MS/MS fragmentation) which was achieved consecutively by both collision-induced dissociation (CID) and electron transfer dissociation (ETD). The aim was to use alternative methods for MS/MS fragmentation in order to increase the opportunity of sequence coverage and PTM identification. ETD provides alternative fragmentation patterns that can complement CID-derived data, improve coverage or even identify novel modifications (Sobott et al., 2009, Juang et al., 2013). Using CID and ETD together in analysis of Gli2 resulted mostly in identification of the same peptide fragments. However ETD would identify the peptide by a different set of MS/MS ion pattern identification and in effect this process mostly enabled ETD to confirm CID identifications. However, a notable exception was that only by ETD was it possible to identify serine phosphorylation (aa559 and aa560) within the Gli2 zinc finger domain. A likely explanation is that the more energetic CID fragmentation removed the specific phosphate moiety whereas the less energetic bombardment of ETD retained the

amino acid to phosphate bond. A summary discussion of all the Gli2 phosphorylation sites identified is provided in section 5-7-02.

5-7-01 Sample preparation methods for proteome analysis

The successful characterisation of HA-Gli2 extracted from HEK293T cells required a substantial change in the methodology from initial attempts at characterising endogenous Gli2 in NIH 3T3 cells. This included switching amongst the two major strategies for protein extraction and peptide processing; in-gel and in-solution digestion. “In-gel” involves denaturing and separation of proteins by SDS PAGE followed by digestion of proteins whilst trapped in the gel (Cohen and Chait, 1997). SDS PAGE is an effective means to resolve, denature and solubilise proteins, yet SDS inhibits enzymatic digestion and proves to be a readily ionised problematic MS contaminant. In comparison, the use of in-solution digestion demonstrated the extent at which peptides can be delivered to the mass spectrometer with minimal handling and intervention. The success of this method also required an abundant amount of Gli2, which was achieved through using an easily transfectable HEK293T cell line to overexpress a tagged HA-Gli2 construct.

An interesting observation made during sample preparation was the thickened HA-Gli2 band revealed after immunoblotting and even when directly silver staining SDS-PAGE gels. The conclusion proposed was that the broad band represented layers of Gli2 PTM, ranging from a high to low number of modifications to Gli2. If these findings are related to PTM then they may also provide a means to detect modifications by examining changes in band thickness. This can be achieved by systematically blocking types of PTM prior to western detection and looking for a reduction in band thickness. In doing so PTMs can be quickly and easily detected allowing input to more specific mass spectrometry parameters for improved PTM detection. In future analysis this would provide a simple means to test for a range of PTM to then provide preliminary evidence to focus mass spectrometry investigations on specific modifications.

Once Gli2 modifications are revealed by MS, specific *Gli2* sequences that encode these regions can be modified by insertional mutagenesis for further expression analysis. In this way, sites of PTM can be associated to functions such as primary cilia localisation and Shh signal pathway activation (Pan et al., 2006, Garcia-Gonzalo and Reiter, 2012).

Nevertheless such methods are still limited on validating pre-identified sites of protein modification. Results may also be deemed unrepresentative if based on levels of protein overexpression that exceed endogenous limits. There is therefore a need to evidence these findings based on endogenous protein detection and do so across alternative cell types. The challenge is to improve traditional “in-gel” and “in-solution” sample preparation techniques so as to improve the sensitivity required to analyse low levels of endogenous protein. A solution may be filter-aided sample preparation (FASP), a method that aims to combine the advantages of in-gel and in-solution digestion techniques (Wisniewski et al., 2009). The method proposes containing proteins in ultra-filtration devices that enable complete depletion of any impurities after treatment. This includes denaturation with SDS as it can be completely cleared by a urea buffer treatment, before enzymatic digestion by trypsin. Peptides retained by ultrafiltration can then be concentrated in µl volumes before automated MS insertion. The success of this method is in the ability to fully denature protein with reduced handling, without retaining impurities and faster peptide processing. This will also reduce the loss and damage of peptide that occurs from “in-gel” sample preparation, particularly important when attempting to analyse low amounts of endogenous protein.

FASP may therefore improve upon the 28% coverage achieved by in-solution digest, particularly as the coverage pattern favoured specific regions. Sequenced regions are hypothesised to be detected due to their accessibility to tryptic digest. Improved protein denaturation by FASP can prepare Gli2 for better accessibility to protein digest whilst still retaining the direct peptide to MS benefits of the in-solution digest.

Finally, uses of additional enzymes in combination with trypsin such as, LysC, chymotrypsin, AspN and elastase, have been reported to also improve MS protein coverage (Winter et al., 2009). This is particularly relevant to phosphorylation analysis as it can inhibit proteolysis by trypsin if adjacent to its target site (Winter et al., 2009).

Chapter 6: Discussion

6-01 General Discussion

The set of specific experimental aims in this thesis were set in the context of a broader investigation relating to the molecular mechanism of Shh signalling in NT development. The starting point for this thesis came from the observation that mice carrying a disruption of the *Tulp3* gene exhibit neural tube defects, and also demonstrate over-activation of the Shh signalling pathway (Cameron et al., 2009, Norman et al., 2009, Patterson et al., 2009). Tulp3 was shown to act as a negative regulator of the Shh signalling pathway, acting between Shh/Smo and cilia/Gli2. Investigations to find interacting protein partners of Tulp3 identified Rgnef and Trim71. Therefore in this thesis, the overall aim was to pursue the hypothesis that Rgnef and Trim71 may themselves play a role in regulating the Shh signalling pathway and how their functions then subsequently relate to NT development.

The study of Gli2 PTM in this thesis was undertaken with the aim of detailing how Shh signal transduction manifests itself on the structure of a member of the Gli family of transcription factors. Precise understanding of exactly how Gli proteins are modified is still lacking. Using the Shh-LIGHT2 assay only reports on Shh activation states but cannot reveal the complex molecular mechanisms of pathway regulation (Section 3-10), particularly when much of what is understood about pathway states of activation involves modifications at a protein level (Section 1-4-02). In this thesis only Gli-dependent pathways are being examined, yet there are proposed examples of non-canonical Shh signalling where Gli proteins are not required (Renault et al., 2010, Polizio et al., 2011). This reiterates the need to encompass an even broader understanding of Shh pathway activation and the molecular mechanisms involved.

Amongst the Gli2 coverage by MS analysis in this thesis there was a consistently detected region between amino acids 784-855 that is of particular interest for Gli2 PTM analysis. This region contains known PKA, CK1 and GSK3 phosphorylation sites that regulate the process of Gli2 proteolytic cleavage to repressor form (Pan et al., 2006, Pan et al., 2009). A homologous region also exists in Gli3 providing the same function as in Gli2 (Pan et al., 2006, Pan et al., 2009). It should therefore be possible to use the same MS preparation and analysis techniques employed for Gli2 to also successfully analyse PTM in this region of Gli3. As well as being the first MS

characterisation to confirm these findings for this region, the results also provide a level of confidence for the novel sites of Gli2 PTM detected in this thesis.

Novel sites include Gli2 PTM identified within the zinc finger domain, a homologous region found in all three Gli proteins and across species in human, mice and *Drosophila*. Further understanding the purpose of modifications within this highly conserved region will therefore have a high probability of translating to human GLI protein function in the Shh signal pathway. Further investigation into Gli protein zinc finger PTM would therefore be an area of great interest particularly as zinc finger region PKA phosphorylation has been reported to negatively regulate Gli1 (Kaesler et al., 2000).

The novel PTMs identified in both the N and C terminals of Gli2 represent regions that are relatively less known in function and appear to show the least homology to other Gli proteins or species orthologues. There is some evidence in Gli1 that ULK3 phosphorylation within these broad regions results in positive regulation of Shh signal pathway (Maloverjan et al., 2010b). However this finding would require further investigation in Gli2 and as such have a high potential of discovering novel regulatory steps in Shh signal transduction relating to PTM.

6-1-01 Rgnef - positive regulator of Shh signalling in neural tube development.

Identifying localised *Rgnef* expression in the neural tube of developing embryos was a key finding in relating Rgnef activity to neural tube development. Functional evidence was then provided by the Shh-LIGHT2 assay in demonstrating that a loss or gain of *Rgnef* expression directly relates to suppression or activation of Shh pathway activity, respectively, and therefore identifies Rgnef as a positive regulator of the Shh signalling pathway. This is clearly opposite to negative regulator Tulp3 (Cameron et al., 2009, Norman et al., 2009, Patterson et al., 2009). Hence this suggests there is an antagonistic relationship between Tulp3 and Rgnef, in relation to Shh signal transduction. The evidence taken together proposes a model in which in Tulp3 deficient mice, *Rgnef* expression in the NT results in the observed activation of the Shh signalling pathway. One limitation with this model is that *Rgnef* has a highly localised expression domain, confined to the cells of the most ventral region of the neural tube (the floor plate). In contrast, *Tulp3* mutants demonstrate enhanced Shh pathway

activation over the ventral two-thirds of the neural tube. This would suggest that activation of the Shh pathway in the absence of Tulp3 is not dependent on the expression of Rgnef and the importance of Rgnef may only be in the NT floorplate.

Mice that have compromised Shh signalling pathway activation, such as *Shh*$^{-/-}$ and *Smo*$^{-/-}$, do not have NTD and in the case of Shh$^{-/-}$ (Chiang et al., 1996, Zhang et al., 2001). Therefore we would also not expect *Rgnef* mutants to show NTDs. Yet in contrast, increased activation of the Shh signalling pathway often does cause NTDs (Ybot-Gonzalez et al., 2002, Ybot-Gonzalez et al., 2007, Greene and Copp, 2009, Murdoch and Copp, 2010). Therefore we would predict that over-expression of Rgnef might lead to NTDs. It would be interesting to investigate the effect of Rgnef over-expression in developing mice and whether that would lead to NTD.

Shh pathway activity is critical for regulating dorso-ventral patterning of the neural tube (Jessell, 2000). We would predict that the *Rgnef*$^{-/-}$ mutant mice would show some disruption of DV patterning. This has not been investigated but would test the hypothesis that a lack of *Rgnef* would result in a more dorsalised DV pattern from suppressed Shh pathway activation. Given the highly localised expression pattern of *Rgnef*, we would expect probably only subtle changes in DV patterning. Attempts to obtain some *Rgnef* mutant embryos to test this idea were, unfortunately, unsuccessful. Conversely, we would expect the opposite effect following *Rgnef* over-expression, with more ventralised DV patterning, similar to (though probably more subtle than) that observed in *Tulp3* deficient mice. Attempts to test the over-expression of *Rgnef* involved construction of the bicistronic plasmid pCAGGS Rgnef (Section 3-6-01), encoding both *Rgnef* and GFP, with the aim of transfecting this into chick embryos. The experiment would have allowed the effect of *Rgnef* expression on patterning to have been tested. Unfortunately, this experiment didn't work.

Investigations into the cellular mechanisms involved have shown that over-expression of *Rgnef* impairs primary cilia formation. Primary cilia are central to the current model of Tulp3 negative regulation in Shh signalling. Hence a lack of primary cilia would remove the very purpose for Tulp3 IFT-A complex formation, proposed as a model of G-coupled receptor ciliary trafficking to induce cAMP driven PKA activation (Mukhopadhyay et al., 2010, Qin et al., 2011, Mukhopadhyay et al., 2013). The

purpose of Tulp3 binding to Rgnef could therefore be to permit Rgnef from impairing ciliogenesis, hence a separate cytoplasmic complex that sequesters Rgnef in the cytoplasm (Figure 6-01). In mode of action the model can be compared to the multiple functions of Sufu; able to bind and sequester Gli transcription factors and yet form a complex with kinase GSK3 to promote proteolytic cleavage of Gli3. Yet all these specific molecular interactions by Sufu are united in the coordinated purpose of Shh pathway suppression (Ding et al., 1999, Dunaeva et al., 2003, Jia et al., 2009, Kise et al., 2009).

An alternative model is to propose that Tulp3 and Rgnef binding relates to Tulp3's role in primary cilia protein traffic regulation across the transition zone (Figure 6-02). Evidence shows that Tulp3 and IFT-A protein binding is modelled on providing a permissive role into the primary cilia for G-coupled receptor protein transport (Mukhopadhyay et al., 2013). Yet the specific purpose of this complex may provide a means of regulation for exiting the primary cilia, particularly as IFT-A protein are required for retrograde transport within the cilia. Furthermore, previous to this thesis, the same yeast-2-hybrid screen that identified Rgnef and Trim71 also detected nuclear pore complex Nup155 as another potential Tulp3 binding partner. Although nuclear pore complex proteins regulate protein traffic through the nuclear membrane, they have recently been localised to the base of cilia transition zones and shown to regulate ciliary traffic (Takao et al., 2014). There is also preliminary evidence that Nup155 is amongst the specific nuclear proteins identified with this dual role (In conversation with Kirsten J Verhey). Hence as a direct binding partner, Rgnef connection with the primary cilia structure should be fully investigated in terms of ciliary transport regulation and not just in terms of ciliogenesis. Hence the high Rgnef expression that results in a lack of primary cilia is instead proposed as evidence that implicates Rgnef in primary cilia mechanism rather than suggest a mode of action. Testing this hypothesis requires investigating Rgnef expression changes at levels that bear more resemblance to its endogenous range. Such investigations require assessing the effects of lower expression increases than induced by pcDNA3-HA-p190RhoGEF or pCAGGS Rgnef. This can be achieved by sub cloning plasmid constructs with reduced or controlled expression capability and investigate the effect of inducing graduated expression changes on Shh pathway activation. Methods include sub cloning low expression

promoters or the use of drug inducible constructs, such as tetracycline-controlled gene expression systems (Gossen and Bujard, 1992, Freundlieb et al., 1997, Gossen, 2006). The approach will help ensure that levels of induced cellular Rgnef are at levels that better reflect endogenous Rgnef expression.

Adapted plasmid expression constructs can also be used to address the question of whether Rgnef acts as a GEF protein in Shh signal pathway activation. Rgnef binding to scaffolding protein JIP-1 has been shown to promote JNK activation without GEF related RhoA activation (Meyer et al., 1999). Single point mutations within Dbl-homology and plekstrin-homology (DH/PH) domains of GEF proteins will inactivate RhoA binding and GTPase activity (Chen et al., 2011b). This can enable comparisons with GEF mutated Rgnef constructs to test if Shh pathway activation is induced without RhoA activation. Although a study of this scale should first follow further protein pull-down investigation conducted in this thesis; that of western analysis of active Rho after Rgnef overexpression. Future analysis would require optimising the experiment for specifying active RhoA pull-down and would be possible by using specific antibodies for RhoA.

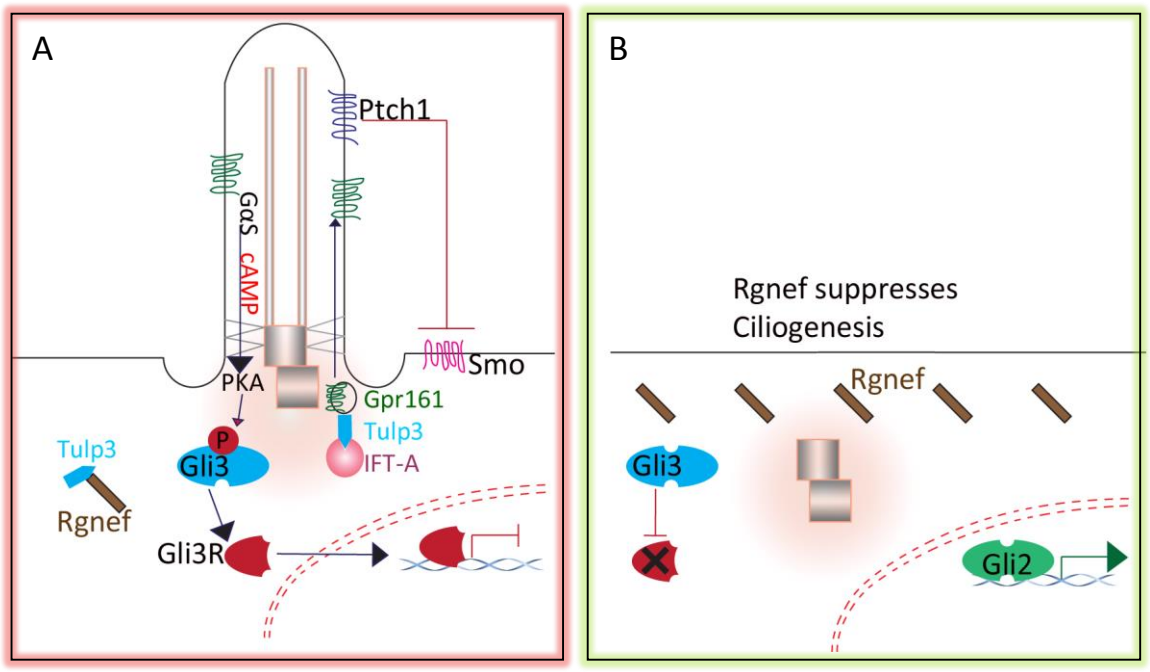

Figure 6-01 Model proposing effects of ciliogenesis on Shh pathway activation by increased Rgnef expression

(A-B) A simplified representation of the Shh signalling pathway proposing the effect of Rgnef overexpression on Shh signalling in relation to ciliogenesis. (A) In the absence of Shh ligand Ptch1 inhibits Smo, preventing its ciliary accumulation. Gpr161 is transported to the cilium in complex with Tulp3 and IFTA proteins. Cilium levels of cAMP are increased by Gs alpha protein coupled receptor activation of the cAMP-dependant pathway. PKA phosphorylates Gli3 and leads to it being targeted for proteolytic cleavage to the repressor form which translocates to the nucleus to repress gene expression. In the cytoplasm Tulp3 binds and sequesters Rgnef from inducing a suppressive effect on ciliogenesis (B) Rgnef overexpression suppresses ciliogenesis and primary cilia mediated Gli3 processing to Gli3 repressor is arrested. Instead Gli2 to Gli activator prevails over Gli3 repressor and induces expression of target genes.

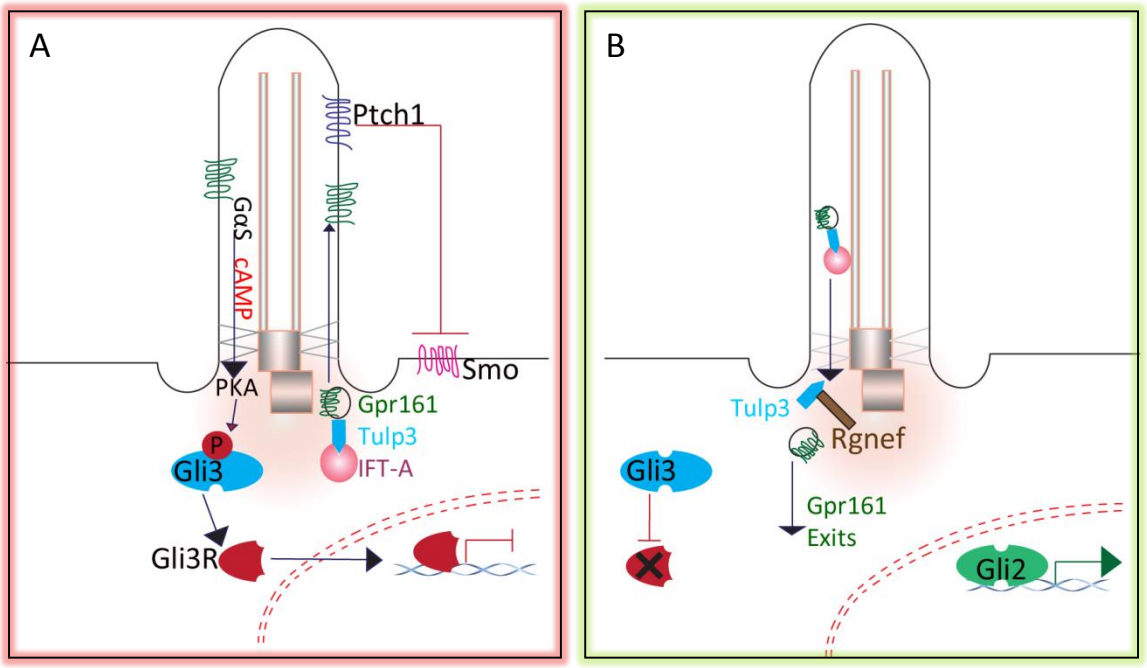

Figure 6-02 Model proposing effect of ciliary IFT transport by increased Rgnef expression leading to Shh pathway activation

(A-B) A simplified representation of the Shh signalling pathway proposing the effect of Rgnef overexpression on Shh signalling in relation to ciliary IFT transportation. (A) In the absence of Shh ligand Ptch1 inhibits Smo, preventing its ciliary accumulation. Gpr161 is transported to the cilium in complex with Tulp3 and IFTA proteins. Cilium levels of cAMP are increased by Gs alpha protein coupled receptor activation of the cAMP-dependant pathway. PKA phosphorylates Gli3 and leads to it being targeted for proteolytic cleavage to the repressor form which translocates to the nucleus to repress gene expression. (B) Increased *Rgnef* expression permits Gpr161 to be transported from the cilium by retrograde IFT transportation through IFTA protein complex bridged by Tulp3. Binding partner Rgnef permits access from the primary cilium. Loss of ciliary cAMP deregulates PKA phosphorylation of Gli3 processing to Gli3 repressor. As Gli3 processing to Gli3 repressor is arrested, Gli2 to Gli activator prevails over Gli3 repressor and induces expression of target genes.

6-1-02 Future plans for investigating Trim71 in Shh signalling and neural tube development.

An investigation of an involvement of Trim71 in Shh signaling has yet to be addressed as results in this thesis were identified to be false positive. Yet there is a strong basis for continuing future investigation into Trim71 in light of evidence in our laboratory that Trim71 and Tulp3 interact (Patterson, 2011). Furthermore *Trim71* deficient mice exhibit neural tube defects (Maller Schulman et al., 2008). The main limitation in this thesis was the lack or low level of *Trim71* expression in Shh-LIGHT2 cells, the cell line used to investigate effects on the Shh pathway. Using Shh-LIGHT2 cells for future investigations are therefore only limited to studying the effects of overexpressing Trim71. A major concern for continuing the use of Shh-LIGHT2 cells, or indeed the NIH 3T3 cells from which Shh-LIGHT2 cells are derived, is about the validity of any given study that is based on inducing *Trim71* expression in a cell that does not normally express it. Hence, a comparison of both knock down and overexpression requires use of a cell line with defined *Trim71* expression as it would indicate its use in signalling mechanisms, and therefore one could be confident that other factors required for its function are also expressed. Interestingly, two cell lines that have been identified with significantly high *Trim71* expression are embryonic cell derived. These are P19, a mouse embryonic carcinoma cell line and J1-ES, a cell line derived from *agouti* embryonic stem cells (Chang et al., 2012). In order to investigate a possible involvement in Shh signaling, changes in *Trim71* expression should be considered in these cells lines relative to Shh pathway activity. This activity can be still be potentially monitored by transient transfection of the Gli reporter construct Gli-BS luciferase, as it is the construct stably transfected in Shh-LIGHT2 cells (Sasaki et al., 1997). Shh pathway activity can be monitored by RT-qPCR expression analysis of *Ptch1* and *Gli1*, hence genes that upregulate in response to pathway activation.

6-02 Conclusion

Investigations into potential Shh pathway protein effectors, like Rgnef and Trim71, should ultimately be understood in terms of regulation by Gli transcription factor PTM, hence commitment to expressing target genes. This advancement in level of detail will help define the regulation involved in a single pathway with such diverse roles. This can in turn help elucidate the highly regulated processes of neural tube closure and

determining differentiation fates for the wide range of neural cells. Future aims are therefore centred on the idea that understanding the complexity of Shh pathway regulation requires deciphering the purpose of Gli transcription factor PTM. Although only Gli2 has been characterised in this thesis, the techniques established can be applied to a full investigation of pathway activation transcription as a whole by also characterising Gli1 and Gli3 PTM.

Future investigations should therefore aim to investigate all three Gli transcription factors for mouse and human and in particular compare against changes in PTM after activation of the Shh signalling pathway. Hence the results are a start to a future framework for investigating the complex transcriptional regulation of Shh pathway signalling. The aim is to identify the overall molecular mechanism of Gli protein PTM related to upstream effectors. Understanding NT development in terms of a more detailed molecular mechanism for Shh signal transduction can better inform the process of identifying specific causes of NTD's and help devise therapeutic strategies.

References

ALCEDO, J., AYZENZON, M., VON OHLEN, T., NOLL, M. & HOOPER, J. E. 1996. The *Drosophila* smoothened gene encodes a seven-pass membrane protein, a putative receptor for the hedgehog signal. *Cell,* 86**,** 221-32.

ALFA, C. E. & HYAMS, J. S. 1991. Microtubules in the fission yeast *Schizosaccharomyces* pombe contain only the tyrosinated form of alpha-tubulin. *Cell Motil Cytoskeleton,* 18**,** 86-93.

ARTHUR, W. T. & BURRIDGE, K. 2001. RhoA inactivation by p190RhoGAP regulates cell spreading and migration by promoting membrane protrusion and polarity. *Mol Biol Cell,* 12**,** 2711-20.

AZA-BLANC, P., RAMIREZ-WEBER, F. A., LAGET, M. P., SCHWARTZ, C. & KORNBERG, T. B. 1997. Proteolysis that is inhibited by hedgehog targets Cubitus interruptus protein to the nucleus and converts it to a repressor. *Cell,* 89**,** 1043-53.

BAI, C. B., STEPHEN, D. & JOYNER, A. L. 2004. All mouse ventral spinal cord patterning by hedgehog is Gli dependent and involves an activator function of Gli3. *Dev Cell,* 6**,** 103-15.

BERBARI, N. F., O'CONNOR, A. K., HAYCRAFT, C. J. & YODER, B. K. 2009. The primary cilium as a complex signaling center. *Curr Biol,* 19**,** R526-35.

BERTRAND, N., MEDEVIELLE, F. & PITUELLO, F. 2000. FGF signalling controls the timing of Pax6 activation in the neural tube. *Development,* 127**,** 4837-43.

BITGOOD, M. J., SHEN, L. & MCMAHON, A. P. 1996. Sertoli cell signaling by Desert hedgehog regulates the male germline. *Curr Biol,* 6**,** 298-304.

BOGGON, T. J., SHAN, W. S., SANTAGATA, S., MYERS, S. C. & SHAPIRO, L. 1999. Implication of tubby proteins as transcription factors by structure-based functional analysis. *Science,* 286**,** 2119-25.

BOYLES, A. L., HAMMOCK, P. & SPEER, M. C. 2005. Candidate gene analysis in human neural tube defects. *Am J Med Genet C Semin Med Genet,* 135C**,** 9-23.

BRISCOE, J. & ERICSON, J. 2001. Specification of neuronal fates in the ventral neural tube. *Curr Opin Neurobiol,* 11**,** 43-9.

BRISCOE, J., PIERANI, A., JESSELL, T. M. & ERICSON, J. 2000. A homeodomain protein code specifies progenitor cell identity and neuronal fate in the ventral neural tube. *Cell,* 101**,** 435-45.

BULGAKOV, O. V., EGGENSCHWILER, J. T., HONG, D. H., ANDERSON, K. V. & LI, T. 2004. FKBP8 is a negative regulator of mouse sonic hedgehog signaling in neural tissues. *Development,* 131**,** 2149-59.

CAMERON, D. A., PENNIMPEDE, T. & PETKOVICH, M. 2009. Tulp3 is a critical repressor of mouse hedgehog signaling. *Dev Dyn,* 238**,** 1140-9.

CANETE-SOLER, R., WU, J., ZHAI, J., SHAMIM, M. & SCHLAEPFER, W. W. 2001. p190RhoGEF Binds to a destabilizing element in the 3' untranslated region of light neurofilament subunit mRNA and alters the stability of the transcript. *J Biol Chem,* 276**,** 32046-50.

CASPARY, T., LARKINS, C. E. & ANDERSON, K. V. 2007. The graded response to Sonic Hedgehog depends on cilia architecture. *Dev Cell,* 12**,** 767-78.

CAYUSO, J., ULLOA, F., COX, B., BRISCOE, J. & MARTI, E. 2006. The Sonic hedgehog pathway independently controls the patterning, proliferation and survival of neuroepithelial cells by regulating Gli activity. *Development,* 133**,** 517-28.

CHANG, H. M., MARTINEZ, N. J., THORNTON, J. E., HAGAN, J. P., NGUYEN, K. D. & GREGORY, R. I. 2012. Trim71 cooperates with microRNAs to repress Cdkn1a expression and promote embryonic stem cell proliferation. *Nat Commun,* 3**,** 923.

CHEN, J., LAI, F. & NISWANDER, L. 2012. The ubiquitin ligase mLin41 temporally promotes neural progenitor cell maintenance through FGF signaling. *Genes Dev,* 26**,** 803-15.

CHEN, J. K., TAIPALE, J., COOPER, M. K. & BEACHY, P. A. 2002. Inhibition of Hedgehog signaling by direct binding of cyclopamine to Smoothened. *Genes Dev,* 16**,** 2743-8.

CHEN, Y., CARDINAUX, J. R., GOODMAN, R. H. & SMOLIK, S. M. 1999. Mutants of cubitus interruptus that are independent of PKA regulation are independent of hedgehog signaling. *Development,* 126**,** 3607-16.

CHEN, Y., GALLAHER, N., GOODMAN, R. H. & SMOLIK, S. M. 1998. Protein kinase A directly regulates the activity and proteolysis of cubitus interruptus. *Proc Natl Acad Sci U S A,* 95**,** 2349-54.

CHEN, Y., YUE, S., XIE, L., PU, X. H., JIN, T. & CHENG, S. Y. 2011a. Dual Phosphorylation of suppressor of fused (Sufu) by PKA and GSK3beta regulates its stability and localization in the primary cilium. *J Biol Chem,* 286**,** 13502-11.

CHEN, Z., GUO, L., SPRANG, S. R. & STERNWEIS, P. C. 2011b. Modulation of a GEF switch: autoinhibition of the intrinsic guanine nucleotide exchange activity of p115-RhoGEF. *Protein Sci,* 20**,** 107-17.

CHEUNG, H. O., ZHANG, X., RIBEIRO, A., MO, R., MAKINO, S., PUVIINDRAN, V., LAW, K. K., BRISCOE, J. & HUI, C. C. 2009. The kinesin protein Kif7 is a critical regulator of Gli transcription factors in mammalian hedgehog signaling. *Sci Signal,* 2**,** ra29.

CHIANG, C., LITINGTUNG, Y., LEE, E., YOUNG, K. E., CORDEN, J. L., WESTPHAL, H. & BEACHY, P. A. 1996. Cyclopia and defective axial patterning in mice lacking Sonic hedgehog gene function. *Nature,* 383**,** 407-13.

CLAES, K., VANDESOMPELE, J., POPPE, B., DAHAN, K., COENE, I., DE PAEPE, A. & MESSIAEN, L. 2002. Pathological splice mutations outside the invariant AG/GT splice sites of BRCA1 exon 5 increase alternative transcript levels in the 5' end of the BRCA1 gene. *Oncogene,* 21**,** 4171-5.

COHEN, S. L. & CHAIT, B. T. 1997. Mass spectrometry of whole proteins eluted from sodium dodecyl sulfate-polyacrylamide gel electrophoresis gels. *Anal Biochem,* 247**,** 257-67.

COLAS, J. F. & SCHOENWOLF, G. C. 2001. Towards a cellular and molecular understanding of neurulation. *Dev Dyn,* 221**,** 117-45.

COOK, A., BONO, F., JINEK, M. & CONTI, E. 2007. Structural biology of nucleocytoplasmic transport. *Annu Rev Biochem,* 76**,** 647-71.

COPP, A. J., GREENE, N. D. & MURDOCH, J. N. 2003a. Dishevelled: linking convergent extension with neural tube closure. *Trends Neurosci,* 26**,** 453-5.

COPP, A. J., GREENE, N. D. & MURDOCH, J. N. 2003b. The genetic basis of mammalian neurulation. *Nat Rev Genet,* 4**,** 784-93.

COPP, A. J., STANIER, P. & GREENE, N. D. 2013. Neural tube defects: recent advances, unsolved questions, and controversies. *Lancet Neurol,* 12**,** 799-810.

CORBIT, K. C., AANSTAD, P., SINGLA, V., NORMAN, A. R., STAINIER, D. Y. & REITER, J. F. 2005. Vertebrate Smoothened functions at the primary cilium. *Nature,* 437**,** 1018-21.

CORDES, S. P. 2005. N-ethyl-N-nitrosourea mutagenesis: boarding the mouse mutant express. *Microbiol Mol Biol Rev,* 69**,** 426-39.

CORTELLINO, S., WANG, C., WANG, B., BASSI, M. R., CARETTI, E., CHAMPEVAL, D., CALMONT, A., JARNIK, M., BURCH, J., ZARET, K. S., LARUE, L. & BELLACOSA, A. 2009. Defective ciliogenesis, embryonic lethality and severe impairment of the Sonic Hedgehog pathway caused by inactivation of the mouse complex A intraflagellar transport gene Ift122/Wdr10, partially overlapping with the DNA repair gene Med1/Mbd4. *Dev Biol,* 325**,** 225-37.

DAVIDSON, B. P., KINDER, S. J., STEINER, K., SCHOENWOLF, G. C. & TAM, P. P. 1999. Impact of node ablation on the morphogenesis of the body axis and the lateral asymmetry of the mouse embryo during early organogenesis. *Dev Biol,* 211**,** 11-26.

DE CASTRO, E., SIGRIST, C. J., GATTIKER, A., BULLIARD, V., LANGENDIJK-GENEVAUX, P. S., GASTEIGER, E., BAIROCH, A. & HULO, N. 2006. ScanProsite: detection of PROSITE signature matches and ProRule-associated functional and structural residues in proteins. *Nucleic Acids Res,* 34**,** W362-5.

DETRAIT, E. R., GEORGE, T. M., ETCHEVERS, H. C., GILBERT, J. R., VEKEMANS, M. & SPEER, M. C. 2005. Human neural tube defects: developmental biology, epidemiology, and genetics. *Neurotoxicol Teratol,* 27**,** 515-24.

DIEZ DEL CORRAL, R., BREITKREUZ, D. N. & STOREY, K. G. 2002. Onset of neuronal differentiation is regulated by paraxial mesoderm and requires attenuation of FGF signalling. *Development,* 129**,** 1681-91.

DIEZ DEL CORRAL, R., OLIVERA-MARTINEZ, I., GORIELY, A., GALE, E., MADEN, M. & STOREY, K. 2003. Opposing FGF and retinoid pathways control ventral neural pattern, neuronal differentiation, and segmentation during body axis extension. *Neuron,* 40**,** 65-79.

DING, Q., FUKAMI, S., MENG, X., NISHIZAKI, Y., ZHANG, X., SASAKI, H., DLUGOSZ, A., NAKAFUKU, M. & HUI, C. 1999. Mouse suppressor of fused is a negative regulator of sonic hedgehog signaling and alters the subcellular distribution of Gli1. *Curr Biol,* 9**,** 1119-22.

DOMPIERRE, J. P., GODIN, J. D., CHARRIN, B. C., CORDELIERES, F. P., KING, S. J., HUMBERT, S. & SAUDOU, F. 2007. Histone deacetylase 6 inhibition compensates for the transport deficit in Huntington's disease by increasing tubulin acetylation. *J Neurosci,* 27**,** 3571-83.

DUNAEVA, M., MICHELSON, P., KOGERMAN, P. & TOFTGARD, R. 2003. Characterization of the physical interaction of Gli proteins with SUFU proteins. *J Biol Chem,* 278**,** 5116-22.

DWIGHT, Z., PALAIS, R. & WITTWER, C. T. 2011. uMELT: prediction of high-resolution melting curves and dynamic melting profiles of PCR products in a rich web application. *Bioinformatics,* 27**,** 1019-20.

ECHELARD, Y., EPSTEIN, D. J., ST-JACQUES, B., SHEN, L., MOHLER, J., MCMAHON, J. A. & MCMAHON, A. P. 1993. Sonic hedgehog, a member of a family of putative signaling molecules, is implicated in the regulation of CNS polarity. *Cell,* 75**,** 1417-30.

ECSEDI, M. & GROSSHANS, H. 2013. LIN-41/TRIM71: emancipation of a miRNA target. *Genes & Development,* 27**,** 581-589.

EGGENSCHWILER, J. T., ESPINOZA, E. & ANDERSON, K. V. 2001. Rab23 is an essential negative regulator of the mouse Sonic hedgehog signalling pathway. *Nature,* 412**,** 194-8.

EICHHOLZER, M., TONZ, O. & ZIMMERMANN, R. 2006. Folic acid: a public-health challenge. *Lancet,* 367**,** 1352-61.

ELDER, G. A., FRIEDRICH, V. L., JR., BOSCO, P., KANG, C., GOUROV, A., TU, P. H., LEE, V. M. & LAZZARINI, R. A. 1998. Absence of the mid-sized neurofilament subunit decreases axonal calibers, levels of light neurofilament (NF-L), and neurofilament content. *J Cell Biol,* 141**,** 727-39.

EPSTEIN, D. J., MARTI, E., SCOTT, M. P. & MCMAHON, A. P. 1996. Antagonizing cAMP-dependent protein kinase A in the dorsal CNS activates a conserved Sonic hedgehog signaling pathway. *Development,* 122**,** 2885-94.

ERICSON, J., MORTON, S., KAWAKAMI, A., ROELINK, H. & JESSELL, T. M. 1996. Two critical periods of Sonic Hedgehog signaling required for the specification of motor neuron identity. *Cell,* 87**,** 661-73.

ERICSON, J., RASHBASS, P., SCHEDL, A., BRENNER-MORTON, S., KAWAKAMI, A., VAN HEYNINGEN, V., JESSELL, T. M. & BRISCOE, J. 1997. Pax6 controls progenitor cell identity and neuronal fate in response to graded Shh signaling. *Cell,* 90**,** 169-80.

EUROCAT prevelance data tables 2008-2012 (2014). prevelance data tables.

FERRANTE, M. I., ZULLO, A., BARRA, A., BIMONTE, S., MESSADDEQ, N., STUDER, M., DOLLE, P. & FRANCO, B. 2006. Oral-facial-digital type I protein is required for primary cilia formation and left-right axis specification. *Nat Genet,* 38**,** 112-7.

FILIPOWICZ, W. 2005. RNAi: the nuts and bolts of the RISC machine. *Cell,* 122**,** 17-20.

FORBES, A. J., NAKANO, Y., TAYLOR, A. M. & INGHAM, P. W. 1993. Genetic analysis of hedgehog signalling in the *Drosophila* embryo. *Dev Suppl***,** 115-24.

FREUNDLIEB, S., BARON, U., BONIN, A. L., GOSSEN, M. & BUJARD, H. 1997. Use of tetracycline-controlled gene expression systems to study mammalian cell cycle. *Methods Enzymol,* 283**,** 159-73.

GAERTIG, J. & WLOGA, D. 2008. Ciliary tubulin and its post-translational modifications. *Curr Top Dev Biol,* 85**,** 83-113.

GARCIA-GONZALO, F. R. & REITER, J. F. 2012. Scoring a backstage pass: mechanisms of ciliogenesis and ciliary access. *J Cell Biol,* 197**,** 697-709.

GEBBINK, M. F., KRANENBURG, O., POLAND, M., VAN HORCK, F. P., HOUSSA, B. & MOOLENAAR, W. H. 1997. Identification of a novel, putative Rho-specific GDP/GTP exchange factor and a RhoA-binding protein: control of neuronal morphology. *J Cell Biol,* 137**,** 1603-13.

GERDES, J. M., DAVIS, E. E. & KATSANIS, N. 2009. The vertebrate primary cilium in development, homeostasis, and disease. *Cell,* 137**,** 32-45.

GOETZ, S. C. & ANDERSON, K. V. 2010. The primary cilium: a signalling centre during vertebrate development. *Nat Rev Genet,* 11**,** 331-44.

GOODRICH, L. V., MILENKOVIC, L., HIGGINS, K. M. & SCOTT, M. P. 1997. Altered neural cell fates and medulloblastoma in mouse patched mutants. *Science,* 277**,** 1109-13.

GORBATYUK, M., JUSTILIEN, V., LIU, J., HAUSWIRTH, W. W. & LEWIN, A. S. 2007. Preservation of photoreceptor morphology and function in P23H rats using an allele independent ribozyme. *Exp Eye Res,* 84**,** 44-52.

GOSSEN, M. 2006. Conditional gene expression: intelligent designs. *Gene Ther,* 13**,** 1251-2.
GOSSEN, M. & BUJARD, H. 1992. Tight control of gene expression in mammalian cells by tetracycline-responsive promoters. *Proc Natl Acad Sci U S A,* 89**,** 5547-51.
GREENE, N. D. & COPP, A. J. 1997. Inositol prevents folate-resistant neural tube defects in the mouse. *Nat Med,* 3**,** 60-6.
GREENE, N. D. & COPP, A. J. 2009. Development of the vertebrate central nervous system: formation of the neural tube. *Prenat Diagn,* 29**,** 303-11.
GUILLEMOT, F. 2007. Spatial and temporal specification of neural fates by transcription factor codes. *Development,* 134**,** 3771-80.
HAYCRAFT, C. J., BANIZS, B., AYDIN-SON, Y., ZHANG, Q., MICHAUD, E. J. & YODER, B. K. 2005. Gli2 and Gli3 localize to cilia and require the intraflagellar transport protein polaris for processing and function. *PLoS Genet,* 1**,** e53.
HIBBARD, B. M., HIBBARD, E. D. & JEFFCOATE, T. N. 1965. Folic acid and reproduction. *Acta Obstet Gynecol Scand,* 44**,** 375-400.
HOOPER, J. E. & SCOTT, M. P. 1989. The *Drosophila* patched gene encodes a putative membrane protein required for segmental patterning. *Cell,* 59**,** 751-65.
HOUDE, C., DICKINSON, R. J., HOUTZAGER, V. M., CULLUM, R., MONTPETIT, R., METZLER, M., SIMPSON, E. M., ROY, S., HAYDEN, M. R., HOODLESS, P. A. & NICHOLSON, D. W. 2006. Hippi is essential for node cilia assembly and Sonic hedgehog signaling. *Dev Biol,* 300**,** 523-33.
HUANGFU, D. & ANDERSON, K. V. 2005. Cilia and Hedgehog responsiveness in the mouse. *Proc Natl Acad Sci U S A,* 102**,** 11325-30.
HUANGFU, D. & ANDERSON, K. V. 2006. Signaling from Smo to Ci/Gli: conservation and divergence of Hedgehog pathways from *Drosophila* to vertebrates. *Development,* 133**,** 3-14.
HUANGFU, D., LIU, A., RAKEMAN, A. S., MURCIA, N. S., NISWANDER, L. & ANDERSON, K. V. 2003. Hedgehog signalling in the mouse requires intraflagellar transport proteins. *Nature,* 426**,** 83-7.
HUMKE, E. W., DORN, K. V., MILENKOVIC, L., SCOTT, M. P. & ROHATGI, R. 2010. The output of Hedgehog signaling is controlled by the dynamic association between Suppressor of Fused and the Gli proteins. *Genes Dev,* 24**,** 670-82.
HYNES, M., YE, W., WANG, K., STONE, D., MURONE, M., SAUVAGE, F. & ROSENTHAL, A. 2000. The seven-transmembrane receptor smoothened cell-autonomously induces multiple ventral cell types. *Nat Neurosci,* 3**,** 41-6.
IKEDA, A., IKEDA, S., GRIDLEY, T., NISHINA, P. M. & NAGGERT, J. K. 2001. Neural tube defects and neuroepithelial cell death in Tulp3 knockout mice. *Hum Mol Genet,* 10**,** 1325-34.
INGHAM, P. W., TAYLOR, A. M. & NAKANO, Y. 1991. Role of the *Drosophila* patched gene in positional signalling. *Nature,* 353**,** 184-7.
JACOBSON, A. G. & MOURY, J. D. 1995. Tissue boundaries and cell behavior during neurulation. *Dev Biol,* 171**,** 98-110.
JANKE, C., ROGOWSKI, K., WLOGA, D., REGNARD, C., KAJAVA, A. V., STRUB, J. M., TEMURAK, N., VAN DIJK, J., BOUCHER, D., VAN DORSSELAER, A., SURYAVANSHI, S., GAERTIG, J. & EDDE, B. 2005. Tubulin polyglutamylase enzymes are members of the TTL domain protein family. *Science,* 308**,** 1758-62.
JESSELL, T. M. 2000. Neuronal specification in the spinal cord: inductive signals and transcriptional codes. *Nat Rev Genet,* 1**,** 20-9.

JIA, J., AMANAI, K., WANG, G., TANG, J., WANG, B. & JIANG, J. 2002. Shaggy/GSK3 antagonizes Hedgehog signalling by regulating Cubitus interruptus. *Nature,* 416**,** 548-52.

JIA, J., KOLTERUD, A., ZENG, H., HOOVER, A., TEGLUND, S., TOFTGARD, R. & LIU, A. 2009. Suppressor of Fused inhibits mammalian Hedgehog signaling in the absence of cilia. *Dev Biol,* 330**,** 452-60.

JIA, J., ZHANG, L., ZHANG, Q., TONG, C., WANG, B., HOU, F., AMANAI, K. & JIANG, J. 2005. Phosphorylation by double-time/CKIepsilon and CKIalpha targets cubitus interruptus for Slimb/beta-TRCP-mediated proteolytic processing. *Dev Cell,* 9**,** 819-30.

JIANG, J. & STRUHL, G. 1998. Regulation of the Hedgehog and Wingless signalling pathways by the F-box/WD40-repeat protein Slimb. *Nature,* 391**,** 493-6.

JOHNSON, K. A. & ROSENBAUM, J. L. 1992. Polarity of flagellar assembly in Chlamydomonas. *J Cell Biol,* 119**,** 1605-11.

JUANG, Y. M., SHE, T. F., CHEN, H. Y. & LAI, C. C. 2013. Comparison of CID versus ETD-based MS/MS fragmentation for the analysis of doubly derivatized steroids. *J Mass Spectrom,* 48**,** 1349-56.

KAESLER, S., LUSCHER, B. & RUTHER, U. 2000. Transcriptional activity of GLI1 is negatively regulated by protein kinase A. *Biol Chem,* 381**,** 545-51.

KANAMOTO, T., TERADA, K., YOSHIKAWA, H. & FURUKAWA, T. 2006. Cloning and regulation of the vertebrate homologue of lin-41 that functions as a heterochronic gene in *Caenorhabditis elegans*. *Dev Dyn,* 235**,** 1142-9.

KASAI, K., TAKAHASHI, M., OSUMI, N., SINNARAJAH, S., TAKEO, T., IKEDA, H., KEHRL, J. H., ITOH, G. & ARNHEITER, H. 2004. The G12 family of heterotrimeric G proteins and Rho GTPase mediate Sonic hedgehog signalling. *Genes Cells,* 9**,** 49-58.

KELLER, R. 2002. Shaping the vertebrate body plan by polarized embryonic cell movements. *Science,* 298**,** 1950-4.

KENNEY, A. M., COLE, M. D. & ROWITCH, D. H. 2003. Nmyc upregulation by sonic hedgehog signaling promotes proliferation in developing cerebellar granule neuron precursors. *Development,* 130**,** 15-28.

KIM, J., KATO, M. & BEACHY, P. A. 2009a. Gli2 trafficking links Hedgehog-dependent activation of Smoothened in the primary cilium to transcriptional activation in the nucleus. *Proc Natl Acad Sci U S A,* 106**,** 21666-71.

KIM, W. Y., WANG, X., WU, Y., DOBLE, B. W., PATEL, S., WOODGETT, J. R. & SNIDER, W. D. 2009b. GSK-3 is a master regulator of neural progenitor homeostasis. *Nat Neurosci,* 12**,** 1390-7.

KISE, Y., MORINAKA, A., TEGLUND, S. & MIKI, H. 2009. Sufu recruits GSK3beta for efficient processing of Gli3. *Biochem Biophys Res Commun,* 387**,** 569-74.

KLOOSTERMAN, W. P., WIENHOLDS, E., KETTING, R. F. & PLASTERK, R. H. 2004. Substrate requirements for let-7 function in the developing zebrafish embryo. *Nucleic Acids Res,* 32**,** 6284-91.

KOVACS, J. J., WHALEN, E. J., LIU, R., XIAO, K., KIM, J., CHEN, M., WANG, J., CHEN, W. & LEFKOWITZ, R. J. 2008. Beta-arrestin-mediated localization of smoothened to the primary cilium. *Science,* 320**,** 1777-81.

KOZMINSKI, K. G., BEECH, P. L. & ROSENBAUM, J. L. 1995. The Chlamydomonas kinesin-like protein FLA10 is involved in motility associated with the flagellar membrane. *J Cell Biol,* 131**,** 1517-27.

KOZMINSKI, K. G., JOHNSON, K. A., FORSCHER, P. & ROSENBAUM, J. L. 1993. A motility in the eukaryotic flagellum unrelated to flagellar beating. *Proc Natl Acad Sci U S A,* 90**,** 5519-23.

LANCMAN, J. J., CARUCCIO, N. C., HARFE, B. D., PASQUINELLI, A. E., SCHAGEMAN, J. J., PERTSEMLIDIS, A. & FALLON, J. F. 2005. Analysis of the regulation of lin-41 during chick and mouse limb development. *Dev Dyn,* 234**,** 948-60.

LECK, I. 1974. Causation of neural tube defects: clues from epidemiology. *Br Med Bull,* 30**,** 158-63.

LIEM, K. F., JR., HE, M., OCBINA, P. J. & ANDERSON, K. V. 2009. Mouse Kif7/Costal2 is a cilia-associated protein that regulates Sonic hedgehog signaling. *Proc Natl Acad Sci U S A,* 106**,** 13377-82.

LITINGTUNG, Y. & CHIANG, C. 2000a. Control of Shh activity and signaling in the neural tube. *Dev Dyn,* 219**,** 143-54.

LITINGTUNG, Y. & CHIANG, C. 2000b. Specification of ventral neuron types is mediated by an antagonistic interaction between Shh and Gli3. *Nat Neurosci,* 3**,** 979-85.

LIU, A., WANG, B. & NISWANDER, L. A. 2005. Mouse intraflagellar transport proteins regulate both the activator and repressor functions of Gli transcription factors. *Development,* 132**,** 3103-11.

LIU, J., CARMELL, M. A., RIVAS, F. V., MARSDEN, C. G., THOMSON, J. M., SONG, J. J., HAMMOND, S. M., JOSHUA-TOR, L. & HANNON, G. J. 2004. Argonaute2 is the catalytic engine of mammalian RNAi. *Science,* 305**,** 1437-41.

LIVAK, K. J. & SCHMITTGEN, T. D. 2001. Analysis of relative gene expression data using real-time quantitative PCR and the 2(-Delta Delta C(T)) Method. *Methods,* 25**,** 402-8.

MACHESKY, L. M. & HALL, A. 1996. Rho: a connection between membrane receptor signalling and the cytoskeleton. *Trends Cell Biol,* 6**,** 304-10.

MALLER SCHULMAN, B. R., LIANG, X., STAHLHUT, C., DELCONTE, C., STEFANI, G. & SLACK, F. J. 2008. The let-7 microRNA target gene, Mlin41/Trim71 is required for mouse embryonic survival and neural tube closure. *Cell Cycle,* 7**,** 3935-42.

MALOVERJAN, A., PIIRSOO, M., KASAK, L., PEIL, L., OSTERLUND, T. & KOGERMAN, P. 2010a. Dual function of UNC-51-like kinase 3 (Ulk3) in the Sonic hedgehog signaling pathway. *J Biol Chem,* 285**,** 30079-90.

MALOVERJAN, A., PIIRSOO, M., MICHELSON, P., KOGERMAN, P. & OSTERLUND, T. 2010b. Identification of a novel serine/threonine kinase ULK3 as a positive regulator of Hedgehog pathway. *Exp Cell Res,* 316**,** 627-37.

MARIGO, V., DAVEY, R. A., ZUO, Y., CUNNINGHAM, J. M. & TABIN, C. J. 1996. Biochemical evidence that patched is the Hedgehog receptor. *Nature,* 384**,** 176-9.

MARSHALL, W. F. 2008. Basal bodies platforms for building cilia. *Curr Top Dev Biol,* 85**,** 1-22.

MARSZALEK, J. R., RUIZ-LOZANO, P., ROBERTS, E., CHIEN, K. R. & GOLDSTEIN, L. S. 1999. Situs inversus and embryonic ciliary morphogenesis defects in mouse mutants lacking the KIF3A subunit of kinesin-II. *Proc Natl Acad Sci U S A,* 96**,** 5043-8.

MARTI, E., BUMCROT, D. A., TAKADA, R. & MCMAHON, A. P. 1995. Requirement of 19K form of Sonic hedgehog for induction of distinct ventral cell types in CNS explants. *Nature,* 375**,** 322-5.

MATISE, M. P. & JOYNER, A. L. 1999. Gli genes in development and cancer. *Oncogene,* 18**,** 7852-9.

MAY, S. R., ASHIQUE, A. M., KARLEN, M., WANG, B., SHEN, Y., ZARBALIS, K., REITER, J., ERICSON, J. & PETERSON, A. S. 2005. Loss of the retrograde motor for IFT disrupts localization of Smo to cilia and prevents the expression of both activator and repressor functions of Gli. *Dev Biol,* 287**,** 378-89.

MCMAHON, A. P., INGHAM, P. W. & TABIN, C. J. 2003. Developmental roles and clinical significance of hedgehog signaling. *Curr Top Dev Biol,* 53**,** 1-114.

MERONI, G. & DIEZ-ROUX, G. 2005. TRIM/RBCC, a novel class of 'single protein RING finger' E3 ubiquitin ligases. *Bioessays,* 27**,** 1147-57.

METHOT, N. & BASLER, K. 1999. Hedgehog controls limb development by regulating the activities of distinct transcriptional activator and repressor forms of Cubitus interruptus. *Cell,* 96**,** 819-31.

MEYER, D., LIU, A. & MARGOLIS, B. 1999. Interaction of c-Jun amino-terminal kinase interacting protein-1 with p190 rhoGEF and its localization in differentiated neurons. *J Biol Chem,* 274**,** 35113-8.

MILLER, N. L., LAWSON, C., CHEN, X. L., LIM, S. T. & SCHLAEPFER, D. D. 2012. Rgnef (p190RhoGEF) knockout inhibits RhoA activity, focal adhesion establishment, and cell motility downstream of integrins. *PLoS One,* 7**,** e37830.

MILLER, N. L., LAWSON, C., KLEINSCHMIDT, E. G., TANCIONI, I., URYU, S. & SCHLAEPFER, D. D. 2013. A non-canonical role for Rgnef in promoting integrin-stimulated focal adhesion kinase activation. *J Cell Sci,* 126**,** 5074-85.

MO, R., FREER, A. M., ZINYK, D. L., CRACKOWER, M. A., MICHAUD, J., HENG, H. H., CHIK, K. W., SHI, X. M., TSUI, L. C., CHENG, S. H., JOYNER, A. L. & HUI, C. 1997. Specific and redundant functions of Gli2 and Gli3 zinc finger genes in skeletal patterning and development. *Development,* 124**,** 113-23.

MOLLA-HERMAN, A., GHOSSOUB, R., BLISNICK, T., MEUNIER, A., SERRES, C., SILBERMANN, F., EMMERSON, C., ROMEO, K., BOURDONCLE, P., SCHMITT, A., SAUNIER, S., SPASSKY, N., BASTIN, P. & BENMERAH, A. 2010. The ciliary pocket: an endocytic membrane domain at the base of primary and motile cilia. *J Cell Sci,* 123**,** 1785-95.

MOTZNY, C. K. & HOLMGREN, R. 1995. The *Drosophila* cubitus interruptus protein and its role in the wingless and hedgehog signal transduction pathways. *Mech Dev,* 52**,** 137-50.

MOURY, J. D. & SCHOENWOLF, G. C. 1995. Cooperative model of epithelial shaping and bending during avian neurulation: autonomous movements of the neural plate, autonomous movements of the epidermis, and interactions in the neural plate/epidermis transition zone. *Dev Dyn,* 204**,** 323-37.

MRC, L. 1991. Prevention of neural tube defects: results of the Medical Research Council Vitamin Study. MRC Vitamin Study Research Group. *Lancet,* 338**,** 131-137.

MUKHOPADHYAY, S. & JACKSON, P. K. 2011. The tubby family proteins. *Genome Biol,* 12**,** 225.

MUKHOPADHYAY, S., WEN, X., CHIH, B., NELSON, C. D., LANE, W. S., SCALES, S. J. & JACKSON, P. K. 2010. TULP3 bridges the IFT-A complex and membrane phosphoinositides to promote trafficking of G protein-coupled receptors into primary cilia. *Genes Dev,* 24**,** 2180-93.

MUKHOPADHYAY, S., WEN, X., RATTI, N., LOKTEV, A., RANGELL, L., SCALES, S. J. & JACKSON, P. K. 2013. The ciliary G-protein-coupled receptor Gpr161 negatively regulates the Sonic hedgehog pathway via cAMP signaling. *Cell,* 152**,** 210-23.

MURDOCH, J. N. & COPP, A. J. 2010. The relationship between sonic Hedgehog signaling, cilia, and neural tube defects. *Birth Defects Res A Clin Mol Teratol,* 88**,** 633-52.

NIWA, H., YAMAMURA, K. & MIYAZAKI, J. 1991. Efficient selection for high-expression transfectants with a novel eukaryotic vector. *Gene,* 108**,** 193-9.

NORMAN, R. X., KO, H. W., HUANG, V., EUN, C. M., ABLER, L. L., ZHANG, Z., SUN, X. & EGGENSCHWILER, J. T. 2009. Tubby-like protein 3 (TULP3) regulates patterning in the mouse embryo through inhibition of Hedgehog signaling. *Hum Mol Genet,* 18**,** 1740-54.

NOVITCH, B. G., WICHTERLE, H., JESSELL, T. M. & SOCKANATHAN, S. 2003. A requirement for retinoic acid-mediated transcriptional activation in ventral neural patterning and motor neuron specification. *Neuron,* 40**,** 81-95.

NUSSLEIN-VOLHARD, C. & WIESCHAUS, E. 1980. Mutations affecting segment number and polarity in *Drosophila*. *Nature,* 287**,** 795-801.

OAKLEY, G. P. 1998. Folic-acid-preventable spina bifida and anencephaly. *Bulletin of the World Health Organisation.* World Health Organisation.

OAKLEY, G. P., JR. 2009. The scientific basis for eliminating folic acid-preventable spina bifida: a modern miracle from epidemiology. *Ann Epidemiol,* 19**,** 226-30.

OH, E. C. & KATSANIS, N. 2012. Cilia in vertebrate development and disease. *Development,* 139**,** 443-8.

PAL, K. & MUKHOPADHYAY, S. 2014. Primary cilium and sonic hedgehog signaling during neural tube patterning: Role of GPCRs and second messengers. *Dev Neurobiol*.

PAN, Y., BAI, C. B., JOYNER, A. L. & WANG, B. 2006. Sonic hedgehog signaling regulates Gli2 transcriptional activity by suppressing its processing and degradation. *Mol Cell Biol,* 26**,** 3365-77.

PAN, Y., WANG, C. & WANG, B. 2009. Phosphorylation of Gli2 by protein kinase A is required for Gli2 processing and degradation and the Sonic Hedgehog-regulated mouse development. *Dev Biol,* 326**,** 177-89.

PASCA DI MAGLIANO, M. & HEBROK, M. 2003. Hedgehog signalling in cancer formation and maintenance. *Nat Rev Cancer,* 3**,** 903-11.

PASQUINELLI, A. E., REINHART, B. J., SLACK, F., MARTINDALE, M. Q., KURODA, M. I., MALLER, B., HAYWARD, D. C., BALL, E. E., DEGNAN, B., MULLER, P., SPRING, J., SRINIVASAN, A., FISHMAN, M., FINNERTY, J., CORBO, J., LEVINE, M., LEAHY, P., DAVIDSON, E. & RUVKUN, G. 2000. Conservation of the sequence and temporal expression of let-7 heterochronic regulatory RNA. *Nature,* 408**,** 86-9.

PATTERSON, V. L. 2011. Characterisation of *hitchiker,* a novel mouse mutant with spina bifida. *Unpublished PhD thesis, University of Oxford*.

PATTERSON, V. L., DAMRAU, C., PAUDYAL, A., REEVE, B., GRIMES, D. T., STEWART, M. E., WILLIAMS, D. J., SIGGERS, P., GREENFIELD, A. & MURDOCH, J. N. 2009. Mouse hitchhiker mutants have spina bifida, dorso-ventral patterning defects and polydactyly: identification of Tulp3 as a novel negative regulator of the Sonic hedgehog pathway. *Hum Mol Genet,* 18**,** 1719-39.

PAZOUR, G. J. & BLOODGOOD, R. A. 2008. Targeting proteins to the ciliary membrane. *Curr Top Dev Biol,* 85**,** 115-49.

PAZOUR, G. J., DICKERT, B. L. & WITMAN, G. B. 1999. The DHC1b (DHC2) isoform of cytoplasmic dynein is required for flagellar assembly. *J Cell Biol,* 144**,** 473-81.
PEDERSEN, L. B. & ROSENBAUM, J. L. 2008. Intraflagellar transport (IFT) role in ciliary assembly, resorption and signalling. *Curr Top Dev Biol,* 85**,** 23-61.
PERKINS, D. N., PAPPIN, D. J., CREASY, D. M. & COTTRELL, J. S. 1999. Probability-based protein identification by searching sequence databases using mass spectrometry data. *Electrophoresis,* 20**,** 3551-67.
PLACZEK, M., TESSIER-LAVIGNE, M., YAMADA, T., JESSELL, T. & DODD, J. 1990. Mesodermal control of neural cell identity: floor plate induction by the notochord. *Science,* 250**,** 985-8.
POLIZIO, A. H., CHINCHILLA, P., CHEN, X., MANNING, D. R. & RIOBO, N. A. 2011. Sonic Hedgehog activates the GTPases Rac1 and RhoA in a Gli-independent manner through coupling of smoothened to Gi proteins. *Sci Signal,* 4**,** pt7.
PORTER, M. E., BOWER, R., KNOTT, J. A., BYRD, P. & DENTLER, W. 1999. Cytoplasmic dynein heavy chain 1b is required for flagellar assembly in *Chlamydomonas*. *Mol Biol Cell,* 10**,** 693-712.
PREAT, T. 1992. Characterization of Suppressor of fused, a complete suppressor of the fused segment polarity gene of *Drosophila melanogaster. Genetics,* 132**,** 725-36.
PRICE, M. A. & KALDERON, D. 1999. Proteolysis of cubitus interruptus in Drosophila requires phosphorylation by protein kinase A. *Development,* 126**,** 4331-9.
PRICE, M. A. & KALDERON, D. 2002. Proteolysis of the Hedgehog signaling effector Cubitus interruptus requires phosphorylation by Glycogen Synthase Kinase 3 and Casein Kinase 1. *Cell,* 108**,** 823-35.
QIN, H., DIENER, D. R., GEIMER, S., COLE, D. G. & ROSENBAUM, J. L. 2004. Intraflagellar transport (IFT) cargo: IFT transports flagellar precursors to the tip and turnover products to the cell body. *J Cell Biol,* 164**,** 255-66.
QIN, J., LIN, Y., NORMAN, R. X., KO, H. W. & EGGENSCHWILER, J. T. 2011. Intraflagellar transport protein 122 antagonizes Sonic Hedgehog signaling and controls ciliary localization of pathway components. *Proc Natl Acad Sci U S A,* 108**,** 1456-61.
REDEKER, V., LEVILLIERS, N., VINOLO, E., ROSSIER, J., JAILLARD, D., BURNETTE, D., GAERTIG, J. & BRE, M. H. 2005. Mutations of tubulin glycylation sites reveal cross-talk between the C termini of alpha- and beta-tubulin and affect the ciliary matrix in Tetrahymena. *J Biol Chem,* 280**,** 596-606.
REED, N. A., CAI, D., BLASIUS, T. L., JIH, G. T., MEYHOFER, E., GAERTIG, J. & VERHEY, K. J. 2006. Microtubule acetylation promotes kinesin-1 binding and transport. *Curr Biol,* 16**,** 2166-72.
REINHART, B. J., SLACK, F. J., BASSON, M., PASQUINELLI, A. E., BETTINGER, J. C., ROUGVIE, A. E., HORVITZ, H. R. & RUVKUN, G. 2000. The 21-nucleotide let-7 RNA regulates developmental timing in *Caenorhabditis elegans*. *Nature,* 403**,** 901-6.
REITER, J. F. & SKARNES, W. C. 2006. Tectonic, a novel regulator of the Hedgehog pathway required for both activation and inhibition. *Genes Dev,* 20**,** 22-7.
RENAULT, M. A., RONCALLI, J., TONGERS, J., THORNE, T., KLYACHKO, E., MISENER, S., VOLPERT, O. V., MEHTA, S., BURG, A., LUEDEMANN, C., QIN, G., KISHORE, R. & LOSORDO, D. W. 2010. Sonic hedgehog induces angiogenesis via Rho kinase-dependent signaling in endothelial cells. *J Mol Cell Cardiol,* 49**,** 490-8.

RINGO, D. L. 1967. Flagellar motion and fine structure of the flagellar apparatus in Chlamydomonas. *J Cell Biol,* 33**,** 543-71.

ROBBINS, D. J., NYBAKKEN, K. E., KOBAYASHI, R., SISSON, J. C., BISHOP, J. M. & THEROND, P. P. 1997. Hedgehog elicits signal transduction by means of a large complex containing the kinesin-related protein costal2. *Cell,* 90**,** 225-34.

ROELINK, H., PORTER, J. A., CHIANG, C., TANABE, Y., CHANG, D. T., BEACHY, P. A. & JESSELL, T. M. 1995. Floor plate and motor neuron induction by different concentrations of the amino-terminal cleavage product of sonic hedgehog autoproteolysis. *Cell,* 81**,** 445-55.

ROHATGI, R., MILENKOVIC, L., CORCORAN, R. B. & SCOTT, M. P. 2009. Hedgehog signal transduction by Smoothened: pharmacologic evidence for a 2-step activation process. *Proc Natl Acad Sci U S A,* 106**,** 3196-201.

ROHATGI, R., MILENKOVIC, L. & SCOTT, M. P. 2007. Patched1 regulates hedgehog signaling at the primary cilium. *Science,* 317**,** 372-6.

ROSENBAUM, J. L. & WITMAN, G. B. 2002. Intraflagellar transport. *Nat Rev Mol Cell Biol,* 3**,** 813-25.

ROWITCH, D. H., B, S. J., LEE, S. M., FLAX, J. D., SNYDER, E. Y. & MCMAHON, A. P. 1999. Sonic hedgehog regulates proliferation and inhibits differentiation of CNS precursor cells. *J Neurosci,* 19**,** 8954-65.

RYBAK, A., FUCHS, H., HADIAN, K., SMIRNOVA, L., WULCZYN, E. A., MICHEL, G., NITSCH, R., KRAPPMANN, D. & WULCZYN, F. G. 2009. The let-7 target gene mouse lin-41 is a stem cell specific E3 ubiquitin ligase for the miRNA pathway protein Ago2. *Nat Cell Biol,* 11**,** 1411-20.

SANTAGATA, S., BOGGON, T. J., BAIRD, C. L., GOMEZ, C. A., ZHAO, J., SHAN, W. S., MYSZKA, D. G. & SHAPIRO, L. 2001. G-protein signaling through tubby proteins. *Science,* 292**,** 2041-50.

SASAKI, H., HUI, C., NAKAFUKU, M. & KONDOH, H. 1997. A binding site for Gli proteins is essential for HNF-3beta floor plate enhancer activity in transgenics and can respond to Shh in vitro. *Development,* 124**,** 1313-22.

SASAKI, H., NISHIZAKI, Y., HUI, C., NAKAFUKU, M. & KONDOH, H. 1999. Regulation of Gli2 and Gli3 activities by an amino-terminal repression domain: implication of Gli2 and Gli3 as primary mediators of Shh signaling. *Development,* 126**,** 3915-24.

SATIR, P. & CHRISTENSEN, S. T. 2007. Overview of structure and function of mammalian cilia. *Annu Rev Physiol,* 69**,** 377-400.

SCHULMAN, B. R., ESQUELA-KERSCHER, A. & SLACK, F. J. 2005. Reciprocal expression of lin-41 and the microRNAs let-7 and mir-125 during mouse embryogenesis. *Dev Dyn,* 234**,** 1046-54.

SHUM, A. S. & COPP, A. J. 1996. Regional differences in morphogenesis of the neuroepithelium suggest multiple mechanisms of spinal neurulation in the mouse. *Anat Embryol (Berl),* 194**,** 65-73.

SLACK, F. J., BASSON, M., LIU, Z., AMBROS, V., HORVITZ, H. R. & RUVKUN, G. 2000. The lin-41 RBCC gene acts in the *C. elegans* heterochronic pathway between the let-7 regulatory RNA and the LIN-29 transcription factor. *Mol Cell,* 5**,** 659-69.

SMITH, J. L. & SCHOENWOLF, G. C. 1989. Notochordal induction of cell wedging in the chick neural plate and its role in neural tube formation. *J Exp Zool,* 250**,** 49-62.

SOBOTT, F., WATT, S. J., SMITH, J., EDELMANN, M. J., KRAMER, H. B. & KESSLER, B. M. 2009. Comparison of CID versus ETD based MS/MS fragmentation for the analysis of protein ubiquitination. *J Am Soc Mass Spectrom,* 20**,** 1652-9.

ST-JACQUES, B., HAMMERSCHMIDT, M. & MCMAHON, A. P. 1999. Indian hedgehog signaling regulates proliferation and differentiation of chondrocytes and is essential for bone formation. *Genes Dev,* 13**,** 2072-86.

STONE, D. M., HYNES, M., ARMANINI, M., SWANSON, T. A., GU, Q., JOHNSON, R. L., SCOTT, M. P., PENNICA, D., GODDARD, A., PHILLIPS, H., NOLL, M., HOOPER, J. E., DE SAUVAGE, F. & ROSENTHAL, A. 1996. The tumour-suppressor gene patched encodes a candidate receptor for Sonic hedgehog. *Nature,* 384**,** 129-34.

TAIPALE, J., CHEN, J. K., COOPER, M. K., WANG, B., MANN, R. K., MILENKOVIC, L., SCOTT, M. P. & BEACHY, P. A. 2000. Effects of oncogenic mutations in Smoothened and Patched can be reversed by cyclopamine. *Nature,* 406**,** 1005-9.

TAKAO, D., DISHINGER, J. F., KEE, H. L., PINSKEY, J. M., ALLEN, B. L. & VERHEY, K. J. 2014. An assay for clogging the ciliary pore complex distinguishes mechanisms of cytosolic and membrane protein entry. *Curr Biol,* 24**,** 2288-94.

TAY, S. Y., INGHAM, P. W. & ROY, S. 2005. A homologue of the *Drosophila* kinesin-like protein Costal2 regulates Hedgehog signal transduction in the vertebrate embryo. *Development,* 132**,** 625-34.

TOMAR, A., LIM, S. T., LIM, Y. & SCHLAEPFER, D. D. 2009. A FAK-p120RasGAP-p190RhoGAP complex regulates polarity in migrating cells. *J Cell Sci,* 122**,** 1852-62.

TRAN, P. V., HAYCRAFT, C. J., BESSCHETNOVA, T. Y., TURBE-DOAN, A., STOTTMANN, R. W., HERRON, B. J., CHESEBRO, A. L., QIU, H., SCHERZ, P. J., SHAH, J. V., YODER, B. K. & BEIER, D. R. 2008. THM1 negatively modulates mouse sonic hedgehog signal transduction and affects retrograde intraflagellar transport in cilia. *Nat Genet,* 40**,** 403-10.

TUKACHINSKY, H., LOPEZ, L. V. & SALIC, A. 2010. A mechanism for vertebrate Hedgehog signaling: recruitment to cilia and dissociation of SuFu-Gli protein complexes. *J Cell Biol,* 191**,** 415-28.

VAN DEN HEUVEL, M. & INGHAM, P. W. 1996. smoothened encodes a receptor-like serpentine protein required for hedgehog signalling. *Nature,* 382**,** 547-51.

VAN DER PUT, N. M., STEEGERS-THEUNISSEN, R. P., FROSST, P., TRIJBELS, F. J., ESKES, T. K., VAN DEN HEUVEL, L. P., MARIMAN, E. C., DEN HEYER, M., ROZEN, R. & BLOM, H. J. 1995. Mutated methylenetetrahydrofolate reductase as a risk factor for spina bifida. *Lancet,* 346**,** 1070-1.

VAN HORCK, F. P., AHMADIAN, M. R., HAEUSLER, L. C., MOOLENAAR, W. H. & KRANENBURG, O. 2001. Characterization of p190RhoGEF, a RhoA-specific guanine nucleotide exchange factor that interacts with microtubules. *J Biol Chem,* 276**,** 4948-56.

VANDESOMPELE, J., DE PRETER, K., PATTYN, F., POPPE, B., VAN ROY, N., DE PAEPE, A. & SPELEMAN, F. 2002. Accurate normalization of real-time quantitative RT-PCR data by geometric averaging of multiple internal control genes. *Genome Biol,* 3**,** RESEARCH0034.

VARJOSALO, M., BJORKLUND, M., CHENG, F., SYVANEN, H., KIVIOJA, T., KILPINEN, S., SUN, Z., KALLIONIEMI, O., STUNNENBERG, H. G., HE, W. W., OJALA, P. &

TAIPALE, J. 2008. Application of active and kinase-deficient kinome collection for identification of kinases regulating hedgehog signaling. *Cell,* 133**,** 537-48.
VELLA, M. C., CHOI, E. Y., LIN, S. Y., REINERT, K. & SLACK, F. J. 2004. The *C. elegans* microRNA let-7 binds to imperfect let-7 complementary sites from the lin-41 3'UTR. *Genes Dev,* 18**,** 132-7.
VERHEY, K. J. & GAERTIG, J. 2007. The tubulin code. *Cell Cycle,* 6**,** 2152-60.
VOICULESCU, O., PAPANAYOTOU, C. & STERN, C. D. 2008. Spatially and temporally controlled electroporation of early chick embryos. *Nat Protoc,* 3**,** 419-26.
WALLINGFORD, J. B. & HARLAND, R. M. 2001. Xenopus Dishevelled signaling regulates both neural and mesodermal convergent extension: parallel forces elongating the body axis. *Development,* 128**,** 2581-92.
WALLINGFORD, J. B. & HARLAND, R. M. 2002. Neural tube closure requires Dishevelled-dependent convergent extension of the midline. *Development,* 129**,** 5815-25.
WANG, B., FALLON, J. F. & BEACHY, P. A. 2000. Hedgehog-regulated processing of Gli3 produces an anterior/posterior repressor gradient in the developing vertebrate limb. *Cell,* 100**,** 423-34.
WESTERMANN, S. & WEBER, K. 2003. Post-translational modifications regulate microtubule function. *Nat Rev Mol Cell Biol,* 4**,** 938-47.
WIJGERDE, M., MCMAHON, J. A., RULE, M. & MCMAHON, A. P. 2002. A direct requirement for Hedgehog signaling for normal specification of all ventral progenitor domains in the presumptive mammalian spinal cord. *Genes Dev,* 16**,** 2849-64.
WILSON, L. & MADEN, M. 2005. The mechanisms of dorsoventral patterning in the vertebrate neural tube. *Dev Biol,* 282**,** 1-13.
WINTER, D., KUGELSTADT, D., SEIDLER, J., KAPPES, B. & LEHMANN, W. D. 2009. Protein phosphorylation influences proteolytic cleavage and kinase substrate properties exemplified by analysis of in vitro phosphorylated Plasmodium falciparum glideosome-associated protein 45 by nano-ultra performance liquid chromatography-tandem mass spectrometry. *Anal Biochem,* 393**,** 41-7.
WISNIEWSKI, J. R., ZOUGMAN, A., NAGARAJ, N. & MANN, M. 2009. Universal sample preparation method for proteome analysis. *Nat Methods,* 6**,** 359-62.
WLOGA, D. & GAERTIG, J. 2010. Post-translational modifications of microtubules. *J Cell Sci,* 123**,** 3447-55.
YAMADA, T., PFAFF, S. L., EDLUND, T. & JESSELL, T. M. 1993. Control of cell pattern in the neural tube: motor neuron induction by diffusible factors from notochord and floor plate. *Cell,* 73**,** 673-86.
YBOT-GONZALEZ, P., COGRAM, P., GERRELLI, D. & COPP, A. J. 2002. Sonic hedgehog and the molecular regulation of mouse neural tube closure. *Development,* 129**,** 2507-17.
YBOT-GONZALEZ, P., GASTON-MASSUET, C., GIRDLER, G., KLINGENSMITH, J., ARKELL, R., GREENE, N. D. & COPP, A. J. 2007. Neural plate morphogenesis during mouse neurulation is regulated by antagonism of Bmp signalling. *Development,* 134**,** 3203-11.
YUAN, A., RAO, M. V., VEERANNA & NIXON, R. A. 2012. Neurofilaments at a glance. *J Cell Sci,* 125**,** 3257-63.

YUM, S. W., ZHANG, J., MO, K., LI, J. & SCHERER, S. S. 2009. A novel recessive Nefl mutation causes a severe, early-onset axonal neuropathy. *Ann Neurol,* 66**,** 759-70.

ZAMIR, E. & GEIGER, B. 2001. Molecular complexity and dynamics of cell-matrix adhesions. *J Cell Sci,* 114**,** 3583-90.

ZHAI, J., LIN, H., NIE, Z., WU, J., CANETE-SOLER, R., SCHLAEPFER, W. W. & SCHLAEPFER, D. D. 2003. Direct interaction of focal adhesion kinase with p190RhoGEF. *J Biol Chem,* 278**,** 24865-73.

ZHANG, W., ZHAO, Y., TONG, C., WANG, G., WANG, B., JIA, J. & JIANG, J. 2005. Hedgehog-regulated Costal2-kinase complexes control phosphorylation and proteolytic processing of Cubitus interruptus. *Dev Cell,* 8**,** 267-78.

ZHANG, X. M., RAMALHO-SANTOS, M. & MCMAHON, A. P. 2001. Smoothened mutants reveal redundant roles for Shh and Ihh signaling including regulation of L/R symmetry by the mouse node. *Cell,* 106**,** 781-92.

ZHU, Q., COUILLARD-DESPRES, S. & JULIEN, J. P. 1997. Delayed maturation of regenerating myelinated axons in mice lacking neurofilaments. *Exp Neurol,* 148**,** 299-316.